Neutrino interactions in hot and dense matter

Sanjay Reddy, Madappa Prakash, and James M. Lattimer

Department of Physics & Astronomy, SUNY at Stony Brook, Stony Brook, New York 11794-3800

(February 1, 2008)

Abstract

We study the charged and neutral current weak interaction rates relevant for the determination of neutrino opacities in dense matter found in supernovae and neutron stars. We establish an efficient formalism for calculating differential cross sections and mean free paths for interacting, asymmetric nuclear matter at arbitrary degeneracy. The formalism is valid for both charged and neutral current reactions. Strong interaction corrections are incorporated through the in-medium single particle energies at the relevant density and temperature. The effects of strong interactions on the weak interaction rates are investigated using both potential and effective field-theoretical models of matter. We investigate the relative importance of charged and neutral currents for different astrophysical situations, and also examine the influence of strangeness-bearing hyperons. Our findings show that the mean free paths are significantly altered by the effects of strong interactions and the multi-component nature of dense matter. The opacities are then discussed in the context of the evolution of the core of a protoneutron star.

PACS number(s): 13.15.+g, 26.60.+c, 97.60Jd

Typeset using REVTEX

arXiv:astro-ph/9710115v1 10 Oct 1997

I. INTRODUCTION

The transport of neutrinos is an essential aspect of simulations of gravitational collapse, supernovae, protoneutron stars and binary mergers of compact objects. The neutrinos of all flavors emitted from newly formed neutron stars in supernova explosions [1] are the only direct probe of the mechanism of supernovae and the structure of protoneutron stars. The most important ingredient of neutrino transport calculations in these simulations is the neutrino opacity at supra-nuclear density [2–8]. Yet, to date, calculations of neutrino opacities in dense matter have received relatively little attention compared to other physical inputs such as the equation of state (EOS).

Both charged current absorption and neutral current scattering reactions are important sources of opacity. Neutral current processes involve all flavors of neutrinos scattering on baryons and leptons. While scattering from electrons is important for energy and momentum transfer in the process of thermalizing neutrinos, for both energy and lepton number transport, neutrino-baryon scattering and absorption are the dominant processes.

Earlier work on neutrino interactions in matter at supra-nuclear densities that have shaped our discussion in this paper are in Refs. [9-32]. Various approximations have almost always been made in the calculations of neutrino cross sections. These approximations concern the degrees of degeneracy or relativity, the composition, or the effects of the baryon-baryon interactions. The cross section for neutrino-nucleon interactions has only been calculated exactly for noninteracting gases by Schinder [26] and for neutrino-electron scattering by Mezzacappa and Bruenn [3] . Other workers have developed limiting expressions for noninteracting gases for the purely elastic case, the completely degenerate case, or the completely nondegenerate case. In fact, most numerical simulations of supernovae, protoneutron star evolution, and binary neutron star coalescence, have employed limiting expressions, derived from those for noninteracting nucleonic matter, in which interactions were included by simple scaling factors [2,4,7,8]. The results may be inconsistent with the underlying nuclear matter EOS.

Only a few attempts exist [10,17,18,27,29] in which the effects of strong interactions on neutrino opacities were considered. But these studies were not performed for the intermediate degeneracies that are often encountered in astrophysical environments. In the case of neutral current opacities, the effects of stong interactions were investigated for nondegenerate nuclear matter by Sawyer [10] and for degenerate neutron matter by Iwamoto & Pethick [17]. Both of these efforts treated nucleons in the nonrelativistic limit and predicted increases in the mean free paths by factors of $\sim 2-3$, for densities in the range of $2-4$ times the nuclear saturation density ($n_0 = 0.16\,\mathrm{fm}^{-3}$). Subsequently, relativistic calculations based on effective Lagrangian models for hot, but neutrino-poor neutron star matter were performed by Horowitz and Wehrberger [27]. The neutral current differential cross sections were calculated using linear response theory and mean free paths were found to be factors of $1.5 - 2$ times that for noninteracting nucleons. In the case of charged current interactions, the effects of interactions have been considered by Sawyer [10] for nondegenerate matter and by Goodwin and Pethick [18] for degenerate matter.

Schinder's exact results for noninteracting nucleons are expressed in terms of a lengthy series of Fermi integrals. We have found, however, a simplification to Schinder's results that not only expresses them in numerically simpler fashion as Polylogarithmic functions, but are

also easily generalized to the case of interacting matter. In contrast to previous work, we calculate both neutral and charged current opacities including effects of interactions arising from the underlying EOS.

Another aspect of opacities which recent work has emphasized concerns the importance of including the multi-component nature of dense matter on neutrino opacities. Prakash *et. al.* [28], and Reddy and Prakash [29,33] have identified neutrino-hyperon absorption and scattering reactions as being important new sources of opacity. These include absorption involving the Λ and Σ^- hyperons and scattering involving the Σ^- hyperon. These could play important roles in calculations of the neutrino signature of an evolving protoneutron star with hyperons [8].

In this paper, we perform neutrino opacity calculations for interacting matter of arbitrary degeneracy and composition at supra-nuclear densities. Interactions between the leptons are negligible and will be ignored. Strong interactions between the baryons, however, significantly alter the energy spectra from their noninteracting forms, especially at high density. One of our objectives is to explore the extent to which interactions among the baryons affect the neutrino cross sections. We will separately consider potential models that are inherently nonrelativistic and relativistic field-theoretical models. Appendices A and B consider the formulation of these models in some detail. We also include effects due to the multicomponent nature of interacting matter and the possible presence of strangeness in the form of hyperons. Where possible, we provide analytical expressions for both charged and neutral current differential scattering cross sections for a given EOS at a fixed density, temperature and lepton concentration for given incoming neutrino energy and scattering angle. The most detailed transport codes [2], which solve the full Boltzmann transport equation, require differential cross sections. However, simpler transport methods [4–8] only need angle and/or energy averaged opacities, which can be usually expressed in the form of mean free paths. In this paper, to facilitate comparisons between our results and those involving various approximations, we present numerical results for mean free paths, leaving for subsequent publications detailed results for the general opacities. In particular, we present results for mean free paths for thermodynamic conditions relevant to the evolution of protoneutron stars.

The paper is organized as follows. In Sec. II, we summarize the basic relations needed to calculate both absorption and scattering opacities in hot and dense matter. We will consider in Sec. III the idealized situation in which the baryons are treated as nonrelativistic, the leptons are assumed to be massless, and the baryon-baryon interactions are neglected. In this case, the baryon energy spectra has the form $E = p^2/2M$. Our results lead naturally to previously obtained limiting cases such as the degenerate, nondegenerate, and elastic approximations. We will next consider, in Sec. IV, the nonrelativistic Skyrme-like potential model [34], in which the spectrum is given by $E = p^2/2M^* + U_{NR}$, where U_{NR} denotes the density-dependent potential contribution and M^* is the Landau effective mass, which is also generally density dependent. Next, in Sec. V, we will consider the effective field-theoretical Walecka-type model [35] at the mean-field level in which the spectrum is $E = \sqrt{p^2 + M^{*2}} + U_R$, where M^*, the Dirac effective mass, and U_R, which accounts for interactions of the fields, are both generally density dependent. The kinetic parts in both nonrelativistic and relativistic approaches contain the effects of interactions insofar as they depend on density-dependent effective masses; further, in both cases, the momentum dependence of the

kinetic energy is formally identical to their noninteracting counterparts. The evaluation of the cross section is therefore similar to the case of noninteracting baryons for these particular models. The numerical results, however, are sensitive to the presence of interactions. In Sec. VI, we show how additional baryonic components, such as hyperons, affect the neutrino opacities. In Sec. VII, we compare our results with those of previous workers. In Sec. VIII, we apply our results to the neutrino opacities encountered in a particular astrophysical event: that of a deleptonizing and cooling protoneutron star. Finally, we summarize and provide an outlook in Sec. IX. Appendices A and B contain supporting material about the potential and field-theoretical models of dense matter.

II. NEUTRINO CROSS SECTIONS

The total opacity of dense matter to neutrinos has contributions from both neutral and charged weak currents. Neutral currents are involved in neutrino-baryon scattering while charged currents are involved in neutrino-baryon absorption reactions. We have considered neutral currents in Ref. [33], in which convenient expressions for the differential and total scattering cross sections were established. Here, we will concentrate upon deriving similar relations for the charged current absorption reactions. Further, the formalism developed here may be easily generalized to include neutral current reactions so that the present work in effect extends and replaces Ref. [33].

The neutrino energies of interest to us are less than a few hundred MeV; we may thus write the relevant interaction Lagrangian from Wienberg–Salam theory [36–38] in terms of a current–current interaction:

$$\mathcal{L}_{int}^{cc} = \frac{G_F C}{\sqrt{2}} \; l_\mu j_W^\mu \qquad \text{for} \qquad \nu_l + B_2 \to l + B_4 \tag{1}$$

$$\mathcal{L}_{int}^{nc} = \frac{G_F}{\sqrt{2}} \; l_\mu^\nu j_Z^\mu \qquad \text{for} \qquad \nu_l + B_2 \to \nu_l + B_4 \,, \tag{2}$$

where $G_F \simeq 1.436 \times 10^{-49}$ erg cm^{-3} is the Fermi weak coupling constant and the Cabibbo factor $C = \cos\theta_c$ for change of strangeness $\Delta S = 0$ and $C = \sin\theta_c$ for $\Delta S = 1$. The lepton and baryon weak charged currents are:

$$l_\mu = \overline{\psi}_l \gamma_\mu \left(1 - \gamma_5\right) \psi_\nu \,, \quad j_W^\mu = \overline{\psi}_4 \gamma^\mu \left(g_V - g_A \gamma_5\right) \psi_2 \,. \tag{3}$$

Similarly, the baryon neutral currents are given by

$$l_\mu^\nu = \overline{\psi}_\nu \gamma_\mu \left(1 - \gamma_5\right) \psi_\nu \,, \quad j_Z^\mu = \frac{1}{2} \overline{\psi}_4 \gamma^\mu \left(c_V - c_A \gamma_5\right) \psi_2 \,, \tag{4}$$

where 2 and 4 are the baryon initial state and final state labels, respectively (these are identical for neutral current reactions). Other particle labels and four-momenta P_i are as shown in Fig. 1(a) for the charged current reaction and Fig. 1(b) for the neutral current reaction. The vector and axial-vector coupling constants g_V and g_A are listed in Table I for the various charged current reactions of interest. Similarly, the couplings c_V and c_A for the neutral current reactions are listed in Table II. Generally, the μ and τ neutrino charged current reactions are kinematically suppressed; μ and τ neutrinos are thermally produced so

that their energies are of order $T << m_\mu$. On the other hand, neutral current reactions are common to all neutrino species and the neutrino-baryon coupling is independent of neutrino flavor. Neutrino coupling to leptons in the same family is modified since the scattering may proceed due to both W and Z exchange; the couplings shown in Tables I and II reflect this fact. Numerical values of the parameters that best fit data on charged current semi-leptonic decays of hyperons are [39]: D=0.756, F=0.477, $\sin^2 \theta_W$=0.23 and $\sin \theta_c = 0.231$. Note that the amplitude for the strangeness changing charged current is suppressed by the factor $\sin \theta_c$. These couplings follow from SU(3) flavor symmetry for the baryons and the quark model. Corrections arising due to explicit $SU(3)$ breaking terms have been recently investigated [40] and in some cases are about 10-30%.

The cross section per unit volume of matter (or equivalently the inverse collision mean free path) may be derived from Fermi's golden rule and is given by

$$
\frac{\sigma(E_1)}{V} = 2 \int \frac{d^3 p_2}{(2\pi)^3} \int \frac{d^3 p_3}{(2\pi)^3} \int \frac{d^3 p_4}{(2\pi)^3} \, (2\pi)^4 \delta^4(P_1 + P_2 - P_3 - P_4) \, W_{fi}
$$
$$
\times \, f_2(E_2)(1 - f_3(E_3))(1 - f_4(E_4)) \,, \tag{5}
$$

where $P_i = (E_i, \vec{p}_i)$ denotes the four-momentum of particle i (particle labels are as shown in Fig. 1(a)) and the transition rate W_{fi} is

$$
W_{fi} = \frac{< |\mathcal{M}|^2 >}{2^4 E_1 E_2 E_3 E_4} \,. \tag{6}
$$

Above, $|\mathcal{M}|^2$ is the squared matrix element and the symbol $< \cdot >$ denotes a sum over final spins and an average over the initial spins. A common expression for both scattering and absorption may be written:

$$
\begin{aligned}
W_{fi} = G_F^2 \quad &\left[(\mathcal{V} + \mathcal{A})^2 (1 - v_2 \cos \theta_{12})(1 - v_4 \cos \theta_{34}) \right. \\
&+ \, (\mathcal{V} - \mathcal{A})^2 (1 - v_2 \cos \theta_{23})(1 - v_4 \cos \theta_{14}) \\
&- \left. (\mathcal{V}^2 - \mathcal{A}^2) \frac{M^2}{E_2 E_4} (1 - \cos \theta_{13}) \right],
\end{aligned} \tag{7}
$$

where the vector and axial couplings $\mathcal{V}$ and $\mathcal{A}$, in the case of absorption, stand for Cg_V and Cg_A, respectively. For the reactions of interest, g_v and g_A are listed in Table I. Similarly, for the scattering reactions of interest, $\mathcal{V}$ and $\mathcal{A}$ stand for $c_V/2$ and $c_A/2$, respectively, which are listed in Table II. The particle velocities are denoted by $v_i = p_i/E_i$, and the angle between the momentum vectors $\vec{p}_i$ and $\vec{p}_j$ is denoted by θ_{ij}. Further, M is the bare nucleon mass. The functions $f_i(E_i)$ in Eq. (5) denote the particle distribution functions, which in thermal equilibrium are given by the Fermi-Dirac functions

$$
f_i(E_i) = \left[1 + \exp\left(\frac{E_i - \mu_i}{T} \right) \right]^{-1}, \tag{8}
$$

where E_i are the single particle energies, μ_i are the corresponding chemical potentials, and T is the temperature.

In general, the single particle energies and chemical potentials depend on the ambient matter conditions, i.e., the density and temperature, and also on the interactions among the

various particles. The various chemical potentials are determined by the conditions of charge neutrality and, in all but the most extremely dynamical situations, chemical equilibrium. In some astrophysical situations, such as in the late stages of core collapse and during the early stages of the evolution of a protoneutron star, neutrinos are trapped on dynamical times within the matter [41,42] and chemical equilibrium is established among the baryons and leptons. In this case, the chemical potentials satisfy the relation

$$\mu_{B_2} - \mu_{B_4} = \mu_e - \mu_{\nu_e}. \tag{9}$$

These situations are characterized by a trapped lepton fraction $Y_L = Y_e + Y_{\nu_e}$, where $Y_e = (n_e - n_{e^+})/n_B$ and $Y_{\nu_e} = (n_{\nu_e} - n_{\overline{\nu}_e})/n_B$ are the net electron and neutrino fractions, respectively. The evolution of a protoneutron star begins from a neutrino-trapped situation with $Y_L \approx 0.4$ to one in which the net neutrino fraction vanishes and chemical equilibrium without neutrinos is established. In this case, the chemical equilibrium is modified by setting $\mu_{\nu_e} = 0$. In all cases, the condition of charge neutrality requires that

$$\sum_i \left(n_{B_i}^{(+)} + n_{\ell_i}^{(+)} \right) = \sum_i \left(n_{B_i}^{(-)} + n_{\ell_i}^{(-)} \right), \tag{10}$$

where the superscript's ($\pm$) on the number densities n signify positive or negative charge.

Although neutrino opacities are required for a wide range of densities, temperatures, and compositions, for the most part we will display results for two limiting situations, namely beta equilibrium matter with either $Y_L = 0.4$ or $Y_\nu = 0$. These are situations encountered in the evolution of a protoneutron star [43], as discussed further in Sec. VII.

III. NONRELATIVISTIC NONINTERACTING BARYONS

For baryon densities $n_B \leq 5n_0$, where $n_0 = 0.16 \text{ fm}^{-3}$ is the empirical nuclear equilibrium density, and in the absence of interactions which could significantly alter their effective masses, baryons may be considered as nonrelativistic. The expression for W_{fi} in Eq. (7) then simplifies considerably, since the baryon velocities $v_i \ll 1$. In this case, the terms involving the baryon velocities may be safely neglected. However, the term involving the angle between the initial and final leptons remains. For reactions involving nucleons, this term gives a small contribution, since it is proportional to $\mathcal{V}^2 - \mathcal{A}^2$. For simplicity, and to make an apposite comparison with earlier results in which this term was also neglected, we drop this term in this section, but will return to a more complete analysis in the succeeding sections.

Under these conditions, the transition rate W_{fi} becomes a constant,

$$W_{fi} = G_F^2(\mathcal{V}^2 + 3\mathcal{A}^2), \tag{11}$$

independent of the momenta of the participating particles, and the differential cross section is given by

$$\frac{1}{V}\frac{d^3\sigma}{d^2\Omega \, dE_3} = \frac{G_F^2}{2\pi}(\mathcal{V}^2 + 3\mathcal{A}^2)(1 - f_3(E_3))S(q_0, q), \tag{12}$$

6

where the three-momentum transfer $\vec{q} = \vec{p_1} - \vec{p_3}$, so that $q = |\vec{q}|$, and the energy transfer $q_0 = E_1 - E_3$. The function $S(q_0, q)$, the so-called dynamic form factor or structure function, characterizes the isospin response of the (nonrelativistic) system. It is simply the total phase space available to transfer energy q_0 and momentum q to the baryons. We note that the differential cross section is needed in multi-energy group neutrino transport codes. However, more approximate neutrino transport algorithms often only require the total cross section as a function of the neutrino energy. The cross section per unit volume given in Eq. (5) then simplifies to

$$\frac{\sigma(E_1)}{V} = G_F^2(\mathcal{V}^2 + 3\mathcal{A}^2) \int \frac{d^3 p_3}{(2\pi)^3} \left(1 - f_3(E_3)\right) S(q_0, q), \tag{13}$$

$$S(q_0, q) = 2 \int \frac{d^3 p_2}{(2\pi)^3} \int \frac{d^3 p_4}{(2\pi)^3} (2\pi)^4 \delta^4(P_1 + P_2 - P_3 - P_4) f_2(E_2)(1 - f_4(E_4)), \tag{14}$$

The total cross section given by Eq. (13) can be recast as a double integral in (q_0, q) space using $d^3 p_3 = 2\pi q(E_3/E_1) \, dq_0 dq$. Since E_3 ranges between 0 and ∞, the limits of q_0 are $-\infty$ and E_1. The limits of q are obtained by inspecting the relation $q^2 = E_1^2 + E_3^2 - 2E_1 E_3 \cos\theta_{13}$ for $\cos\theta_{13} = \pm 1$. Thus, $|q_0| < q < 2E_1 - q_0$. One finds

$$\frac{\sigma(E_1)}{V} = \frac{G_F^2}{4\pi^2}(\mathcal{V}^2 + 3\mathcal{A}^2) \int_{-\infty}^{E_1} dq_0 \, \frac{E_3}{E_1}(1 - f_3(E_3)) \int_{|q_0|}^{2E_1 - q_0} dq \, qS(q_0, q). \tag{15}$$

This, of course, applies to both scattering and absorption with appropriate changes of particle labels and coupling constants.

The integrals in Eq. (14) can be performed analytically and the result expressed in closed form for the noninteracting case and for certain models of interacting matter. The integral over the final state momentum p_4 in Eq. (14) may be performed by exploiting the momentum delta function to obtain

$$S(q_0, q) = \frac{1}{2\pi^2} \int d^3 p_2 \, \delta(q_0 + E_2 - E_4) f_2(E_2)(1 - f_4(E_4)). \tag{16}$$

We note that $E_4 = (\vec{p_2} + \vec{q})^2/2M$, and we ignore the difference between M_2 and M_4 as it is small compared to other energy scales at high density for noninteracting matter. We may rewrite the energy delta function in terms of the angle between $\vec{p_2}$ and $\vec{q}$:

$$\delta(q_0 + E_2 - E_4) = \frac{M}{p_2 q}\delta(\cos\theta - \cos\theta_0)\Theta(p_2^2 - p_-^2), \tag{17}$$

where

$$\cos\theta_0 = \frac{M}{p_2 q}\left(q_0 - \frac{q^2}{2M}\right), \quad p_-^2 = \frac{M^2}{q^2}\left(q_0 - \frac{q^2}{2M}\right)^2 \tag{18}$$

and $\Theta(x) = 1$ for $x \geq 0$ and zero otherwise. Substituting these results in Eq. (16) and performing the angular integrals we obtain

$$S(q_0, q) = \frac{M}{\pi q} \int_{p_-}^{\infty} dp_2 \, p_2 \, f_2(E_2) \, (1 - f_4(E_4)). \tag{19}$$

7

The remaining p_2 integral is performed by using the relation

$$\int \frac{dx}{1 + \exp(x)} \frac{1}{1 + \exp(-x - z)} = -\frac{1}{1 - \exp(-z)} \ln \frac{1 + \exp(x)}{1 + \exp(x + z)}. \tag{20}$$

Thus, the free gas isospin density response function is given by

$$S(q_0, q) = \frac{M^2 T}{\pi q} \left[\frac{z}{1 - \exp(-z)} \left(1 + \frac{\xi_-}{z} \right) \right], \tag{21}$$

where

$$z = \frac{q_0 + \hat{\mu}}{T}, \quad \hat{\mu} = \mu_2 - \mu_4,$$

$$\xi_- = \ln \left[\frac{1 + \exp((e_- - \mu_2)/T)}{1 + \exp((e_- + q_0 - \mu_4)/T)} \right], \quad e_- = \frac{p_-^2}{2M} = \frac{1}{4} \frac{(q_0 - q^2/2M)^2}{q^2/2M}. \tag{22}$$

This result generalizes a result obtained earlier for noninteracting symmetric nuclear matter [44], in which $\hat{\mu} = 0$, to the case of asymmetric nuclear matter for conditions of arbitrary degeneracy. This result, which we further generalize to include nuclear interactions in the next section, proves to be the key to being able to efficiently calculate opacities. These results are easily specialized to the case of scattering by noting that particle labels 2 and 4 are identical; thus $\mu_2 = \mu_4$. The integrals in Eq. (15), even with an analytical expression for $S(q_0, q)$, require numerical evaluation; closed form expressions for arbitrary degeneracy cannot be obtained. However, in some limiting cases these integrals become analytic and correspond to results obtained earlier and which are often used in astrophysical simulations.

Highly Degenerate Baryons $(\mu_i/T \gg 1)$: In this situation, the participating particles all lie close to their respective Fermi surfaces. In this case, the q integration may be performed trivially, since the factor $(1 + \xi_-/z)$ may be replaced by $\Theta(\mu_2 - e_-)$ or, equivalently, $\Theta(q - (p_{F_2} - p_{F_4}))$, where $\Theta(x) = 1$ for $x \geq 0$ and zero otherwise. The integral to be performed is then

$$I_q = \int_{|q_0|}^{2E_1 - q_0} dq \, \Theta(q - (p_{F_2} - p_{F_4})) \cong \int_{|\hat{\mu}|}^{2E_1 + \hat{\mu}} dq \, \Theta(q - (p_{F_2} - p_{F_4})), \tag{23}$$

where in writing the rightmost relation, we have set $q_0 = -\hat{\mu}$, since the exponentials in the q_0 integral are highly peaked at this value at low temperature. Thus,

$$I_q = \begin{cases} 2E_1 \Theta(\hat{\mu} - (p_{F_2} - p_{F_4})) & : \quad \text{for} \ \hat{\mu} > p_{F_2} - p_{F_4} \\ (2E_1 - \hat{\mu} - p_{F_2} + p_{F_4})\Theta(2E_1 - \hat{\mu} - p_{F_2} + p_{F_4}) & : \quad \text{for} \ \hat{\mu} \leq p_{F_2} - p_{F_4} \end{cases} \tag{24}$$

The upper limit on the remaining q_0 integral can be replaced by $+\infty$ since the integrand vanishes exponentially for positive values of q_0 due to final state Pauli blocking of the electron degeneracy. With this substitution, it is straighforward to perform the q_0 integral by noting that

$$\int_{-\infty}^{+\infty} dz \frac{z}{1 - \exp(-z)} \frac{1}{1 + \exp(z + \eta)} = \frac{1}{2} \left[\frac{\pi^2 + \eta^2}{1 + \exp(\eta)} \right]. \tag{25}$$

8

The final result for the cross section per unit volume in the degenerate approximation is given by

$$\frac{\sigma(E_1)}{V} = \frac{G_F^2}{4\pi^3}(\mathcal{V}^2 + 3\mathcal{A}^2)M^2 T^2 \Xi \left(E_1 + \hat{\mu}\right) \left[\pi^2 + \left(\frac{E_1 - \mu_1}{kT}\right)^2\right] \frac{1}{1 + \exp\left((\mu_1 - E_1)/T\right)}$$

$$\text{with} \quad \Xi = \Theta(p_{F_4} + p_{F_3} - p_{F_2} - p_{F_1})$$

$$+ \frac{p_{F_4} + p_{F_3} - p_{F_2} + p_{F_1}}{2E_1} \, \Theta(p_{F_1} - |p_{F_4} + p_{F_3} - p_{F_2}|) \,. \tag{26}$$

In the above expression all terms proportional to T/μ_i are neglected as they are small. Further, if we were to assume that the incoming neutrino energy E_1 were equal to the neutrino chemical potential, the factor $(E_1 + \hat{\mu})$ could be replaced by μ_e. With this substitution, the above result coincides exactly with that derived earlier by Sawyer and Soni [15].

In the case of scattering, this expression simplifies to

$$\frac{\sigma(E_1)}{V} = \frac{G_F^2}{16\pi^3}(c_V^2 + 3c_A^2)M^2 T^2 E_1 \left[\pi^2 + \left(\frac{E_1 - \mu_1}{kT}\right)^2\right] \frac{1}{1 + \exp((\mu_1 - E_1)/T)} \,. \tag{27}$$

An analogous result was derived earlier by Iwamoto and Pethick [17].

Note that the energy e_- arises due to the kinematical condition that ensures three-momentum conservation. For $e_- \gg \mu_2$, in the degenerate limit, the phase space rapidly vanishes. Thus, at low temperatures, this leads to the condition

$$q \geq |p_{F_2} - p_{F_4}| \,, \tag{28}$$

which is the threshold condition for the so-called direct Urca process [45]. Note that the maximum possible momentum transer is $q = E_1 + p_{F_3}$. For a free gas in beta equilibrium with zero neutrino chemical potential, the condition in Eq. (28) is usually not satisfied, since the neutron Fermi momenta are usually much larger than those of protons and electrons. In contrast, in the case when neutrinos are trapped, significantly larger proton fractions are favored in beta equilibrium condition. This enables the threshold condition to be easily fulfilled. Similarly, strong interactions also tend to increase the proton fraction, which in some cases allows Eq. (28) to be satisfied even in the vicinity of nuclear densities [45]. The factor $1 + \xi_-/z$ naturally accounts for the threshold-like behavior with decreasing temperature.

Nondegenerate matter $(\mu_i/T \ll -1)$: In the nondegenerate limit, one has

$$z\left(1 + \frac{\xi_-}{z}\right) = z + \xi_- \cong \exp\left(\frac{\mu_2 - e_-}{T}\right) \left[1 - \exp(-z)\right] \tag{29}$$

after expanding the logarithmic terms in Eq. (22) to leading order. Thus, $S(q_0, q) \simeq (M^2 T/\pi q)\exp((\mu_2 - e_-)/T)$. Assuming further that the effects due to final state Pauli blocking may be neglected and the relevant energy transfer is small, $q_0 \ll E_1$, one finds

$$\frac{\sigma(E_1)}{V} = \frac{G_F^2(\mathcal{V}^2 + 3\mathcal{A}^2)M^2 T}{4\pi^3} \exp\left(\frac{\mu_2}{T}\right) \int_{-\infty}^{E_1} dq_0 \int_0^{2E_1} dq \, \exp\left(-\frac{e_-}{T}\right) \tag{30}$$

In this case, the q_0 integration may be performed first. To leading order in q and T/M the result is $q(2\pi T/M)^{1/2}$. The remaining q integration is elementary and we obtain

9

$$\frac{\sigma(E_1)}{V} = \frac{G_F^2}{\pi}(\mathcal{V}^2 + 3\mathcal{A}^2)E_1^2 \, n_2 \,, \tag{31}$$

where $n_2 = 2(MT/2\pi)^{3/2} \, \exp(\mu_2/T)$ is the neutron number density in the nondegenerate limit. In this limiting situation, the total cross section is simply that on a single baryon times the baryon number density [9].

The Elastic Approximation: We can also derive the result of the so-called elastic approximation [2], in which it is assumed there is no energy or momentum transfer to the nucleons. The effects of final state Pauli blocking and nucleon degeneracy are still fully included. In this case, the cross section may be obtained by considering the response function for $q_0 \to 0$ and $q \to 0$:

$$S(q_0 \to 0, q \to 0) = 2\pi\delta(E_1 - E_3) \int \frac{d^3p_2}{(2\pi)^3} \, f_2(E_2)(1 - f_4(E_2))$$

$$= 2\pi\delta(q_0)\frac{n_2 - n_4}{1 - \exp((\mu_4 - \mu_2)/T)} \,, \tag{32}$$

where n_2 and n_4 are the number densities of species 2 and 4, respectively. In obtaining this result, the identity

$$f_2(E_2)(1 - f_4(E_2)) = \frac{f_2(E_2) - f_4(E_2)}{1 - \exp((\mu_4 - \mu_2)/T)} \tag{33}$$

was used. One then finds

$$\frac{\sigma(E_1)}{V} = \frac{G_F^2}{\pi}(\mathcal{V}^2 + 3\mathcal{A}^2) \ \frac{n_2 - n_4}{1 - \exp((\mu_4 - \mu_2)/T)} \ E_1^2 \, (1 - f_3(E_1)) \,. \tag{34}$$

To specialize this result to the case of scattering, we need to take the limit $(\mu_2 - \mu_4) \to 0$:

$$\frac{\sigma(E_1)}{V} = \frac{G_F^2}{4\pi}(c_V^2 + 3c_A^2) \left.\frac{\partial n_2}{\partial(\mu_2/T)}\right|_T E_1^2 \, (1 - f_3(E_1)) \,. \tag{35}$$

We now present some results for noninteracting matter containing nucleons, electrons, and trapped neutrinos for n_B and T chosen to lie in the range $(0.25-5)n_0$ and $(5-60)$ MeV, respectively. For the beginning of the evolution of a nascent neutron star, it is appropriate to consider the neutrino trapped case in which the electron lepton fraction $Y_L = Y_e + Y_{\nu_e}$ is held fixed at 0.4. At later times the neutrino chemical potential vanishes and the matter contains thermally produced pairs; under these circumstances, Y_{ν_e} and μ_{ν_e} vanish and $Y_L = Y_e$ is determined by charge and chemical equilibrium.

Fig. 2 shows the composition and the chemical potentials versus the density (in units of the nuclear equilibrium density n_0) for $T = 5, 30$, and 60 MeV for the neutrino-trapped case. The major effect of trapping is to keep the electron concentration high so that matter is more proton rich in comparison to the case in which neutrinos do not carry net lepton number; thus the threshold conditon for the charged current rate is easily satisfied for all relevant densities and temperatures of interest. There is little variation in the individual concentrations with either density or temperature. The individual chemical potentials and

10

$\hat{\mu} = \mu_n - \mu_p$ increase significantly with density, but are relatively insensitive to variations in temperature as leptons are degenerate except at the lowest densities.

In the neutrino-trapped case, in which the neutrinos are degenerate, Pauli blocking ensures that the transport processes involve only neutrinos close to the Fermi surface. Thus it is appropriate to calculate the neutrino mean free path for a neutrino energy given by $E_1 = \mu_{\nu_e}$. The neutrino absorption mean free path, $\lambda = (\sigma/V)^{-1}$, is shown in Fig. 3, as solid lines for temperatures $T = 5, 30$, and 60 MeV as a function of density. As expected, the mean free path decreases with increasing density since μ_e increases with density. For comparison, we also show the results of the three limiting expressions for the extremely degenerate (Eq. (26), dashed curve), nondegenerate (Eq. (31), dot-dashed curve), and elastic (Eq. (34), long dashed curve) approximations. It is evident that, for the densities and temperatures of interest to us, it is essential to include Pauli blocking of the final state electrons to obtain reliable results. This is chiefly due to the fact that electrons are degenerate. When all participating particles are extremely degenerate, Eq. (26) provides an excellent approximation to the exact result. The failure of the elastic approximation in this regime is related to the fact that the favored energy transfer is not zero as is assumed, but $q_0 = -\hat{\mu}$, which is generally large in magnitude. At high temperatures and relatively low density, in which the nucleons are not extremely degenerate, the cross section in Eq. (34), based on the elastic approximation, reasonably reproduces the exact results. As expected, the nondegenerate approximation is only realistic for extremely low densities.

Similarly, we have calculated the mean free path due to scattering reactions assuming $E_1 = \mu_{\nu_e}$, and these are compared with the charged current results in Fig. 4 for $T = 10$ MeV as a function of density. The total scattering opacity, which has contributions from neutrons (dashed curve), protons (dot-dashed curve), and electrons (dot-long dashed curve), is shown as the long-dashed curve labelled λ_S. The results for electron scattering are actually taken from the relativistic formulation presented in Sec. V; they cannot be evaluated from the nonrelativistic formulation in this section because the electrons are highly relativistic. In the right panel, the ratio of scattering mean free path to that of the absorption mean free path is plotted. The solid curve is the ratio of the total scattering mean free path to that of the absorption mean free path, the dashed curve is the ratio of the mean free due to the reaction $\nu_e + n \rightarrow \nu_e + n$ to that of absorption. $\nu_e + n \rightarrow e^- + p$. Clearly, the scattering mean free path is dominated by neutrons since the electron and proton fractions are small. However, the net electron-neutrino mean free path in the trapped regime is dominated by the absorption reaction, for two reasons. First, the charged current matrix element is four times larger and second, the rate is proportional to μ_e while the scattering rate is proportional to μ_{ν_e}.

In the neutrino-free case $(Y_{\nu_e} = 0)$, neutrinos still exist, but as pairs and do not carry net lepton number. Thus the reference to this phase as neutrino-free is somewhat misleading. Fig. 5 shows the composition and the chemical potentials. Compared to the neutrino-trapped case, Fig. 2, matter contains a smaller proton fraction. Consequently, the difference between the neutron Fermi momentum and proton (and electron) Fermi momenta are large, making simultaneous energy and momentum conservation impossibile. Thus, at low temperatures for all densities shown, neutrino absorption due the reaction $\nu + n \rightarrow e^- + p$ is kinematically suppressed and is unimportant; the dominant absorption rates are those due to the modified Urca reaction $\nu + n + X \rightarrow p + X + e^-$ where X is a bystander particle. The modified Urca reaction, however, gives a small contribution to the total opacity when compared with the

total scattering opacity and can be neglected. Although the direct reaction $(\nu + n \rightarrow e^- + p)$ is kinematically forbidden at zero temperature, it exhibits a strong temperature dependance. We also note, as can be seen in Fig. 5, that beta-equilibrium and charge neutrality favors a larger proton fraction at higher temperatures, which enhances the importance of the direct process. In this sense, finite temperature effects on the neutrino absorption reaction are similar to those encountered due to the presence of a finite neutrino chemical potential. It increases both the neutrino energy and the proton fraction so as to simultaneously fulfill momentum and energy conservation.

In Fig. 6, we plot the neutrino mean free path for neutrino-free matter with $Y_{\nu_e} = 0$. Because the neutrinos are thermal, we choose $E_1 = 3T$ as the relevant energy for calculating the mean free path. At low temperatures, the neutrino absorption mean free paths are very large and increase with density as matter becomes increasingly degenerate. For higher temperatures, this behaviour is not seen and the larger neutrino energy and a higher proton fraction both ensure that momentum and energy conservation for the direct reaction are easily satisfied. The extent to which the elastic and nondegenerate approximations reproduce the exact numerical results may be gauged from Fig. 6. Note that the degenerate approximation is not an appropriate limit because when the theta functions in Eq. (26) are zero causing the mean free paths to be infinite; thus the degenerate limit is not plotted in this case.

From Fig. 6 we see that the absorption rate shows a strong temperature dependance. In Fig. 7, we show the temperature dependance of the absorption and scattering mean free paths at nuclear saturation density. The individual scattering contributions are shown in the left panel together with the total scattering mean free path, which is shown as the long dashed curve. For this density, the scattering opacity is dominated by neutron scattering. The right panels show the ratio of the total scattering mean free path to that of the absorption reaction $\nu + n \rightarrow e^- + p$. For low temperatures, where the absorption is kinematically suppressed, scattering dominates the net opacity. However, with increasing temperature, absorption increases and eventually dominates for $T \geq 10$ MeV.

IV. NONRELATIVISTIC INTERACTING BARYONS

We turn now to the effects of strong interactions on the charged and neutral current neutrino cross sections. To begin, we will continue to use the nonrelativistic approximation for baryons. Nonrelativistic potential model descriptions of dense matter are based on a two-body potential fitted to nucleon-nucleon scattering and a three-body term whose form is suggested by theory and whose parameters are determined by the binding of few-body nuclei and the saturation properties of nuclear matter (see for example, Ref. [46]). However, microscopic calculations of this type which encompass asymmetric matter at an entropy/baryon in the range $s = 1 - 2$ are not yet available. We therefore use a schematic potential model [47], which is designed to reproduce the results of more microscopic calculations of both symmetric and neutron matter at zero temperature and which can be extended to asymmetric matter at finite temperature. In addition to employing local contact interactions, momentum dependent interactions arising from finite range exchange forces can also be considered in such an approach. The relevant details are given in Appendix A.

The calculation of the neutrino opacities is greatly simplified if the finite range interactions are approximated by effective local interactions. A notable feature of this approximation is that the particle effective masses generally drop more rapidly with increasing density compared to the case in which the full nonlocality is retained. In this case, one retains only a quadratic momentum dependence in the single particle spectrum, so that it takes a form (*cf.* Appendix A) closely resembling that of a free gas:

$$E_i(p_i) = \frac{p_i^2}{2M_i^*} + U_i, \quad i = n, p. \tag{36}$$

Both the single particle potentials U_i and the (Landau) effective masses M_i^* are density dependent. Because the functional dependence of the spectra on the momenta is identical to that of the noninteracting case, the methods employed in the previous section are amenable to the incorporation of the effects of strong interactions. However, it is important now to retain the distinction between the masses of the nucleons, in particular the effective masses, M_2^* and M_4^*.

The dynamic form factor in Eq. (14), with the single particle spectrum in Eq. (36), may be expressed in essentially the same functional form as in Eq. (21). The energy delta function can be recast in terms of the angle between $\vec{p_2}$ and $\vec{q}$:

$$\delta(q_0 + E_2 - E_4) = \frac{M_4^*}{p_2 q} \delta(\cos\theta - \cos\theta_0) \, \Theta(E_2 - e_-)\Theta(e_+ - E_2), \tag{37}$$

where

$$\cos\theta_0 = \frac{M_4^*}{p_2 q}\left(c - \frac{\chi p_2^2}{2M_4^*}\right), \quad p_\pm^2 = \frac{2q^2}{\chi^2}\left[\left(1 + \frac{\chi M_4^* c}{q^2}\right) \pm \sqrt{1 + \frac{2\chi M_4^* c}{q^2}}\right],$$

$$E_2 = \frac{p_2^2}{2M_2^*}, \quad e_\pm = \frac{p_\pm^2}{2M_2^*}, \tag{38}$$

where the new variables appearing above are defined by the relations

$$\chi = 1 - \frac{M_4^*}{M_2^*}, \quad c = q_0 + U_2 - U_4 - \frac{q^2}{2M_4^*}. \tag{39}$$

The factor $U_2 - U_4$ is the potential energy gained in converting a particle of species "2" to a particle of species "4". When the intial and final state baryon masses are different, the p_2 integration is restricted to the interval $p_+^2 \geq p_2^2 \geq p_-^2$. Note also that the effective chemical potential $\mu_2 - U_2$ replaces μ_2. With these changes, the response function incorporates the effects of strong interactions at the mean field level. We can now generalize the definition of ξ_-, which appears in the noninteracting response function, with $\xi_\pm$:

$$\xi_\pm = \ln\left[\frac{1 + \exp((e_\pm - \mu_2 + U_2)/T)}{1 + \exp((e_\pm + q_0 - \mu_4 + U_2)/T)}\right]. \tag{40}$$

Collecting these modifications together, and using the relation in Eq. (20), we have

$$S(q_0, q) = \frac{M_2^* M_4^* T}{\pi q} \frac{\xi_- - \xi_+}{1 - \exp(-z)}. \tag{41}$$

13

For the charged current, modifications due to interactions are twofold. First, the difference in the neutron and proton single particle potentials appears in the response function and also in $\hat{\mu}$. Second, the response depends upon the nucleon effective mass. Since both U_i and M_i^* are strongly density dependent, the opacities are significantly altered from those for the noninteracting case at high density.

Finally, note that we can make the nondegenerate, elastic, and degenerate approximations in analogy to those found for the noninteracting case. The expression for the degenerate approximation is nearly indentical to that for the noninteracting case, because the condition $e_- \geq \mu_2 - U_2$ is equivalent to $q \geq |p_{F_2} - p_{F_4}|$. We must only replace M^2 in Eq. (26) by $M_2^* M_4^*$. The expression for the nondegenerate approximation is identical to that for the noninteracting case (Eq. (31)), because for nondegenerate nucleons, the number density is proportional to $(M_2^* T)^{3/2} \exp((\mu_2 - U_2)/T)$. Finally, in the elastic case, we need only replace $\mu_4 - \mu_2$ in Eq. (34) with $\mu_4 - \mu_2 + U_2 - U_4$.

For the neutral currents, since the initial and final state particle labels are identical for both leptons and baryons, we have the simplifications

$$z = \frac{q_0}{T}, \quad \mu_2 = \mu_4, \quad e_- = \frac{M_2^*}{2q^2}\left(q_0 - \frac{q^2}{2M_2^*}\right)^2, \quad e_+ = \infty. \tag{42}$$

Thus, $\xi_+ = -z$, and one finds a result formally similar to the noninteracting expression:

$$S(q_0, q) = \frac{M_2^{*2} T}{\pi q}\left[\frac{z}{1 - \exp(-z)}\left(1 + \frac{\xi_-}{z}\right)\right]. \tag{43}$$

Fig. 8 shows the composition and the chemical potentials versus the density for charge-neutral matter containing interacting nucleons, electrons, and trapped neutrinos in beta equilibrium. While these results are qualitatively similar to the case of noninteracting nucleons, interactions lead to lower values of Y_{ν_e} and μ_{ν_e}, and larger values of $\hat{\mu}$, especially at high densities. The influence of these changes on the neutrino mean free paths are depicted in Fig. 9, using $E_1 = \mu_{\nu_e}$ as before for the trapped-neutrino case, and the dynamic form factor Eq. (41). Shown for comparison are the three limiting behaviors for the degenerate, nondegenerate, and elastic approximations discussed in connection with the noninteracting case.

The counter-intuitive result, that the mean free paths increase at high density, is chiefly due to the use of nonrelativistic kinematics coupled with the behavior of the Landau effective mass of the nucleons, which are displayed in Fig. 10. The cross section is proportional to $M_2^* M_4^*$, and the dropping effective masses more than compensate for the higher neutrino chemical potential at high densities. However, the net effect of a decreasing cross section at high density may be an anomalous result of using a nonrelativistic theory in a situation in which the nucleons are at least partially relativistic. This also explains why the elastic approximation, which is applicable in the case when the mass of the absorber is large, provides a much poorer representation of the exact results than in the noninteracting situation. Related to this is the fact that the high density behavior of the nonrelativistic Skyrme-like EOS becomes dominated by the $u^{8/3}$ density-dependence in the energy density. This leads to eventual acausality, i.e., the speed of sound exceeds the speed of light. While it is possible to avoid this behavior in nonrelativistic potential model approaches by including more general

14

forms of momentum dependence (see for example, Ref. [48]), a nonrelativistic description of matter at very high densities is difficult to justify at a fundamental level. In addition, the calculation of the opacity is then greatly complicated by the fact that the energy spectrum no longer resembles that of a free gas. In the next section, we consider field-theoretical models with relativistic kinematics which do not have the above problems.

In the neutrino-free case, interactions change the composition significantly. The proton fraction is larger when compared with the neutrino-free noninteracting case. Quantitatively, the proton fraction is sensitive to the density dependence of the symmetry energy, which for the Skyrme interaction we chose is nearly linearly increasing with density. The composition and chemical potentials are shown in Fig. 11. We shall first focus on the charged current reaction. At zero temperature, the direct Urca reaction $\nu + n \rightarrow e^- + p$ is kinematically possible for low energy neutrinos at and above a threshold density when the proton fraction exceeds $1/9$ [45]. In the presence of muons, the proton fraction at threshold density is slightly larger. The threshold density for the model chosen here occurs at $n = 1.5n_0$ (for a free gas, by comparison, the threshold density is $n = 73n_0$!).

In Fig. 12 the neutrino mean free paths are calculated for the neutrino-free case. At low temperature, the absorption mean free path increases sharply below the threshold density $(1.5n_0)$. The mean free paths show similar behavior to that of the neutrino-trapped case shown in Fig. 9, although in general they are about 3 times smaller. This factor can largely be understood by examining the last three terms in the noninteracting expression Eq. (26). In the neutrino-trapped case in which $E_1 \approx \mu_\nu$ these terms yield $\mu_e(Y_L = 0.4)\pi^2/2$. In the neutrino-free case in which $\mu_\nu = 0$ and $E_1 = 3T$, these terms yield $\mu_e(Y_\nu = 0)(\pi^2 + 9)$. The ratio of these two cases is thus approximately $\mu_e(Y_L = 0.4)/4.5\mu_e(Y_\nu = 0) \simeq 0.3$ using values for μ_e from Figs. 8 and 11.

V. RELATIVISTIC INTERACTING BARYONS

At several times the nuclear equilibrium density n_0, the Fermi momentum and effective nucleon mass are both expected to be comparable. Thus, a relativistic description may be more appropriate. Relativistic local quantum field-theoretical models of finite nuclei and infinite nuclear matter have had some success [35], albeit with rather more schematic interactions and with less sophisticated approximations than their nonrelativistic counterparts. Appendix B contains a description of this approach in which the set of baryons B has been augmented to include strangeness-bearing hyperons.

The usual starting point for relativistic field theory calculations is the mean-field approximation. In this approximation, the presence of baryons generates nonzero average values of the meson fields. Baryons move independently in these self-consistently generated mean fields. In a model of baryons Yukawa coupled to vector (ω_μ), isovector (b_μ) and scalar (σ) mesons, the latter simulating correlated pion-exchange, the single particle energies are

$$E_B = \sqrt{\mathbf{p}^2 + M_B^{*2}} + g_{\omega B}\omega_0 + g_{\rho B}t_{3B}b_0 \equiv \sqrt{\mathbf{p}^2 + M_B^{*2}} + U \, , \tag{44}$$

where $M_B^* = M_B - g_{\sigma B}\sigma$ are the Dirac effective masses, σ, ω_0, and b_0 are the average values of the meson fields, and $g_{\sigma B}$, $g_{\omega B}$, and $g_{\rho B}$ are the strong interaction couplings of the different meson fields to baryons, and t_{3B} is the third component of isospin for the baryons. This equation defines the effective potential U. For more details, see Appendix B.

15

We turn now to calculate the cross section for absorption of electron neutrinos in a multi-component system described by a Walecka-type effective field-theoretical model at the mean field level. In this model, the nucleons become increasingly relativistic due to the rapidly dropping nucleon effective masses. The nonrelativistic approximation for the hadronic current discussed thus far cannot be justified, since, at high density, terms of order p/M^* are of order unity and must be retained. It is convenient to express the angles appearing in Eq. (7) in terms of energy and momentum transfers (q_0, q), and to define the response functions in terms of appropriate current-current correlation or polarization functions [27]. To see how this is accomplished, we start with a general expression for the differential cross section [49,50]

$$\frac{1}{V}\frac{d^3\sigma}{d^2\Omega_3 dE_3} = -\frac{G_F^2}{128\pi^2}\frac{E_3}{E_1}\left[1 - \exp\left(\frac{-q_0 - (\mu_2 - \mu_4)}{T}\right)\right]^{-1}(1 - f_3(E_3))\ \text{Im}\ (L^{\alpha\beta}\Pi_{\alpha\beta}^R), \quad (45)$$

where the incoming neutrino energy is E_1 and the outgoing electron energy is E_3. The factor $[1 - \exp((-q_0 - \mu_2 + \mu_4)/T)]^{-1}$ arises due to the fluctuation-dissipation theorem, since particles labeled '2' and '4' are in thermal equilibrium at temperature T and in chemical equilibrium with chemical potentials μ_2 and μ_4, respectively. The final state blocking of the outgoing lepton is accounted for by the Pauli blocking factor $(1 - f_3(E_3))$. The lepton tensor $L_{\alpha\beta}$ is given by

$$L^{\alpha\beta} = 8[2k^\alpha k^\beta + (k \cdot q)g^{\alpha\beta} - (k^\alpha q^\beta + q^\alpha k^\beta) \mp i\epsilon^{\alpha\beta\mu\nu}k_\mu q_\nu] \quad (46)$$

The target particle retarded polarization tensor is

$$\text{Im}\Pi_{\alpha\beta}^R = \tanh\left(\frac{q_0 + (\mu_2 - \mu_4)}{2T}\right)\text{Im}\ \Pi_{\alpha\beta}, \quad (47)$$

where $\Pi_{\alpha\beta}$ is the time ordered or causal polarization and is given by

$$\Pi_{\alpha\beta} = -i\int\frac{d^4p}{(2\pi)^4}\text{Tr}\ [T(G_2(p)J_\alpha G_4(p+q)J_\beta)]. \quad (48)$$

Above, k_μ is the incoming neutrino four-momentum and q_μ is the four-momentum transfer. In writting the lepton tensor, we have neglected the electron mass term, since typical electron energies are of the order of a few hundred MeV. The Greens' functions $G_i(p)$ (the index i labels particle species) describe the propagation of baryons at finite density and temperature. The current operator J_μ is γ_μ for the vector current and $\gamma_\mu\gamma_5$ for the axial current. Given the structure of the particle currents, we have

$$\Pi_{\alpha\beta} = \mathcal{V}^2\Pi_{\alpha\beta}^V + \mathcal{A}^2\Pi_{\alpha\beta}^A - 2\mathcal{V}\mathcal{A}\Pi_{\alpha\beta}^{VA}. \quad (49)$$

For the vector polarization, $\{J_\alpha, J_\beta\} :: \{\gamma_\alpha, \gamma_\beta\}$, for the axial polarization, $\{J_\alpha, J_\beta\} :: \{\gamma_\alpha\gamma_5, \gamma_\beta\gamma_5\}$ and for the mixed part, $\{J_\alpha, J_\beta\} :: \{\gamma_\alpha\gamma_5, \gamma_\beta\}$. Using vector current conservation and translational invariance, $\Pi_{\alpha\beta}^V$ may be written in terms of two independent components. In a frame where $q_\mu = (q_0, |q|, 0, 0)$, we have

$$\Pi_T = \Pi_{22}^V \qquad \text{and} \qquad \Pi_L = -\frac{q_\mu^2}{|q|^2}\Pi_{00}^V.$$

The axial current-current correlation function can be written as a vector piece plus a correction term:

$$\Pi_{\mu\nu}^A = \Pi_{\mu\nu}^V + g_{\mu\nu}\Pi^A. \tag{50}$$

The mixed, axial current-vector current correlation function is

$$\Pi_{\mu\nu}^{VA} = i\epsilon_{\mu,\nu,\alpha,0}q^\alpha\Pi^{VA}. \tag{51}$$

The above mean field or Hartree polarizations, which characterize the medium response to the neutrino, have been explicitly evaluated in previous work [51,52] for the case of neutrino scattering. Since the structure of the charged current is similar to that of the neutral current, we may write

$$\frac{1}{V}\frac{d^3\sigma}{d^2\Omega dE_\nu} = -\frac{G_F^2}{16\pi^3}\frac{E_3}{E_1}q_\mu^2\,(1-f_3(E_3))\,\left[1-\exp\frac{-q_0-(\mu_2-\mu_4)}{T}\right]^{-1}[AR_1+R_2+BR_3],$$

$$A = \frac{4E_1E_3+q_\mu^2}{2q^2}, \quad B = E_1+E_3. \tag{52}$$

From Eq. (52), we see that the response of a relativistic system to the charged or neutral current probe may be written in terms of three response functions R_1, R_2, and R_3. (In contrast, the response in a nonrelativistic system, Eq. (14), is characterized by a single isospin density response function. This is due to the fact that when the baryon velocity $v_i \sim 1$, the angular terms in Eq. (7) cannot be dropped.). The various response functions required have been studied in earlier works for neutral current reactions [27,33]. Their generalization to the case of charged current reactions are:

$$R_1 = (\mathcal{V}^2+\mathcal{A}^2)\,[\mathrm{Im}\,\Pi_L^R(q_0,q)+\mathrm{Im}\,\Pi_T^R(q_0,q)] \tag{53}$$

$$R_2 = (\mathcal{V}^2+\mathcal{A}^2)\,\mathrm{Im}\,\Pi_T^R(q_0,q)-\mathcal{A}^2\,\mathrm{Im}\,\Pi_A^R(q_0,q) \tag{54}$$

$$R_3 = 2\mathcal{V}\mathcal{A}\,\mathrm{Im}\,\Pi_{VA}^R(q_0,q). \tag{55}$$

These response functions have been written in terms of the imaginary part of the polarization functions, whose causal components are given in Ref. [51,52] for symmetric nuclear matter. We present extensions of these results to asymmetric matter, and, in particular, to unlike particle-hole excitations. For space like excitations, $q_\mu^2 \le 0$, they are given by

$$\mathrm{Im}\,\Pi_L(q_0,\vec{q}) = 2\pi\int\frac{d^3p}{(2\pi)^3}\,\frac{E_p^{*2}-|p|^2\cos^2\theta}{E_p^*E_{p+q}^*}\,\Theta \tag{56}$$

$$\mathrm{Im}\,\Pi_T(q_0,\vec{q}) = \pi\int\frac{d^3p}{(2\pi)^3}\,\frac{q_\mu^2/2-|p|^2(1-\cos^2\theta)}{E_p^*E_{p+q}^*}\,\Theta \tag{57}$$

$$\mathrm{Im}\,\Pi_A(q_0,\vec{q}) = 2\pi\int\frac{d^3p}{(2\pi)^3}\,\frac{M_2^{*2}}{E_p^*E_{p+q}^*}\,\Theta \tag{58}$$

$$\mathrm{Im}\,\Pi_{VA}(q_0,\vec{q}) = 2\pi\int\frac{d^3p}{(2\pi)^3}\,\frac{q_\mu^2M_2^*}{|q^2|E_p^*E_{p+q}^*}\,\Theta. \tag{59}$$

In the above,

$$\Theta = F(E_p^*, E_{p+q}^*)[\delta(q_0 - (E_{p+q} - E_p)) + \delta(q_0 - (E_p - E_{p+q}))] \tag{60}$$

$$F(E_p^*, E_{p+q}^*) = f_2(E_p^*)(1 - f_4(E_{p+q}^*)) \tag{61}$$

$$E_p^* = \sqrt{|p|^2 + M_2^{*2}}, \qquad E_p = E_p^* + U \tag{62}$$

The particle distribution functions $f_i(E)$ are given by the Fermi-Dirac distribution functions

$$f_i(E_p^*) = \frac{1}{1 + \exp((E_p^* - \nu_i)/kT)}, \tag{63}$$

where ν is the effective chemical potential defined by

$$\nu_i = \mu_i - U_i = \mu_i - (g_{\omega B_i}\omega_0 + t_{3B_i}g_{\rho B_i}b_0), \tag{64}$$

The single particle spectrum in Eq. (44) is discussed in Appendix B. The angular integrals are performed by exploiting the delta functions. The three dimensional integrals can be reduced to the following one dimensional integrals:

$$\text{Im } \Pi_L(q_0, q) = \frac{q_\mu^2}{2\pi|q|^3} \int_{e_-}^\infty dE \ [(E + q_0/2)^2 - |q|^2/4]$$
$$\times [F(E, E + q_0) + F(E + q_0, E)] \tag{65}$$

$$\text{Im } \Pi_T(q_0, q) = \frac{q_\mu^2}{4\pi|q|^3} \int_{e_-}^\infty dE \ [(E^* + q_0/2)^2 + |q|^2/4 + |q|^2 M_2^{*2}/q_\mu^2)]$$
$$\times [F(E, E + q_0) + F(E + q_0, E)] \tag{66}$$

$$\text{Im } \Pi_A(q_0, q) = \frac{M_2^{*2}}{2\pi|q|} \int_{e_-}^\infty dE \ [F(E, E + q_0) + F(E + q_0, E)] \tag{67}$$

$$\text{Im } \Pi_{VA}(q_0, q) = \frac{q_\mu^2}{8\pi|q|^3} \int_{e_-}^\infty dE \ [2E + q_0][F(E, E + q_0) + F(E + q_0, E)] \ . \tag{68}$$

The lower cut-off e_- arises due to kinematical restrictions and is given by

$$e_- = -\beta\frac{\tilde{q}_0}{2} + \frac{q}{2}\sqrt{\beta^2 - 4\frac{M_2^{*2}}{q^2 - \tilde{q}_0^2}}, \tag{69}$$

where

$$\tilde{q}_0 = q_0 + U_2 - U_4, \quad \beta = 1 + \frac{M_4^{*2} - M_2^{*2}}{q^2 - \tilde{q}_0^2}. \tag{70}$$

It is convenient to reexpress the polarization functions as follows:

$$\text{Im } \Pi_L^R(q_0, q) = \frac{q_\mu^2}{2\pi|q|^3} \left[I_2 + q_0 I_1 + \frac{q_\mu^2}{4}I_0\right] \tag{71}$$

$$\text{Im } \Pi_T^R(q_0, q) = \frac{q_\mu^2}{4\pi|q|^3} \left[I_2 + q_0 I_1 + \left(\frac{q_\mu^2}{4} + \frac{q^2}{2} + M_2^{*2}\frac{q^2}{q_\mu^2}\right) I_0\right] \tag{72}$$

$$\text{Im } \Pi_A^R(q_0, q) = \frac{M_2^{*2}}{2\pi|q|}I_0 \tag{73}$$

$$\text{Im } \Pi_{VA}^R(q_0, q) = \frac{q_\mu^2}{8\pi|q|^3}[q_0 I_0 + 2I_1], \tag{74}$$

18

where we used the one-dimensional integrals

$$I_n = \tanh\left(\frac{q_0 + (\mu_2 - \mu_4)}{2T}\right) \int_{e_-}^{\infty} dE \; E^n \; [F(E, E + q_0) + F(E + q_0, E)]. \tag{75}$$

These integrals may be explicitly expressed in terms of the Polylogarithmic functions

$$Li_n(z) = \int_0^z \frac{Li_{n-1}(x)}{x} \, dx \,, \qquad Li_1(x) = \ln(1-x) \tag{76}$$

which are defined to conform to the definitions of Lewin [53]. This Polylogarithm representation is particularly useful and compact:

$$I_0 = T \; z \left(1 + \frac{\xi_1}{z}\right), \tag{77}$$

$$I_1 = T^2 \; z \left(\frac{\mu_2 - U_2}{T} - \frac{z}{2} + \frac{\xi_2}{z} + \frac{e_- \xi_1}{zT}\right), \tag{78}$$

$$I_2 = T^3 \; z \left(\frac{(\mu_2 - U_2)^2}{T^2} - z\frac{\mu_2 - U_2}{T} + \frac{\pi^2}{3} + \frac{z^2}{3} - 2\frac{\xi_3}{z} + 2\frac{e_- \xi_2}{Tz} + \frac{e_-^2 \xi_1}{T^2 z}\right), \tag{79}$$

where $z = (q_0 + (\mu_2 - \mu_4))/T$ and the factors ξ_n are given by

$$\xi_n = Li_n(-\alpha_1) - Li_n(-\alpha_2), \tag{80}$$

with

$$\alpha_1 = \exp\left((e_- - \mu_2 + U_2)/T\right), \quad \alpha_2 = \exp\left((e_- + q_0 - \mu_4 + U_2)/T\right). \tag{81}$$

We note that the nonrelativistic structure function for neutral current scattering, Eq. (43) is, aside from the factor $M_2^{*2}T/\pi q$, equal to I_0 since $\xi_1 \equiv \xi_-$.

The total cross section is the double integral in (q_0, q) space:

$$\frac{\sigma(E_1)}{V} = \frac{G_F^2}{2\pi^2 E_1^2} \int_{-\infty}^{E_1} dq_0 \; \frac{(1 - f_3(E_3))}{1 - \exp\frac{-q_0 - (\mu_2 - \mu_4)}{T}} \int_{|q_0|}^{2E_1 - q_0} dq \; q \; q_\mu^2 \; [AR_1 + R_2 + BR_3]. \tag{82}$$

Eq. (82) allows us to calculate the cross section per unit volume, or equivalently the inverse mean free path, consistently with the relativistic field-theoretical model in the mean field approximation. This naturally incorporates the effects of strong interactions, Pauli blocking of final state particles and the contribution of relativistic terms to the baryon currents. In the case of neutral currents, some of the terms in the above are slightly simplified:

$$z = \frac{q_0}{T}, \quad \mu_2 = \mu_4, \quad e_- = -\frac{q_0}{2} + \frac{q}{2}\sqrt{1 - 4\frac{M_2^{*2}}{q_\mu^2}} \tag{83}$$

We note that other expressions for the cross sections, based on a similar formalism, have been derived earlier in the literature [27,33]. However, negative values of q_0 were not taken into account in Ref. [27] and the response functions used in Refs. [27,33] inadvertently

19

omitted the factor $(1 - \exp(-z))$ in the denominator of Eqs. (52). While the qualitative results in Refs. [27,33] remain unchanged, they are quantitatively affected.

In Fig. 13, the individual particle fractions and the relevant chemical potentials are shown for a lepton fraction $Y_L = 0.4$. As in the case of the potential model, interactions in this model lead to larger proton fractions compared to the noninteracting case. These results are almost indistinguishable from those of the potential model. The absorption (upper panels) and scattering (lower panels) mean free paths, calculated using Eq. (82), are shown in Fig. 14 for three different temperatures, $T = 5, 30$, and 60 MeV, as a function of baryon density. At low temperatures, the neutrino mean free path has relatively little variation with density due to the dropping baryon effective masses at high density. Nevertheless, the mean free paths eventually decrease with increasing density, unlike in the potential model. We attribute this to the inclusion of relativistic kinematics.

The results for the neutrino-free case are shown in Figs. 15 and 16. Qualitatively, the results have similar density and temperature behaviour as in both the neutrino-trapped case and in the nonrelativistic case. The upper panels show the absorption mean free paths and the lower panels show the scattering mean free path. The threshold density for the charged current reaction to be kinematically allowed at zero temperature in this model occurs at $1.7n_0$. This accounts for the sudden increase in absorption mean free path below this density at low temperatures. At higher temperatures, this threshold-like behaviour is much less pronounced, neutrino absorption mean free path dominate the total opacity for electron neutrinos. From the leftmost panels in Fig. 16, we see that even at $T = 5$ MeV, despite kinematical restrictions at low density the absorption reaction always dominates over the scattering reaction.

VI. COMPARISON WITH OTHER WORKS

Calculations of protoneutron star evolution have been performed by several groups [4–8]. At supra-nuclear densities, these groups used for the most part neutrino cross sections as originally described in Burrows and Lattimer [4]. Those cross sections were generated by interpolation among limiting formulae for degenerate and nondegenerate matter and neutrinos analogous to the limiting formulae given in Sec. III for noninteracting, nonrelativistic baryonic matter. A direct comparision of those results with the results obtained here for arbitrary degeneracy and including interactions is therefore not straightforward. First, the limiting expressions should include the effects of interactions. Second, the results will be sensitive to the interpolation algorithm, especially the interpolation parameter.

In addition, relativistic effects become increasingly important with density in a field-theoretical description, since the nucleon effective mass decreases with increasing density. Quantitatively, the effects arising due to the relativistic structure of the baryon currents is small and is typically of order $E\nu/M^*$. However, relativistic kinematics introduces important corrections (of order p_f/M^*) in the degenerate limit. To facilitate an illustrative comparision of our results with other results often used in the literature, we study the neutrino mean free path in the trapped regime. In this case, the dominant neutrino cross sections are those due to absorption (on neutrons) and scattering off neutrons and protons. The appropriate limiting expressions for the absorption and scattering cross sections for the degenerate case become

$$\frac{\sigma_{D,n}^A(E_\nu)}{V} = \frac{G_F^2}{4\pi^3}(g_V^2 + 3g_A^2)E_{F_n}^{*2}T^2\mu_e\left[\pi^2 + \left(\frac{E_\nu - \mu_\nu}{kT}\right)^2\right]\frac{1}{1 + \exp((\mu_\nu - E_\nu)/T)},\qquad(84)$$

$$\frac{\sigma_{D,i}^S(E_\nu)}{V} = \frac{G_F^2}{16\pi^3}(c_V^2 + 3c_A^2)E_{F_i}^{*2}T^2 E_\nu\left[\pi^2 + \left(\frac{E_\nu - \mu_\nu}{kT}\right)^2\right]\frac{1}{1 + \exp((\mu_\nu - E_\nu)/T)},\qquad(85)$$

where $E_{F_i}^2 = p_{Fi}^2 + M_i^{*2}$ replaces M_i^2 appearing in the formulae for nonrelativistic, noninteracting nucleons Eq. (26) $(i = n, p)$. For scattering off neutrons and protons, c_V and c_A are appropriately chosen. The nondegenerate cross sections $\sigma_{ND,n}^A$ and $\sigma_{ND,i}^S$ are unchanged from Eq. (31).

We compare the results for the total cross section obtained by interpolation as opposed to the exact integrations (σ_{rpl}) for the case of neutrino-trapped matter with $Y_L = 0.4$. For this exercise, we chose a field-theoretical model and therefore used the limiting formulas for the σ_D's and σ_{ND}'s just described. The total cross section is the sum of those from absorption on neutrons and scattering off neutrons and protons. As an illustration, we first employ the particular interpolation scheme of Keil and Janka [8]:

$$\sigma_1 = \sum_{i=n,p}\left(\sigma_{D,i}^S\frac{X_i}{1 + X_i} + \sigma_{ND,i}^S\frac{1}{1 + X_i}\right) + \sigma_{D,n}^A\frac{X_n}{1 + X_n} + \sigma_{ND,n}^A\frac{1}{1 + X_n},\qquad(86)$$

where $X_i = \max[0, \eta_i]$ where η_i is the degeneracy parameter. For a relativistic model, the appropriate degeneracy parameter is $\eta_i = (\nu_i - M_i^*)/T$ which can be seen by reference to Eq. (63). Fig. 17 (lower left panel) shows the ratio of our exact integration compared with σ_1 as a function of density and temperature and assuming $E_\nu = \mu_\nu$. This interpolation gives reasonable cross sections in the nondegenerate limit but is poor in the degenerate limit. This behavior is easily understood by examining the ratio σ_{ND}^A/σ_D^A, which for $E_\nu = \mu_\nu$ is proportional to $nE_\nu^2/(E_{F_n}^{*2}T^2\mu_e)$. We can neglect the relatively weak density dependence of $E_{F_n}^*$, since the drop in M_n^* is compensated somewhat by the increase of k_{F_n}, and note that in the neutrino-trapped case both $E_\nu = \mu_\nu$ and μ_e scale as $n^{1/3}$. Thus, $\sigma_{ND}^A/\sigma_D^A \sim n^{4/3}/T^2 \sim (E_{Fn}/T)^2 = \eta^2$ where E_{F_n} is the nonrelativistic neutron Fermi energy. In the degenerate limit, therefore, the σ_{ND}^A contribution can still dominate that from σ_D^A. This may also be inferred by comparing with the ratio σ_{rpl}/σ_{ND} in the degenerate regions as shown in the upper left panel of Fig. 17, where $\sigma_{ND} = \sigma_{ND}^A + \sigma_{ND}^S$.

These results suggest that a better interpolation formula is

$$\sigma_3 = \sum_{i=n,p}\left(\sigma_{D,i}^S\frac{X_i^3}{1 + X_i^3} + \sigma_{ND,i}^S\frac{1}{1 + X_i^3}\right) + \sigma_{D,n}^A\frac{X_n^3}{1 + X_n^3} + \sigma_{ND,n}^A\frac{1}{1 + X_n^3}.\qquad(87)$$

The ratio of the exact to these interpolated results are shown Fig. 17. The interpolation now correctly goes to the required limits; for reference the exact result is compared directly with the two limiting forms in the upper left (nondegenerate) and upper right (degenerate) panels. Nevertheless, significant errors for intermediate degeneracies still exist, which underscores the importance of the relatively simple exact formulae we have found. There is no significant need to use interpolations any longer.

VII. MULTI-COMPONENT ENVIRONMENT

Strangeness-bearing components can appear in dense matter either in the form of hyperons, kaon condensate, or quarks. In this section, we investigate the effects of multi-components on the neutrino mean free paths by concentrating on the possible presence of hyperons. We present specific results for a relativistic field-theoretical model in which the baryons, B, interact via the exchange of σ, ω, and ρ mesons [35]. The relevant details are presented in Appendix B.

For a typical case, the particle fractions in matter containing hyperons are shown in the upper panels of Fig. 18 for different temperatures in the neutrino-trapped case, $Y_L = 0.4$. The lower panels show the behaviour of the relevant chemical potentials. Note that the neutrino chemical potential increases rapidly with the onset of hyperons in matter (compare with the results in Fig. 12) due to the increase in the positive charge in the system. This is typical for matter in which strangeness, due to any source, appears. Consequently, in matter with hyperons neutrino energies are somewhat larger than those in nucleons-only matter.

The absorption mean free paths in matter containing hyperons are shown in Fig. 19. The various reactions that contribute to the total absorption opacity are calculated using Eq. (82) by using the appropriate chemical potentials and neutrino coupling constants. Strangeness-changing reactions are Cabibbo suppressed and hence their contribution to the total opacity is negligible. The relative importance of the various reactions are shown in the upper panels. Pauli blocking and kinematic restrictions account for the threshold-like structure seen at low temperatures, particularly for the reaction $\nu_e + \Sigma^- \rightarrow \Lambda + e^-$. This is analogous to the threshold behavior seen for the reaction $\nu_e + n \rightarrow e^- + p$ in hyperon-free matter. The kinematical restrictions on reactions involving baryons require that the initial and final state baryon Fermi momenta not be vastly different. When too large a difference exists, the phase space is highly suppressed. At higher temperatures, these kinematical restrictions are relaxed. The higher neutrino energy and the lower degeneracy of the baryons account for the qualitative trends of the results at the higher temperatures $T = 30$ MeV and $T = 60$ MeV. The solid lines in the lower panels show the net mean free path from all contributions from absorption reactions. For comparison, the net mean free path in a model without hyperons is shown by the dashed curves. In general, the presence of hyperons has the effect of decreasing the neutrino mean free path.

In Fig. 20, the scattering mean free paths are shown. The upper panels show the individual contributions to the total scattering mean free path due to the various reactions of interest. In the lower panels, the net mean free paths in hyperonic matter (solid curves) are compared with those in nucleons-only matter (dashed curves). The appearance of hyperons again decreases the neutrino mean free path. The overall scattering mean free path is less than 50% larger than the absorption mean free path, so that scattering provides an important contribution.

In summary, the decrease in mean free paths in a multi-component environment may be understood by noting that: (1) A larger neutrino chemical potential results in larger neutrino energies, (2) hyperons decrease the degeneracy of baryons, and (3) hyperons provide additional channels of scattering reactions to occur.

When neutrinos carry no net lepton number, they do not play a role in determining the composition of matter. In neutrino-free matter, the hyperons appear in larger numbers and

at threshold densities which are lower than in neutrino-rich matter. In Fig. 21, particle fractions (upper panels) and the electron chemical potentials (lower panels) in neutrino-free matter with hyperons are shown. Since the neutrinos in this case are thermal, we present results for absorption and scattering mean free paths calculated for $E_\nu = 3T$.

In Fig. 22 are shown the relative contributions of the dominant charged current reactions (upper panels) and the total neutrino absorption mean free paths (lower panels). At low temperatures, the reactions show the expected threshold-like behavior. The total absorption opacity due to all possible reactions (solid curves) is shown in the lower panels. For comparison, results in matter without hyperons is also shown by the dashed curves. As in the neutrinos-trapped case, the neutrino mean free paths are smaller in matter with hyperons, albeit by a smaller amount. Scattering off hyperons, shown in Fig. 23, clearly leads to important modifications to the neutrino mean free path in the neutrino-free case.

VIII. NEUTRINO TRANSPORT IN AN EVOLVING PROTONEUTRON STAR

A. Introduction

One of the most important applications of dense matter opacity calculations is the environment of a newly formed neutron star. A protoneutron star is formed subsequent to the core bounce of a massive star in a gravitational collapse supernova. Its early evolution has been investigated in Refs. [4–8]. Detailed studies of the dynamics of core collapse and supernova indicate that within milliseconds of the shock wave formation the formerly collapsing stellar core settles into nearly hydrostatic equilibrium, with a relatively low entropy and large lepton content.

The entropy per baryon, s, is about one or less (measured in units of Boltzmann's constant), which corresponds to a temperature of about 10-20 MeV. The electron lepton fraction $Y_L = Y_e + Y_{\nu_e}$ at bounce in the interior is estimated to be about 0.4. The ν_e's formed and trapped in the core during collapse are degenerate with a chemical potential of about 300 MeV. In addition, because no μ- or τ- leptons were present when neutrino trapping occurred, the net numbers of either μ or τ leptons is zero: e.g., $Y_{\nu_\mu} = -Y_\mu \approx 0$. The μ and ν_μ chemical potentials in beta equilibrium are related by $\mu_\mu - \mu_{\nu_\mu} = \mu_e - \mu_{\nu_e}$, each side of which has a value of order 100 MeV. Unless $\mu_\mu > m_\mu c^2$, however, the net number of μ's or ν_μ's present is zero.

The temperature and entropy increase beyond about 0.5 $M_\odot$ from the center because of shock heating [4]. During the early deleptonization or neutrino loss phase, the stellar interior gains entropy because of resistive neutrino diffusion, and the regions near the protoneutron star surface lose entropy because of neutrino losses. Eventually, this reverses the positive temperature and entropy gradients in the interior. On time scales of about 10-15 s, the center reaches a maximum entropy of about 2 and a maximum temperature of 40–60 MeV. This time coincides with the loss of virtually all the net trapped neutrino fraction Y_{ν_e} in the interior, although there are still considerable numbers of neutrino pairs of all flavors present in thermal equilibrium. This time, therefore, marks both the end of the deleptonization phase and the onset of the cooling phase of the protoneutron star.

The baryonic composition of dense matter is greatly affected by the degree to which neutrinos are trapped. Thus there exists an unambiguous compositional difference between

the initial deleptonization (neutrino-trapped) and cooling (neutrino-free) phases [47]. This difference could be enhanced if strangeness, in the form of hyperons, kaons or quark matter, is considered. Neutrino trapping delays the appearance of the strange matter components to higher baryon densities. This implies that during the early deleptonization phase, matter may consist mostly of nonstrange baryons, except possibly at the very center of the star. But the cooling phase may be characterized by the presence of a substantial amount of strange matter, due to both the decreasing threshold density for their appearance and to the increasing central density of the star. It is therefore of considerable interest to examine the behavior of neutrino opacities in matter characterized by these different thermodynamic conditions.

B. Semi-analytic treatment of neutrino transport

The neutrino transport in the bulk of the interior may be treated in the diffusion approximation, since neutrinos are very nearly in thermal equilibrium due to the large weak-interaction rates and the typical mean free path is very small compared to the stellar radius until after about a minute when the mean neutrino energy becomes very small. In the diffusion approximation, neglecting the effects of general relativity, the rate of change of electron lepton number is related to the electron neutrino number gradient by

$$n\frac{\partial Y_L}{\partial t} = \frac{1}{r^2}\frac{\partial}{\partial r}\left[r^2 \int \frac{c}{3}\left(\lambda_\nu(E_\nu)\frac{\partial n_\nu(E_\nu)}{\partial r} - \lambda_{\bar\nu}(E_\nu)\frac{\partial n_{\bar\nu}(E_\nu)}{\partial r}\right)\right]dE_\nu,\tag{88}$$

where n is the baryon number density,

$$n_\nu(E_\nu) = \frac{E_\nu^2}{2\pi^2(\hbar c)^3}f_\nu(E_\nu), \qquad n_{\bar\nu}(E_\nu) = \frac{E_\nu^2}{2\pi^2(\hbar c)^3}f_{\bar\nu}(E_\nu)\tag{89}$$

are the electron neutrino and antineutrino number densities, respectively, at energy E_ν, $f_\nu = (1 + e^{(E_\nu-\mu_\nu)/T})^{-1}$ and $f_{\bar\nu} = (1 + e^{(E_\nu+\mu_\nu)/T})^{-1}$ are the neutrino and anti-neutrino distribution functions, and $Y_L = Y_\nu + Y_e$ is the total number of leptons per baryon. The net neutrino mean free path is due to both absorption and scattering:

$$\lambda_\nu^{-1}(E_\nu) = \frac{1}{1 - f_\nu(E_\nu)}\sum_{i=a,s}\frac{\sigma_i(E_\nu)}{V},\tag{90}$$

where σ_a and σ_s are the absorption and scattering cross sections, respectively, and the factor $1 - f_\nu(E_\nu)$ accounts for the inverse process [17]. A similar relation exists for the antineutrino mean free path, but uses $f_{\bar\nu}$ and the appropriate absorption and scattering cross sections $(\bar\sigma_a, \bar\sigma_s)$ for $\bar\nu_e$s. Eq. (88) can be rewritten in terms of the diffusion coefficients

$$D_n = \int_0^\infty dE_\nu \ E_\nu^n \ \lambda_\nu(E_\nu) \ f_\nu(E_\nu)(1 - f_\nu(E_\nu))\tag{91}$$

and a similarly defined $D_{\bar n}$ as follows:

$$n\frac{\partial Y_L}{\partial t} = \frac{c}{6\pi^2(\hbar c)^3}\frac{1}{r^2}\frac{\partial}{\partial r}\left[r^2\left((D_2 + D_{\bar 2})\frac{\partial(\mu_\nu/T)}{\partial r} - (D_3 - D_{\bar 3})\frac{\partial(1/T)}{\partial r}\right)\right].\tag{92}$$

24

The diffusion constants are related to the conventional Rosseland mean free paths by

$$\lambda_n = \frac{D_n}{\int_0^\infty dE_\nu \ E_\nu^n \ f(E_\nu)(1 - f(E_\nu))}. \tag{93}$$

The diffusion constants $D_2, D_3, D_{\bar{2}}$ and $D_{\bar{3}}$ only contain contributions from electron-type neutrinos, since only these are associated with changes in electron-neutrino number.

During the deleptonization phase, the neutrinos are mostly degenerate. Thus, the diffusion of antineutrinos can be essentially ignored and the neutrino properties are essentially only a function of μ_ν. For nearly degenerate matter in beta equilibrium, one can show that

$$\frac{\partial Y_L}{\partial Y_\nu} \simeq \left(\frac{\partial Y_L}{\partial Y_\nu}\right)_o \frac{\mu_{\nu,o}}{\mu_\nu} \tag{94}$$

where the subscript o indicates values at the beginning of deleptonization. For example, for $\mu_{\nu,o} \sim 200$ MeV, $(\partial Y_L/\partial Y_\nu)_o \simeq 3$. It is instructive to explore the transport behavior for various assumptions concerning the energy dependence of the mean free path. Supposing that $\lambda_\nu(E_\nu) = \lambda_o(n, T)(\mu_{\nu,o}/E_\nu)^m$, one finds in the degenerate limit

$$D_n = \lambda_o T \mu_{\nu,o}^m \mu_\nu^{n-m} . \qquad n \geq m \tag{95}$$

Therefore, assuming that during the deleptonization phase the remnant is nearly hydrostatic, Eq. (92) can be written in terms of the neutrino chemical potential as

$$\left(\frac{\partial Y_L}{\partial Y_\nu}\right)_o \frac{3\mu_{\nu,o}^{1-m}\mu_\nu}{c} \frac{\partial \mu_\nu}{\partial t} = \frac{1}{r^2} \frac{\partial}{\partial r} \left[r^2 \lambda_o \mu_\nu^{2-m} \frac{\partial \mu_\nu}{\partial r}\right] . \tag{96}$$

Note that the terms involving the temperature gradient in Eq. (92) vanish in the degenerate limit irrespective of the value of m. The temperature now only enters through $\lambda_o(n, T)$. Inasmuch as the temperature in the interior of the neutron star varies with time only by a factor of about two during the deleptonization, while μ_ν varies by a much larger factor, a simple understanding of deleptonization can be obtained by treating λ_o as a constant in both space and time.

As shown in Ref. [47], approximate solutions of Eq. (96) can be found by separating the time and radial dependences in μ_ν:

$$\mu_\nu = \mu_{\nu,o}\phi(t)\psi(r) , \tag{97}$$

with $\phi(0) = 1$ and $\psi(0) = 1$. This separation is justifiable since the remnant is essentially hydrostatic. The functional forms of ϕ and ψ, and the eigenvalue of the solution, depend upon the value of m. In Ref. [47], it was assumed that $m = 2$, in which case ϕ decreases linearly with time: $\phi = 1 - t/\tau$. If, instead, $m = 0$, then ϕ varies like $(1 + t/\tau)^{-1}$. In the case of $m = 1$, ϕ varies like $\exp -(t/\tau)$. In each case, τ is a deleptonization time and is proportional to $R^2/c\lambda_o$ where R is the stellar radius. In detail, one finds

$$\tau = \left(\frac{\partial Y_L}{\partial Y_\nu}\right)_o \frac{3R^2}{c\lambda_o} \frac{(3 - m)^{2/(3-m)}}{\xi_{n,1}^2} , \tag{98}$$

25

where $\xi_{n,1}$ is the Lane-Emden radial eigenvalue for index $n = 2/(3 - m)$ [54]. For the cases $m = 0, 1$ and 2, one finds $n = 2/3, 1$, and 2, and $\xi_{n,1} = 2.871, \pi$, and 4.353, respectively. Below, we examine the behavior of D_2 with respect to μ_ν, for fixed temperature, in the interior of a star at the onset of deleptonization, as it appears that the details of deleptonization fundamentally depend upon this behavior.

As the net electron-neutrino fraction disappears, the number diffusion equation becomes irrelevant and one should consider the energy diffusion equation [47]

$$nT\frac{\partial s}{\partial t} = \frac{1}{r^2}\frac{\partial}{\partial r}\left[r^2 \int \frac{c}{3}\sum_\ell \lambda_{\nu,\ell}\frac{\partial \epsilon_{\nu,\ell}(E_\nu)}{\partial r}dE_\nu\right] - n\mu_\nu\frac{\partial Y_L}{\partial t}. \tag{99}$$

Here, s is the entropy per baryon and $\epsilon_{\nu,\ell} = n_{\nu,\ell}E_\nu$ are the energy densities, at energy E_ν, of neutrinos (or antineutrinos) of species ℓ. Similarly, $\lambda_{\nu,\ell}$ represents the net mean free path of each neutrino and antineutrino species. This equation assumes the matter to be in beta equilibrium. The energy densities and mean free paths, in contrast to the deleptonization situation, contain important contributions from all three types of neutrinos. The λ's of electron-type neutrinos are due to both absorption and scattering, but those of tau-type neutrons have only scattering contributions. Those pertaining to muon-type neutrinos, besides having scattering contributions, may also have absorption contributions if muons are present, which is generally the situation only when $Y_\nu < 0.02$ above nuclear densities.

In the neutrino-free case, setting $\mu_\nu = 0$ in Eq. (99) results in

$$nT\frac{\partial s}{\partial t} = \frac{c}{6\pi(\hbar c)^3}\frac{1}{r^2}\frac{\partial}{\partial r}\left[r^2 \sum_\ell \frac{D_{4,\ell}}{T^2}\frac{\partial T}{\partial r}\right]. \tag{100}$$

As is the case with the mean free paths, the diffusion coefficients $D_{4,\ell}$ have contributions from all three types of neutrinos. Since the baryon matter, which dominates the specific heat, remains fairly degenerate throughout the cooling epoch, the entropy varies practically linearly with the temperature. In the nondegenerate approximation for the baryons and the neutrinos, the relativistic cross sections are expected to vary as $E_\nu^2 n$, so that $D_{4,\ell} \propto T^3/n$. However, the baryons are degenerate so we should expect the cross sections to be modified by an extra degeneracy factor of T/μ_n. Therefore, we can anticipate that the diffusion constants $D_{4,\ell}$ will behave as $T^2\mu_n/n$. A separation of Eq. (100) into temporal and spatial variations reveals that the temperature in the star is then expected to be roughly linearly decreasing with time. The predicted temperature profile will depend somewhat upon the density profile of the star; assuming the density to be approximately constant, one finds that the temperature profile is that of an $n = 2$ Lane-Emden polytrope. This is different from the predictions in Ref. [47], which, however, did not account for the degenerate nature of baryonic matter during the cooling stage. However, numerical simulations have demonstrated the qualitative correctness of these remarks.

C. Results

Fig. 24 shows D_2 plotted versus density for beta equilibrium matter with $Y_L = 0.4$ for temperatures between 5 and 30 MeV for the field-theoretical model adopted earlier. Both nucleons-only matter and matter in which hyperons are assumed to appear are shown. One

sees that both nucleons-only matter and matter containing hyperons have relatively small variations of D_2 with density at fixed temperature for $n \geq 1.5 n_s$. In the limit of degenerate matter and neutrinos, this results from the asymptotic behavior of the cross sections at the Fermi surface, which is $\sigma \propto T^2 \mu_e \mu_n \mu_p$ in the relativistic case. (In the nonrelativistic case, see Eqs. (26) and (27).) Thus, D_2 is expected to behave like $\mu_\nu^2 / (T \mu_e \mu_n \mu_p)$ in this case, and this has relatively little density dependence at high densities since the increase in $\mu_e \mu_n \mu_p$ is compensated by the increase in μ_ν^2. This implies that the case $m = 2$ could approximate the deleptonization stage of a protoneutron star, which implies that μ_ν should decrease linearly with time. Since D_2 is roughly proportional to $1/T$, one has that λ_o is roughly proportional to $1/T^2$. The rising temperature during deleptonization will modify the linear decrease of μ_ν. However, numerical simulations show that the linear behavior is approximately correct.

The effect of hyperons appearing during the deleptonization phase at first does not appear to be appreciable, especially if hyperons appear only relatively late in the evolution. In the presence of hyperons, the diffusion constant D_2 decreases from its value for the nucleons-only case for a given temperature. However, the appearance of hyperons is accompanied by a general temperature decrease because of the addional degrees of freedom which increase the heat capacity of the system. This results in a very small net change for deleptonization times. More important effects from hyperons can be expected at the late stages of deleptonization and during the cooling epoch following deleptonization. The total $D_4 = \sum_\ell D_{4,\ell}$ is shown as a function of density for several values of the temperature between 5 and 30 MeV in Fig. 25. As suggested in the previous section, an overall T^2 behavior is observed. The large (factor of 2) decrease in D_4 in hyperon-bearing matter relative to nucleons-only matter for a given T would, at first glance seems to imply longer diffusion and cooling times. However, the fact that the temperatures are smaller in the presence of hyperons somewhat compensates for this effect and preliminary calculations [55] show that there is an overall increase in cooling times for models which contain hyperons. Thus, there are important feedbacks operating between the stellar structure, the EOS and the opacities that may only be addressed in detailed simulations.

IX. SUMMARY AND OUTLOOK

In summary, we have calculated both charged and neutral current neutrino cross sections in dense matter at supra-nuclear densities. We have identified new sources of neutrino opacities involving strange particles and have computed their weak interaction couplings. The weak interaction cross sections are greatly affected by the composition of matter which is chiefly determined by the strong interactions between the baryons. We have, therefore, performed baseline calculations by considering the effects strong interactions on the in-medium single particle spectra, which also determines the composition through the EOS. The formalism we have developed allows us to calculate the cross sections efficiently for matter at arbitrary matter degeneracy. From our results, various limiting forms used earlier in the literature are also easily derived. This, in addition to providing valuable physical insights, allows us to assess the extent to which the various approximations are valid in both free and interacting matter.

To explore the influence of baryonic interactions on the neutrino cross sections, we have examined both nonrelativistic potential and relativistic field-theoretical models that are

commonly used in the calculation of the EOS. We sought to identify the common features shared by these models. At the mean-field level in both cases, a relatively simple structure for the single particle spectrum leads to analytic expressions for the response function, which in turn facilitates a first study of the role of strong interactions on the neutrino cross sections at temperatures of relevance in astrophysical applications. Specifically, when the effects of momentum dependent potential interactions can be treated adequately in the effective mass approximation (*i.e.,* only the quadratic term in momentum is retained), analytic expressions obtained for noninteracting matter are straighforwardly extended to include interactions. Effective field-theoretical models at the mean-field level offer a similar opportunity since the single particle specturm is that of a free Dirac spectrum, but with a density dependent effective mass. Note that in both cases, energy shifts in the spectrum arising through density dependent interactions are naturally included. Investigating the effects of more complicated momentum dependent interactions will be necessarily more involved. We have also calculated neutrino cross sections in matter containing hyperons and assessed their influence on the total opacities.

We have examined the role played by neutrino opacities in determining the deleptonization and cooling times of a newly born neutron star as it evolves in time. We showed analytically how these times are related to the relevant diffusion constants and, thus, the opacities. Although the main physical issues involved are clarified in such an approach, a quantitative assesment must await calculations using a more complete protoneutron star evolution code. The results of such a calculation will be reported elsewhere [55].

Some important aspects of our work are:

1. An exact and efficient calculation of the phase space valid for arbitrary degeneracy of asymmetric matter for both nonrelativistic and relativistic interacting baryons. The simplicity of the resulting formulae may be especially useful in the calculation of electron scattering, for example.

2. With the formalism presented here, it is no longer necessary or desirable to employ "generic" (*i.e.,* EOS independent) neutrino opacities in astrophysical simulations. Rather, tables of opacities can be constructed directly from quantities already known from the EOS determination. For example, the needed quantities are the chemical potentials, effective masses and single particle potentials of the baryon components. The first of these are generally tabulated in the EOS itself. In the nonrelativistic formalism, the effective masses and single particle potentials are simple functions of the particle number densities and kinetic energy densities. In the relativistic formalism, the effective masses and single particle potentials are straightforwardly related to the particle number densities, internal energy and pressure by the minimization conditions.

In the near future, we will prepare tables of both nonrelativistic potential and relativistic mean-field models of the EOS combined with their opacities, and make these generally available. Models including hyperons, kaon condensates and/or quarks will be computed.

It is difficult to state categorically how the opacities reported here will affect the current generation of supernova or protoneutron star calculations. For example, although it seems clear that the addition of hyperons in matter will decrease mean free paths for a given density and temperature, the hyperon-bearing matter has a smaller temperature for a given entropy and density. Smaller temperatures tend to increase the mean free paths, and this

effect appears to more than cancel the original decrease. The feedback between opacities and EOS in a given astrophysical setting must be calculated consistently.

It must be stressed that while we have included some effects of strong interactions through density dependent single particle excitations, there remain important collective effects from both density and spin/isospin dependent excitations [10,17,27] and from other density dependent in-medium correlations [56]. The magnitude of these effects has so far only been assesed in some special cases such as nondegenerate symmetric matter or pure degenerate neutron matter or neutrino-poor beta-equilibrated matter. Furthermore, coupling to the $\Delta(1230)$ isobar [57] and screening by virtual particle-hole pairs created in the final state interactions [16] could reduce the effective matrix elements. The net impact of such effects could be a reduction of some cross sections by as much as a factor of 2 at high densities. Work is in progress to calculate the role these effects on the neutrino cross sections at all temperatures of relevance and for all possible compositions, and will be reported subsequently.

ACKNOWLEDGMENTS

APPENDIX A: POTENTIAL MODELS

Here, we outline a potential model for a system of neutrons and protons at finite temperature. With suitable choices of finite range interactions and parameters, this model reproduces the results of the more microscopic calculations (for more details, see, for example, Ref. [47]). We begin with the energy density

$$\varepsilon = \varepsilon_n^{(kin)} + \varepsilon_p^{(kin)} + V(n_n, n_p, T), \tag{101}$$

where n_n (n_p) is the neutron (proton) density and the total density $n = n_n + n_p$. The contributions arising from the kinetic parts are

$$\varepsilon_n^{(kin)} + \varepsilon_p^{(kin)} = 2 \int \frac{d^3k}{(2\pi)^3} \frac{\hbar^2 k^2}{2m} (f_n + f_p), \tag{102}$$

where the factor 2 denotes the spin degeneracy and f_i for $i = n, p$ are the usual Fermi-Dirac distribution functions and m is the nucleon mass. It is common to employ local contact interactions to model the nuclear potential. Such forces lead to power law density-dependent terms in $V(n)$. Including the effect of finite-range forces between nucleons, we parameterize the potential contribution as

$$
\begin{aligned}
V(n_n, n_p, T) = {} & A n_0 \left[\tfrac{1}{2} - \tfrac{1}{3} \left(\tfrac{1}{2} + x_0 \right) (1 - 2x)^2 \right] u^2 \\
& + B n_0 \left[1 - \tfrac{2}{3} \left(\tfrac{1}{2} + x_3 \right) (1 - 2x)^2 \right] u^{\sigma+1} \\
& + \tfrac{2}{5} u \sum_{i=1,2} \left\{ (2C_i + 4Z_i) 2 \int \frac{d^3k}{(2\pi)^3} g(k, \Lambda_i) (f_n + f_p) \right. \\
& \left. + (C_i - 8Z_i) \, 2 \int \frac{d^3k}{(2\pi)^3} g(k, \Lambda_i)[f_n(1 - x) + f_p x] \right\},
\end{aligned}
\tag{103}
$$

where $x = n_p/n$ and $u = n/n_0$, with n_0 denoting equilibrium nuclear matter density. The function $g(k, \Lambda_i)$ is suitably chosen to simulate finite range effects. The constants A, B, σ, C_1, and C_2, which enter in the description of symmetric nuclear matter, and the additional constants x_0, x_3, Z_1, and Z_2, which determine the properties of asymmetric nuclear matter, are treated as parameters that are constrained by empirical knowledge.

The single particle spectrum e_i entering the Fermi-Dirac distribution functions f_i may be written as

$$e_i(k) = \frac{\hbar^2 k^2}{2m_i} + U_i(k; n, x, T), \tag{104}$$

where the single particle potential $U_i(n, x, k; T)$, which is explicitly momentum dependent, is obtained by a functional differentiation of the potential energy density in Eq. (103), with respect to the distribution functions f_i. Explicitly,

$$
\begin{aligned}
U_i(n, x, k; T) = {} & \tfrac{1}{5} u \left[\sum_{i=1,2} \{ 5C_i \pm (C_i - 8Z_i)(1 - 2x) \} \right] g(k, \Lambda_i) \\
& + A u \left[1 \mp \tfrac{2}{3} \left(\tfrac{1}{2} + x_0 \right) (1 - 2x) \right]
\end{aligned}
$$

$$+ Bu^\sigma \left[1 \mp \tfrac{4}{3} \frac{1}{\sigma + 1}(1 - 2x) - \tfrac{2}{3} \frac{(\sigma - 1)}{(\sigma + 1)} \left(\tfrac{1}{2} + x_3 \right) (1 - 2x)^2 \right]$$

$$+ \tfrac{2}{5} \frac{1}{n_0} \sum_{i=1,2} \left\{ (2C_i + 4Z_i) 2 \int \frac{d^3 k}{(2\pi)^3}\, g(k, \Lambda_i) f_i(k) \right.$$

$$\left. + (3C_i - 4Z_i) 2 \int \frac{d^3 k}{(2\pi)^3}\, g(k, \Lambda_i) f_j(k) \right\}, \tag{105}$$

where the upper (lower) sign in $\mp$ is for neutrons (protons) and $i \neq j$.

The Landau effective mass is defined through the relation

$$\frac{m_i^*}{m} = \frac{k_{F_i}}{m_i} \left[\frac{\partial e_k}{\partial k}\bigg|_{k_{F_i}} \right]^{-1}$$

$$= \left[1 + \frac{1}{5} u \sum_{i=1,2} \left\{ 5C_i \pm (C_i - 8Z_i)(1 - 2x) g'(k, \Lambda_i)|_{k_{F_i}} \right\} \right]^{-1}, \tag{106}$$

where the prime denotes a derivative with respect to momentum. The finite range interactions may be approximated by effective local interactions by retaining only the quadratic momentum dependence: i.e., $g(k, \Lambda_i) = 1 - (k/\Lambda_i)^2$. The energy density in Eq. (103) and the single particle potential in Eq. (105) then take the forms stemming from Skyrme's effective interactions [34]. Combining the finite range quadratic momentum term with the free kinetic energy term, the single particle spectrum in Eq. (104) may be written for Skyrme-like interactions as

$$e_i(k) = \frac{\hbar^2 k^2}{2m_i^*} + \tilde{U}_i(n, x, ; T). \tag{107}$$

This resembles the free particle spectrum, but with a density dependent effective mass m_i^* given by Eq. (106) with $g'(k, \Lambda_i)|_{k_{F_i}} = 1/(R_i^2 E_F^{(0)})$, where $R_i = \Lambda_i/(\hbar k_F^{(0)})$ and $E_F^{(0)} = (\hbar k_F^{(0)})^2/(2m)$ is the Fermi energy of symmetric nuclear matter at the equilibrium density. Other forms of $g(k, \Lambda_i)$, with more than a quadratic momentum dependence, also offer a viable description of the energy density and the single particle potential (see for example, Ref. ([47])), but do not lead to a spectrum resembling the free particle spectrum in Eq. (107). This simple form of the spectrum allows a direct evaluation of the neutrino opacities including the effects of interactions along the lines developed for noninteracting baryons in Sec. III. For more general momentum dependent interactions, the evaluation of the neutrino opacities requires more complicated techniques which take into account the full momentum dependence in the four-momentum conserving delta functions.

The parameters A, B, σ, C_1, and C_2, are determined from constraints provided by the empirical properties of symmetric nuclear matter at the equilibrium density $n_0 = 0.16$ fm^{-3}. With appropriate choices of the parameters, it is possible to parametrically vary the nuclear incompressibility K_0 so that the dependence on the stiffness of the EOS may be explored. In this work, we have chosen $K_0 = 180$ MeV for which

$$A = 159.47, \quad B = -109.04, \quad \sigma = 0.844, \quad C_1 = -41.28 \quad \text{and} \quad C_2 = 23. \tag{108}$$

Except for the dimensionless σ, all quantities above are in MeV. The finite-range parameters $\Lambda_1 = 1.5p_F^{(0)}$ and $\Lambda_2 = 3p_F^{(0)}$.

In the same vein, by suitably choosing the parameters x_0, x_3, Z_1, and Z_2, it is possible to obtain different forms for the density dependence of the symmetry energy $S(n)$ defined by the relation

$$E(n, x) = \varepsilon(n, x)/n = E(n, 1/2) + S(n)(1 - 2x)^2 + \cdots , \tag{109}$$

where E is the energy per particle, and $x = n_p/n$ is the proton fraction. Inasmuch as the density dependent terms associated with powers higher than $(1 - 2x)^2$ are generally small, even down to $x = 0$, $S(n)$ adequately describes the properties of asymmetric matter. The need to explore different forms of $S(n)$ stems from the uncertain behavior at high density and has been amply detailed in earlier publications [45,48]. In this work, we have chosen the potential part of the symmetry energy to vary as u. For this case,

$$x_0 = -0.410, \quad x_3 = -0.5 \quad Z_1 = -11.56 \text{ MeV}, \quad \text{and} \quad Z_2 = -4.421 \text{ MeV} \tag{110}$$

Since repulsive contributions that vary faster than linearly give rise to acausal behavior at high densities, care must be taken to screen such repulsive interactions [48]. This may be achieved by dividing the term proportional to $u^{\sigma+1}$ (when $\sigma > 1$) by the factor

$$1 + \tfrac{2}{3}B' \left[\tfrac{3}{2} - \left(\tfrac{1}{2} + x_3 \right)(1 - 2x)^2 \right] u^{\sigma-1} , \tag{111}$$

where B' is a small parameter introduced to maintain causality. Note that the single particle potential in Eq. (105) must then be accordingly modified. The appropriate terms may be obtained by using the relations $(\partial/\partial n_n)|_{n_p} = \partial/\partial n - (x/n)\partial/\partial x$ for neutrons and $(\partial/\partial n_p)|_{n_n} = \partial/\partial n + [(1 - x)/n]\partial/\partial x$ for protons.

For a fixed baryon density n, proton fraction x, and temperature T, an iterative procedure may now be employed to calculate the density dependent single particle potentials $\tilde{U}_n$ and $\tilde{U}_p$, and the chemical potentials μ_n and μ_p. The calculational procedure is detailed in Ref. [47]. These quantities, in conjunction with the requirements of chemical equilibrium in Eq. (9) and charge neutrality in Eq. (10) determines the composition of stellar matter at finite temperature. The specification of the spectrum in Eq. (107) then allows for a calculation of the neutrino opacities which are consistent with the underlying EOS.

APPENDIX B: EFFECTIVE FIELD-THEORETICAL MODELS

In a Walecka-type relativistic field-theoretical model the interactions between baryons are mediated by the exchange of σ, ω, and ρ mesons. The Lagrangian density is given by [35],

$$
\begin{aligned}
L &= L_H + L_\ell \\
&= \sum_B \overline{B}(-i\gamma^\mu\partial_\mu - g_{\omega B}\gamma^\mu\omega_\mu - g_{\rho B}\gamma^\mu\mathbf{b}_\mu\cdot\mathbf{t} - M_B + g_{\sigma B}\sigma)B \\
&\quad - \frac{1}{4}W_{\mu\nu}W^{\mu\nu} + \frac{1}{2}m_\omega^2\omega_\mu\omega^\mu - \frac{1}{4}\mathbf{B}_{\mu\nu}\mathbf{B}^{\mu\nu} + \frac{1}{2}m_\rho^2 b_\mu b^\mu \\
&\quad + \frac{1}{2}\partial_\mu\sigma\partial^\mu\sigma - \frac{1}{2}m_\sigma^2\sigma^2 - U(\sigma) \\
&\quad + \sum_l \overline{l}(-i\gamma^\mu\partial_\mu - m_l)l \,.
\end{aligned}
$$

Here, B are the Dirac spinors for baryons and $\mathbf{t}$ is the isospin operator. The sums include baryons $B = n, p, \Lambda, \Sigma$, and Ξ, and leptons, $l = e^-$ and μ^-. The field strength tensors for the ω and ρ mesons are $W_{\mu\nu} = \partial_\mu\omega_\nu - \partial_\nu\omega_\mu$ and $\mathbf{B}_{\mu\nu} = \partial_\mu\mathbf{b}_\nu - \partial_\nu\mathbf{b}_\mu$, respectively. The potential $U(\sigma)$ represents the self-interactions of the scalar field and is taken to be of the form

$$
U(\sigma) = \frac{1}{3}bM_n(g_{\sigma N}\sigma)^3 + \frac{1}{4}c(g_{\sigma N}\sigma)^4 \,. \tag{112}
$$

Electrons and muons are included in the model as noninteracting particles, since their interactions give small contributions compared to those of their free Fermi gas parts.

In the mean field approximation, the partition function (denoted by Z_H) for the hadronic degrees of freedom is given by

$$
\begin{aligned}
\ln Z_H \;=\;& \beta V\left[\tfrac{1}{2}m_\omega^2\omega_0^2 + \tfrac{1}{2}m_\rho^2 b_0^2 - \tfrac{1}{2}m_\sigma^2\sigma^2 - U(\sigma)\right] \\
&+ 2V\sum_B\int\frac{d^3k}{(2\pi)^3}\ln\left(1 + e^{-\beta(E_B^* - \nu_B)}\right) \,,
\end{aligned} \tag{113}
$$

where $\beta = (kT)^{-1}$ and V is the volume. The contribution of antibaryons is not significant for the thermodynamics of interest here, and is therefore not included in Eq. (113). Here, the effective baryon masses $M_B^* = M_B - g_{\sigma B}\sigma$ and $E_B^* = \sqrt{k^2 + M_B^{*2}}$. The chemical potentials are given by

$$
\mu_B = \nu_B + g_{\omega B}\omega_0 + g_{\rho B}t_{3B}b_0 \,, \tag{114}
$$

where t_{3B} is the third component of isospin for the baryon. Note that particles with $t_{3B} = 0$, such as the Λ and Σ^0 do not couple to the ρ. The effective chemical potential ν_B sets the scale of the temperature dependence of the thermodynamical functions.

Using Z_H, the thermodynamic quantities can be obtained in the standard way. The pressure $P_H = TV^{-1}\ln Z_H$, the number density for species B, and the energy density ε_H are given by

$$n_B = 2 \int \frac{d^3k}{(2\pi)^3} \left(e^{\beta(E_B^* - \nu_B)} + 1 \right)^{-1},$$

$$\varepsilon_H = \tfrac{1}{2} m_\sigma^2 \sigma^2 + U(\sigma) + \tfrac{1}{2} m_\omega^2 \omega_0^2 + \tfrac{1}{2} m_\rho^2 b_0^2 + 2 \sum_B \int \frac{d^3k}{(2\pi)^3} E_B^* \left(e^{\beta(E_B^* - \nu_B)} + 1 \right)^{-1}. \tag{115}$$

The entropy density is then given by $s_H = \beta(\varepsilon_H + P_H - \sum_B \mu_B n_B)$.

The meson fields are obtained by extremization of the partition function, which yields the equations

$$m_\omega^2 \omega_0 = \sum_B g_{\omega B} n_B \quad ; \quad m_\rho^2 b_0 = \sum_B g_{\rho B} t_{3B} n_B,$$

$$m_\sigma^2 \sigma = -\frac{dU(\sigma)}{d\sigma} + \sum_B g_{\sigma B} \; 2 \int \frac{d^3k}{(2\pi)^3} \frac{M_B^*}{E_B^*} \left(e^{\beta(E_B^* - \nu_B)} + 1 \right)^{-1}. \tag{116}$$

The total partition function $Z_{total} = Z_H Z_L$, where Z_L is the standard noninteracting partition function of the leptons.

The additional conditions needed to obtain a solution are provided by the charge neutrality requirement, and, when neutrinos are not trapped, the set of equilibrium chemical potential relations required by the general condition

$$\mu_i = b_i \mu_n - q_i \mu_l, \tag{117}$$

where b_i is the baryon number of particle i and q_i is its charge. For example, when $\ell = e^-$, this implies the equalities

$$\mu_\Lambda = \mu_{\Sigma^0} = \mu_{\Xi^0} = \mu_n,$$
$$\mu_{\Sigma^-} = \mu_{\Xi^-} = \mu_n + \mu_e,$$
$$\mu_p = \mu_{\Sigma^+} = \mu_n - \mu_e. \tag{118}$$

In the case that the neutrinos are trapped, Eq. (117) is replaced by

$$\mu_i = b_i \mu_n - q_i(\mu_l - \mu_{\nu_\ell}). \tag{119}$$

The new equalities are then obtained by the replacement $\mu_e \to \mu_e - \mu_{\nu_e}$ in Eq. (118). The introduction of additional variables, the neutrino chemical potentials, requires additional constraints, which we supply by fixing the lepton fractions, $Y_{L\ell}$, appropriate for conditions prevailing in the evolution of the protoneutron star. The contribution to pressure from neutrinos of a given species is $P_\nu = (1/24\pi^2)\mu_\nu^4$.

In the nucleon sector, the constants $g_{\sigma N}, g_{\omega N}, g_{\rho N}, b$, and c are determined by reproducing the nuclear matter equilibrium density $n_0 = 0.16$ fm^{-3}, and the binding energy per nucleon (~ 16 MeV), the symmetry energy ($\sim 30 - 35$ MeV), the compression modulus (200 MeV $\leq K_0 \leq 300$ MeV), and the nucleon Dirac effective mass $M^* = (0.6 - 0.7) \times 939$ MeV at n_0. Numerical values of the coupling constants so chosen are:

$$g_{\sigma N}/m_\sigma = 3.434 \text{ fm}, \quad g_{\omega N}/m_\omega = 2.674 \text{ fm}, \quad g_{\rho N}/m_\rho = 2.1 \text{ fm},$$
$$b = 0.00295, \quad \text{and} \quad c = -0.00107. \tag{120}$$

These couplings yield a symmetry energy of 32.5 MeV, a compression modulus of 300 MeV, and $M^*/M = 0.7$. This particular choice of model parameters are from Glendenning and Moszkowski [58] and will be referred to as GM1 hereafter. The prevalent uncertainty in the nuclear matter compression modulus and the effective mass M^* does not allow for a unique choice of these coupling constants. The high density behaviour of the EOS is sensitive to the strength of the meson coupling constants employed. Lacking definitive experimental and theoretical constraints, this choice of parameters may be considered typical.

The hyperon coupling constants may be determined by reproducing the binding energy of the Λ hyperon in nuclear matter [58]. Parameterizing the hyperon-meson couplings in terms of nucleon-meson couplings through

$$x_{\sigma H} = g_{\sigma H}/g_{\sigma N}, \quad x_{\omega H} = g_{\omega H}/g_{\omega N}, \quad x_{\rho H} = g_{\rho H}/g_{\rho N}, \tag{121}$$

the Λ binding energy at nuclear density is given by

$$(B/A)_{\Lambda} = -28 = x_{\omega \Lambda} g_{\omega N} \omega_0 - x_{\sigma \Lambda} g_{\sigma N} \sigma_0, \tag{122}$$

in units of MeV. Thus, a particular choice of $x_{\sigma \Lambda}$ determines $x_{\omega \Lambda}$ uniquely. To keep the number of parameters small, the coupling constant ratios for all the different hyperons are assumed to be the same. That is

$$x_{\sigma} = x_{\sigma \Lambda} = x_{\sigma \Sigma} = x_{\sigma \Xi} = 0.6, \tag{123}$$

and similarly for the ω

$$x_{\omega} = x_{\omega \Lambda} = x_{\omega \Sigma} = x_{\omega \Xi} = 0.653. \tag{124}$$

The ρ-coupling is of less consequence and is taken to be of similar order, i.e. $x_{\rho} = x_{\sigma}$.

TABLE I: Charged current vector and axial couplings. Numerical values are quoted using D=0.756 , F=0.477, $\sin^2\theta_W$=0.23 and $\sin^2\theta_c = 0.053$ (see Ref. [39]). The couplings for the same reactions involving antineutrinos are identical, and ℓ stands for $e-$, $\mu-$ or $\tau-$ type leptons. For corrections arising due to explicit $SU(3)$ breaking terms, see Ref. [40].

Reaction	g_V	g_A	ΔS
$\nu_\ell + n \to \ell^- + p$	1	$D + F = 1.23$	0
$\nu_\ell + \Sigma^- \to \ell^- + \Lambda$	0	$\sqrt{2/3}D = 0.62$	0
$\nu_\ell + \Sigma^- \to \ell^- + \Sigma^0$	$\sqrt{2}$	$\sqrt{2}F = 0.67$	0
$\nu_\ell + \Sigma^0 \to \ell^- + \Sigma^+$	$-\sqrt{2}$	$-\sqrt{2}F = -0.67$	0
$\nu_\ell + \Lambda \to \ell^- + \Sigma^+$	0	$-\sqrt{2/3}D = -0.62$	0
$\nu_\ell + \Lambda \to \ell^- + p$	$-\sqrt{3/2}$	$-\sqrt{3/2}(F + D/3) = 0.89$	1
$\nu_\ell + \Sigma^0 \to \ell^- + p$	1	$\sqrt{1/2}D = 0.54$	1
$\nu_\ell + \Sigma^- \to \ell^- + n$	-1	$D - F = 0.28$	1
$\nu_e + \mu^- \to \nu_\mu + e^-$	1	1	0

TABLE II: Neutral current vector and axial couplings. Neutral current couplings with baryons of all neutrino species, including antineutrinos, are identical, and ℓ stands for $e-, \mu-$, or $\tau-$ type neutrinos. Neutrino interactions with leptons have the same matrix elements as those with antineutrinos of the same flavor. For corrections arising due to explicit $SU(3)$ breaking terms, see Ref. [40].

Reaction	c_V	c_A
$\nu_e + e^- \to \nu_e + e^-$	$1 + 4\sin^2\theta_W = 1.92$	1
$\nu_\mu + \mu^- \to \nu_\mu + \mu^-$	$1 + 4\sin^2\theta_W = 1.92$	1
$\nu_e + \mu^- \to \nu_e + \mu^-$	$-1 + 4\sin^2\theta_W = -0.08$	-1
$\nu_{\mu,\tau} + e^- \to \nu_{\mu,\tau} + e^-$	$-1 + 4\sin^2\theta_W = -0.08$	-1
$\nu_\ell + n \to \nu_\ell + n$	-1	$-D - F = -1.23$
$\nu_\ell + p \to \nu_\ell + p$	$1 - 4\sin^2\theta_W = 0.08$	$D + F = 1.23$
$\nu_\ell + \Lambda \to \nu_\ell + \Lambda$	-1	$-F - D/3 = -0.73$
$\nu_\ell + \Sigma^- \to \nu_\ell + \Sigma^-$	$-3 + 4\sin^2\theta_W = -2.08$	$D - 3F = -0.68$
$\nu_\ell + \Sigma^+ \to \nu_\ell + \Sigma^+$	$1 - 4\sin^2\theta_W = 0.08$	D+F =1.23
$\nu_\ell + \Sigma^0 \to \nu_\ell + \Sigma^0$	-1	$D - F = 0.28$
$\nu_\ell + \Xi^- \to \nu_\ell + \Xi^-$	$-3 + 4\sin^2\theta_W = -2.08$	$D - 3F = -0.68$
$\nu_\ell + \Xi^0 \to \nu_\ell + \Xi^0$	-1	$-D - F = -1.23$
$\nu_\ell + \Sigma^0 \to \nu_\ell + \Lambda$	0	$2D/\sqrt{3} = 0.87$

36

REFERENCES

[1] K. Hirata, et. al., Phys. Rev. Lett., **58** (1987) 1490; R. M. Bionta, et. al., Phys. Rev. Lett., **58** (1987) 1494.

[2] S. W. Bruenn, Astrophys. Jl. Suppl. **58** (1985) 771.

[3] A. Mezzacappa and S. W. Bruenn, Astrophys. Jl. **405** (1993) 637.

[4] A. Burrows and J. M. Lattimer, Astrophys. Jl., **307** (1986) 178; A. Burrows, Ann. Rev. Nucl. Sci., **40** (1990) 181; and references therein.

[5] J. R. Wilson and R. Mayle, in *The Nuclear Equation of State*, eds. W. Greiner and H. Stöcker (Plenum Press, New York, 1989) 731.

[6] H. Suzuki and K. Sato, in *The Structure and Evolution of Neutron Stars*, eds. D. Pines, R. Tamagaki, and S. Tsuruta (New York: Addison-Wesley, 1992), 276.

[7] W. Keil, Prog. part. Nucl. Phys. **32** (1994) 105.

[8] W. Keil and H. T. Janka, Astronomy and Astrophysics, **296** (1995) 145.

[9] D. L. Tubbs and D. N. Schramm, Astrophys. Jl. **201** (1975) 467.

[10] R. F. Sawyer, Phys. Rev. **D11** (1975) 2740; Phys. Rev. **C40** (1989) 865.

[11] D. Q. Lamb and C. J. Pethick, Astrophys. Jl. **209** (1976) L77.

[12] D. Q. Lamb, Phys. Rev. Lett **41** (1978) 1623.

[13] D. L. Tubbs, Astrophys. Jl. Suppl. **37** (1978) 287.

[14] S. Bludman and K. Van Riper, Astrophys. Jl. **224** (1978) 631.

[15] R. F. Sawyer and A. Soni, Astrophys. Jl. **230** (1979) 859.

[16] N. Iwamoto, Ann. Phys. **141** (1982) 1.

[17] N. Iwamoto and C. J. Pethick, Phys. Rev. **D25** (1982) 313.

[18] B. T. Goodwin and C. J. Pethick, Astrophys. Jl. **253** (1982) 816.

[19] A. Burrows and T. J. Mazurek, Astrophys. Jl. **259** (1982) 330.

[20] B. T. Goodwin, Astrophys. Jl. **261** (1982) 321.

[21] S. W. Bruenn, Astrophys. Jl. Suppl. **58** (1985) 771.

[22] L. Van Den Horn and J. Cooperstein, Astrophys. Jl. **300** (1986) 142.

[23] O. V. Maxwell, Astrophys. Jl. **316** (1987) 691.

[24] J. Cooperstein, Phys. Rep. **163** (1988) 95.

[25] A. Burrows, Astrophys. Jl. **334** (1988) 891.

[26] P. J. Schinder, Astrophys. Jl. Suppl. **74** (1990) 249.

[27] C. J. Horowitz and K. Wehrberger, Nucl. Phys. **A531** (1991) 665; Phys. Rev. Lett. **66** (1991) 272; Phys. Lett. **B226** (1992) 236.

[28] M. Prakash, Manju Prakash, J. M. Lattimer and C. J. Pethick, Astrophys. Jl. **390** (1992) L80.

[29] S. Reddy and M. Prakash, in Proc. 11th Winter Workshop on Nuclear Dynamics, Advances in Nuclear Dynamics, ed. W. Bauer and Migerney (New York: Plenum) (1995) 237.

[30] W. Keil, H-T. Janka and G. Raffelt, Phys. Rev. **D51** (1995) 6635.

[31] H-T. Janka, W. Keil, G. Raffelt, and D. Seckel, Phys. Rev. Lett. **76** (1996) 2621.

[32] G. Sigl, Phys. Rev. Lett. **76** (1996) 2625.

[33] S. Reddy and M. Prakash, Astrophys. Jl. **423** (1997) 689.

[34] D. Vautherin and D.M. Brink, Phys. Rev. **C5** (1972) 626.

[35] B. D. Serot and J. D. Walecka, Advances in Nuclear Physics, **16**, eds. J. W. Negele and E. Vogt, (New York: Plenum); B.D. Serot, Rep. Prog. Phys. **55** (1992) 1855.

[36] S. Weinberg, Phys. Rev. Lett. **19** (1967) 1264.

[37] A. Salam, in Proc. Eighth Nobel Symp., Elementary Particle Theory: Relativistic Groups and Analyticity, ed. N. Svartholm (Stockholm: Almquist and Wicksell)

[38] S. L. Glashow, Nucl. Phys. **22** (1961) 579.

[39] J.-M. Gaillard and G. Sauvage, Ann. Rev. Nucl. Part. Sci., **34** (1984) 351.

[40] M.J. Savage and J. Walden, Phys. Rev. **D55** (1997) 5376.

[41] K. Sato, Prog. Theor. Phys. **53** (1975) 595.

[42] T. J. Mazurek, Astrophys. Space Sci. **35** (1975) 117.

[43] H. A. Bethe, G. E. Brown, J. Applegate, and J. M. Lattimer, Nucl. Phys. **A324** (1979) 487.

[44] F. C. Khanna and H. R. Glyde, Can. Jl. Phys. **54** (1976) 648.

[45] J. M. Lattimer, C.J. Pethick, M. Prakash, and P. Haensel, Phys. Rev. Lett. **66** (1991) 2701.

[46] R. B. Wiringa, V. Fiks and A. Fabrocine, Phys. Rev. **C38** (1988) 1010.

[47] M. Prakash, I. Bombaci, Manju Prakash, P. J. Ellis, J. M. Lattimer and R. Knorren, Phys. Rep **280** (1997) 1.

[48] M. Prakash, T. L. Ainsworth and J. M. Lattimer, Phys. Rev. Lett. **61** (1988) 2518.

[49] A.L. Fetter and J.D. Walecka, *Quantum Theory of Many Particle Systems* (New York: McGraw-Hill), 1971.

[50] S. Doniach and E. H. Sondheimer, *Green's Functions for Solid State Physicists* (Reading, The Benjamin/Cummings Publishing Company, Inc.), 1974.

[51] K. Lim and C. J. Horowitz, Nucl. Phys. **A501** (1989) 729.

[52] K. Saito, T. Maruyama and K. Soutame, Phys. Rev. **C40** (1989) 407.

[53] L. Lewin, *Polylogarithms and Associated Functions* (New York: North-Holland) 1983.

[54] S. Chandrasekhar, *An Introduction to the Study of Stellar Structure* (Dover, New York, 1967).

[55] J. Pons, S. Reddy, M. Prakash and J. M. Lattimer, to be published.

[56] D. H. Wilkinson, Phys. Rev. **C7** (1973) 930; M. Rho, Nucl. Phys. **A231** (1974) 493.

[57] G. E. Brown and M. Rho, Phys. Rev. Lett. **66** (1991) 2720.

[58] N. K. Glendenning and S. Moszkowski, Phys. Rev. Lett. **67** (1991) 2414.

Fig. 1. Lowest order Feynman diagram for $\nu_l + B_2 \rightarrow l + B_4$. The symbols B_i and l denote baryons and leptons, respectively. P_i are the particles' four-momenta and $q_\mu = (q_0, \vec{q})$ is the four-momentum transfer. Fig. (1a) is the absorption reaction and Fig. (1b) is the scattering reaction.

Fig. 2. Composition and chemical potentials for noninteracting matter in beta equilibrium at $Y_L = 0.4$ at different temperatures. Top panels: Individual concentrations $Y_i = n_i/n_B$, where $i = n$, p, e^- and ν_e. Bottom panels: The lepton chemical potentials and $\mu = \mu_n - \mu_p = \mu_e - \mu_{\nu_e}$.

Fig. 3. Absorption mean free paths $\lambda = \sigma/V$ in noninteracting matter in beta equilibrium at different temperatures. The neutrino energy is taken to be the Fermi energy ($E_\nu = \mu_\nu$). The solid curves show exact results from Eqs. (15) and (21), the dashed curves are from the degenerate approximation (Eq. (26)), the dot-dashed curves are the nondegenerate results from Eq. (31), and the long dashed curves represent the elastic approximation from Eq. (34).

Fig. 4. Comparison between scattering and absorption reactions at $T = 10$ MeV for neutrino-trapped matter ($Y_L = 0.4$), assuming $E_\nu = \mu_\nu$. The neutrino energy was set equal to the local neutrino chemical potential. In the left panels the contribution to the neutrino mean free path due to individual reactions are shown. In the right panel, the solid curve is the ratio of the scattering to absorption mean free paths and the the dashed curve is the neutron scattering/absorption ratio.

Fig. 5. Compositions and chemical potentials for noninteracting matter in beta equilibrium with no trapped neutrinos ($Y_\nu = 0$) at different temperatures. Top panels: Individual concentrations $Y_i = n_i/n_B$, where $i = n$, p, and e^-. Bottom panels: The electron chemical potential $\mu_e = \mu_n - \mu_p$.

Fig. 6. Absorption mean free paths $\lambda = \sigma/V$ in noninteracting matter in beta equilibrium with no trapped neutrinos at different temperatures. The neutrino energy is taken to be $E_1 = 3T$. The leftmost panel clearly shows that at low temperatures the mean free path is very large since the reaction is kinematically supressed.

Fig. 7. Temperature dependance of the neutrino mean free path at nuclear saturation density for $Y_\nu = 0$ and $E_\nu = 3T$. Left panel: Individual contributions due to scattering and absorption reactions to the mean free path, the long-dashed curve is the total scattering opacity. Right panel: Ratio of the total scattering opacity to that of absorption.

Fig. 8. Particle fractions (upper panels) and lepton chemical potentials (lower panels) in the nonrelativistic potential Skyrme model for $Y_L = 0.4$ at various temperatures. Note that the proton fraction is larger than in the noninteracting case.

Fig. 9. Neutrino absorption mean free path in neutrino-trapped matter with $Y_L = 0.4$. Results for the limiting cases discussed in the text are also shown, with the same notation as in Fig. 3.

Fig. 10. Neutron (solid curve) and proton (dashed curve) effective masses as a function of baryon density in the Skyrme model. The curves shown are for $T = 30 MeV$.

Fig. 11. Compositions (upper panels) and electron chemical potentials (lower panels) for neutrino-free matter at various temperatures in the Skryme model. Note that the proton fraction is larger when compared with the noninteracting case and, at low densities, is quite sensitive to the temperature.

Fig. 12. Upper panel: Neutrino absorption mean free path in neutrino-free matter with the Skyrme model, assuming $E_\nu = 3T$. The exact and limiting cases discussed in the text are shown, with the same notation as in Fig. 3. For $T = 5$ MeV, the elastic approximation is off-scale. Lower panel: Comparison of absorption and scattering mean free paths for this case.

Fig. 13. Compositions (upper panels) and chemical potentials (lower panels) in field-theoretical model for nucleonic matter in beta equilibrium with fixed lepton number $Y_L = 0.4$.

Fig. 14. Absorption (upper panels) and scattering (lower panels) mean free paths $\lambda = \sigma/V$ for neutrino energy $E_\nu = \mu_{\nu_e}$ in beta equilibrium matter with $Y_L = 0.4$, for the field-theoretical model.

Fig. 15. Composition (upper panels) and chemical potentials (lower panels) matter in beta equilibrium with no trapped neutrinos ($Y_\nu = 0$) for the field-theoretical model.

Fig. 16. Absorption (upper panels) and scattering (lower panels) mean free paths $\lambda = \sigma/V$ for neutrino energy $E_\nu = 3T$ in matter with no trapped neutrinos for the field-theoretical model.

Fig. 17. Comparision with previous cross sections employed in protoneutron star calculations. The upper panels show comparisions with limiting forms valid for the nondegenerate (left) and degenerate (right) matter. The lower panels show comparisions with interpolated cross sections; the interpolation scheme in Eq. (86)is shown in the left panel and that in Eq. (87) is shown in the right panel.

Fig. 18. Compositions (upper panels) and chemical potentials (lower panels) for neutrino-trapped matter ($Y_L = 0.4$) including hyperons in the field-theoretical model. $\mu = \mu_n - \mu_p = \mu_e - \mu_{\nu_e}$.

Fig. 19. Absorption mean free paths $\lambda = (\sigma/V)^{-1}$ for neutrino energy $E_\nu = \mu_{\nu_e}$ in matter with fixed lepton number ($Y_L = 0.4$) in the field-theoretical model. Upper panels show both the results for matter without hyperons (dashed curves) and with hyperons (solid curves). Lower panels show the relative contributions to the absorption mean free path for matter with hyperons.

Fig. 20. Scattering mean free paths for neutrino energy $E_\nu = \mu_{\nu_e}$ in matter with fixed lepton number ($Y_L = 0.4$) in the field-theoretical model. Upper panels show the results for the toal

scattering mean free path for matter without hyperons (dashed curves) and with hyperons (solid curves). Lower panels show the relative contributions to the scattering mean free path for matter with hyperons.

Fig. 21. Compositions (upper panels) and chemical potentials (lower panels) for neutrino-free matter ($Y_\nu = 0$) including hyperons in the field-theoretical model.

Fig. 22. Absorption mean free paths $\lambda = (\sigma/V)^{-1}$ for neutrino energy $E_\nu = 3T$ in matter with no trapped neutrinos ($Y_\nu = 0$) in the field-theoretical model. Upper panels show both the results for matter without hyperons (dashed curves) and with hyperons (sold curves). Lower panels show the relative contributions to the absorption mean free path for matter with hyperons.

Fig. 23. Scattering mean free path for neutrino energy $E_\nu = 3T$ in matter with no trapped neutrinos ($Y_\nu = 0$) in the field-theoretical model. Upper panels show the results for the total scattering mean free path for matter without hyperons (dashed curves) and with hyperons (solid curves). Lower panels show the relative contributions to the scattering mean free path for matter with hyperons.

Fig. 24. Neutrino diffusion coefficient D_2 defined in Eq. (91) in matter with and with out hyperons for $Y_L = 0.4$ in the field-theoretical model. The left panel shows D_2 as a function of baryon density in matter containing only nucleons and leptons. The ratio of D_2 in matter without hyperons to D_2 in matter with hyperons is shown in the right panel.

Fig. 25. Neutrino diffusion coefficient D_4 defined in Eq. (91) in matter with and with out hyperons for $Y_\nu = 0$ in the field-theoretical model. The left panel shows D_4 as a function of baryon density in matter containing only nucleons and leptons. The ratio of D_4 in matter without hyperons to D_4 in matter with hyperons is shown in the right panel.

FIGURES

(a)Absorption:

(b)Scattering:
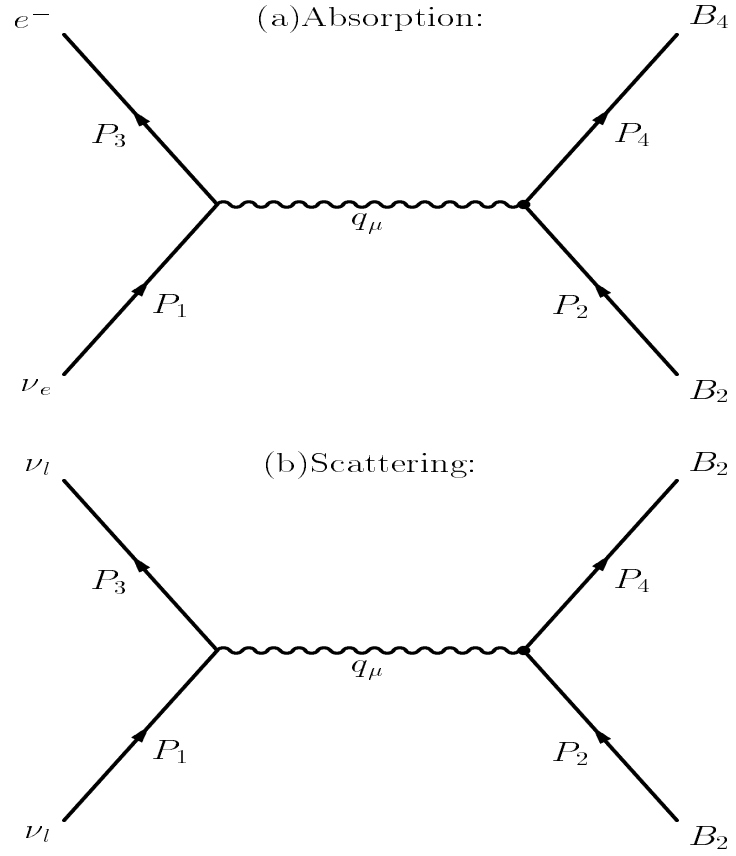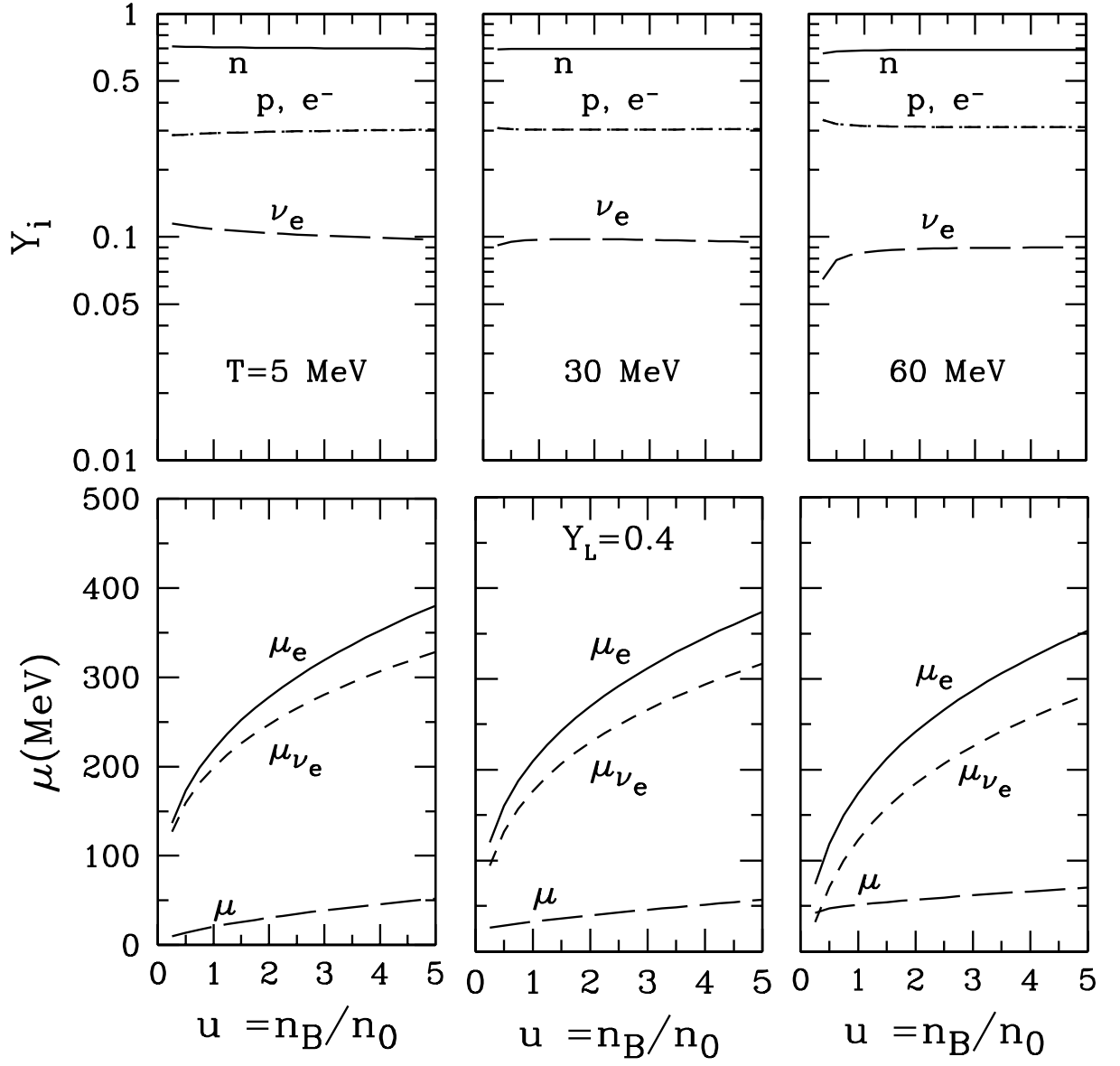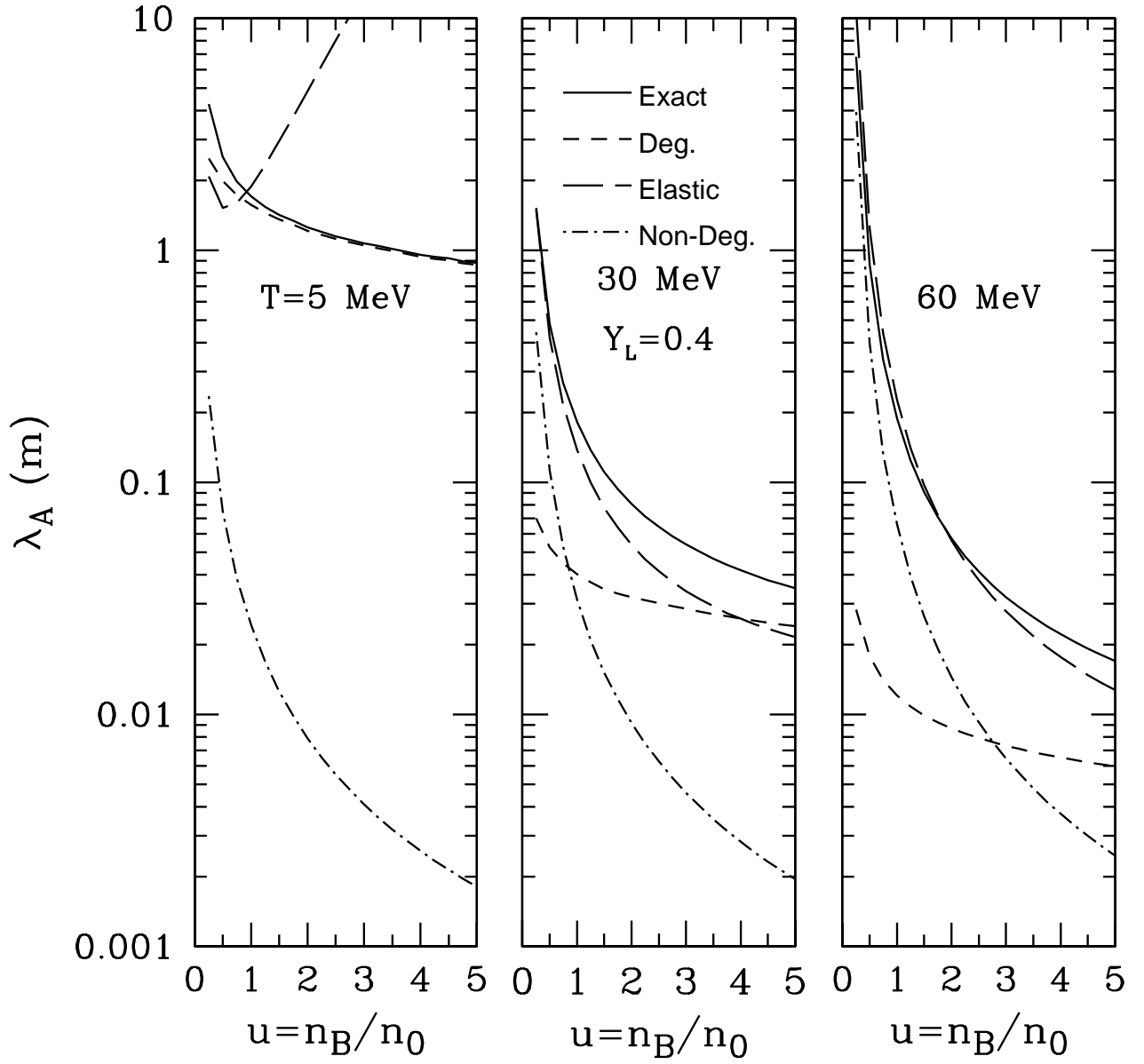
FIG. 1.

FIG. 2.

FIG. 3.

FIG. 4.

FIG. 5.

FIG. 6.

47

FIG. 7.

FIG. 8.

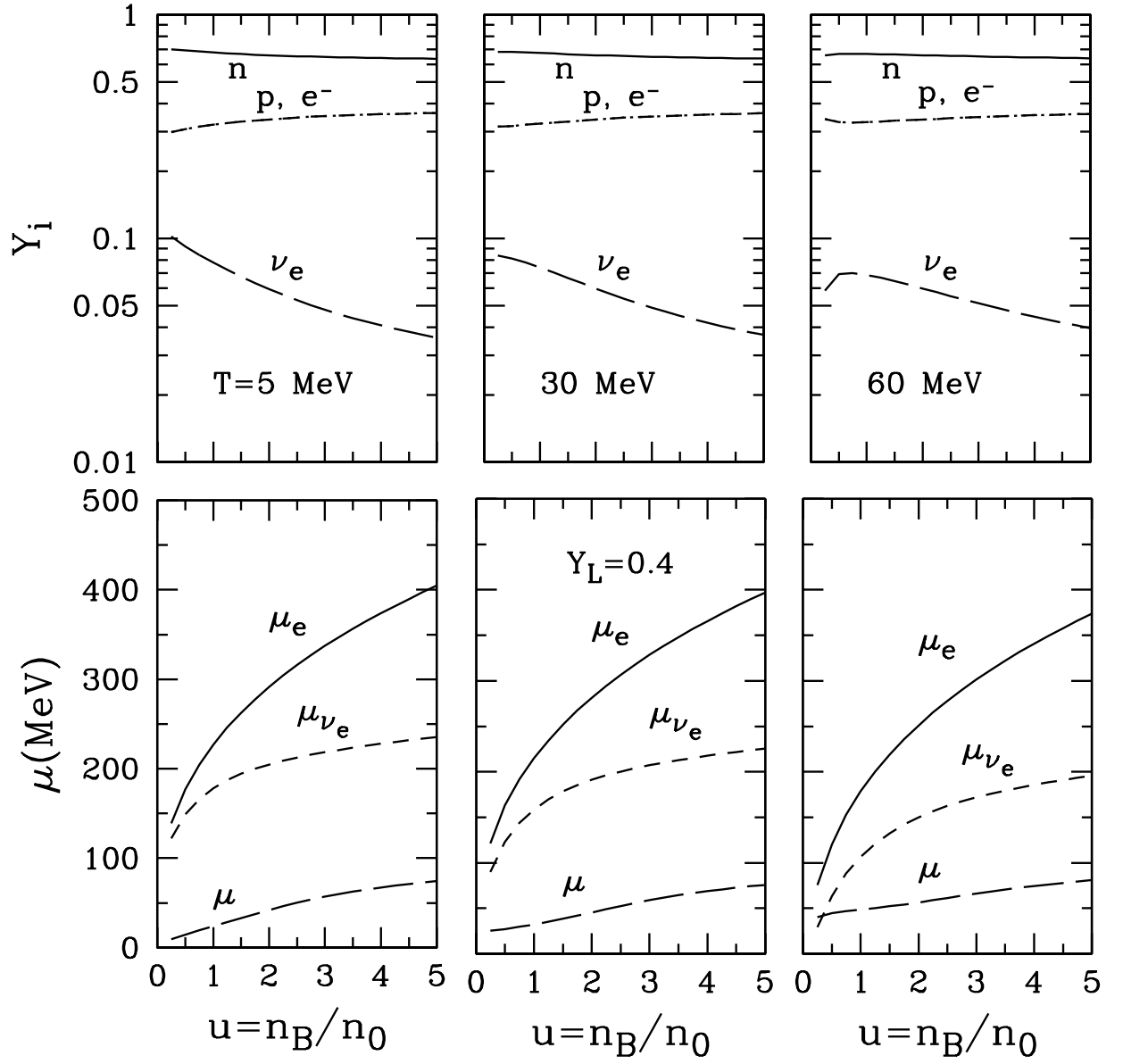FIG. 9.

$Y_L = 0.4$

$\dfrac{M^*}{M}$
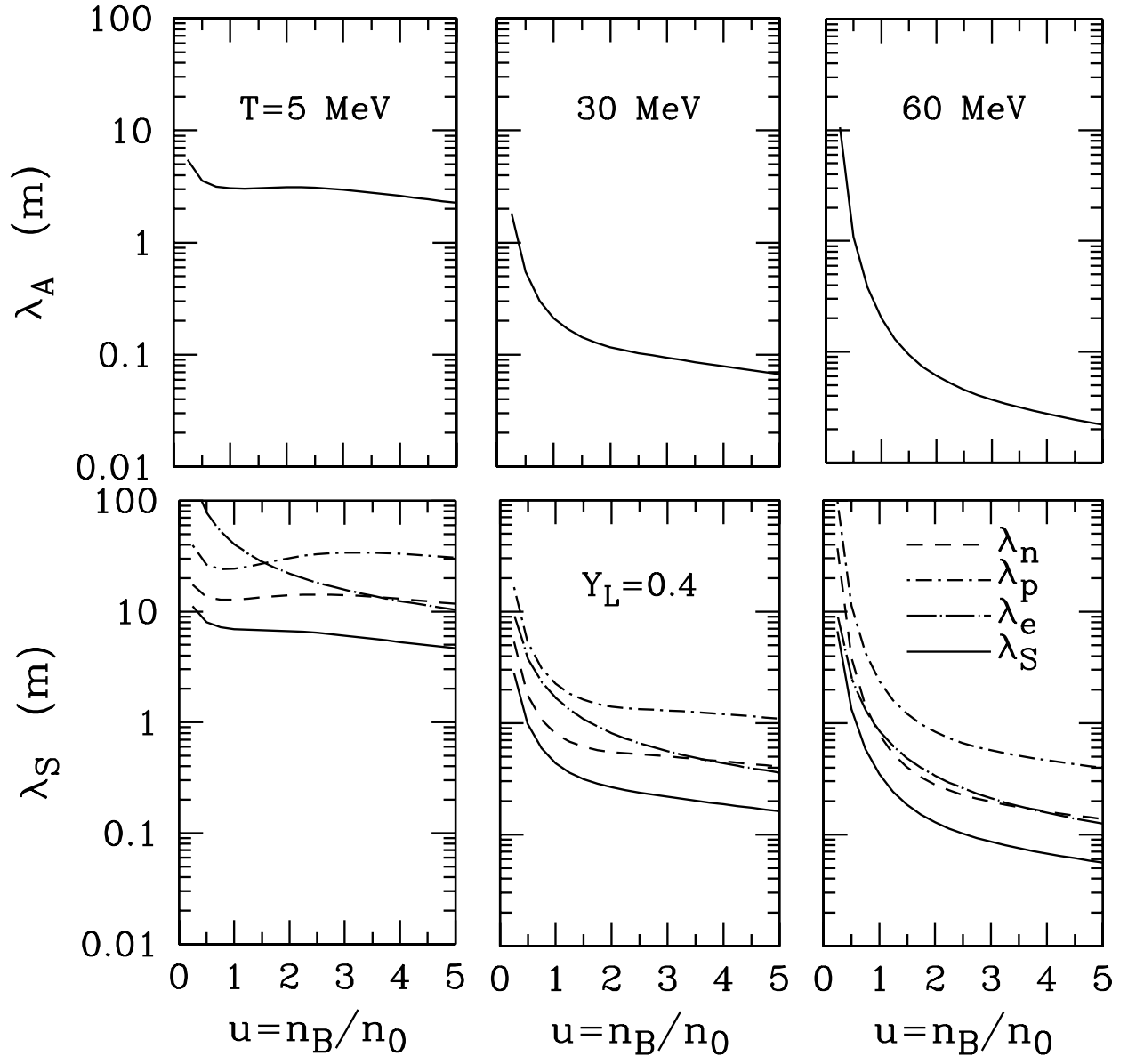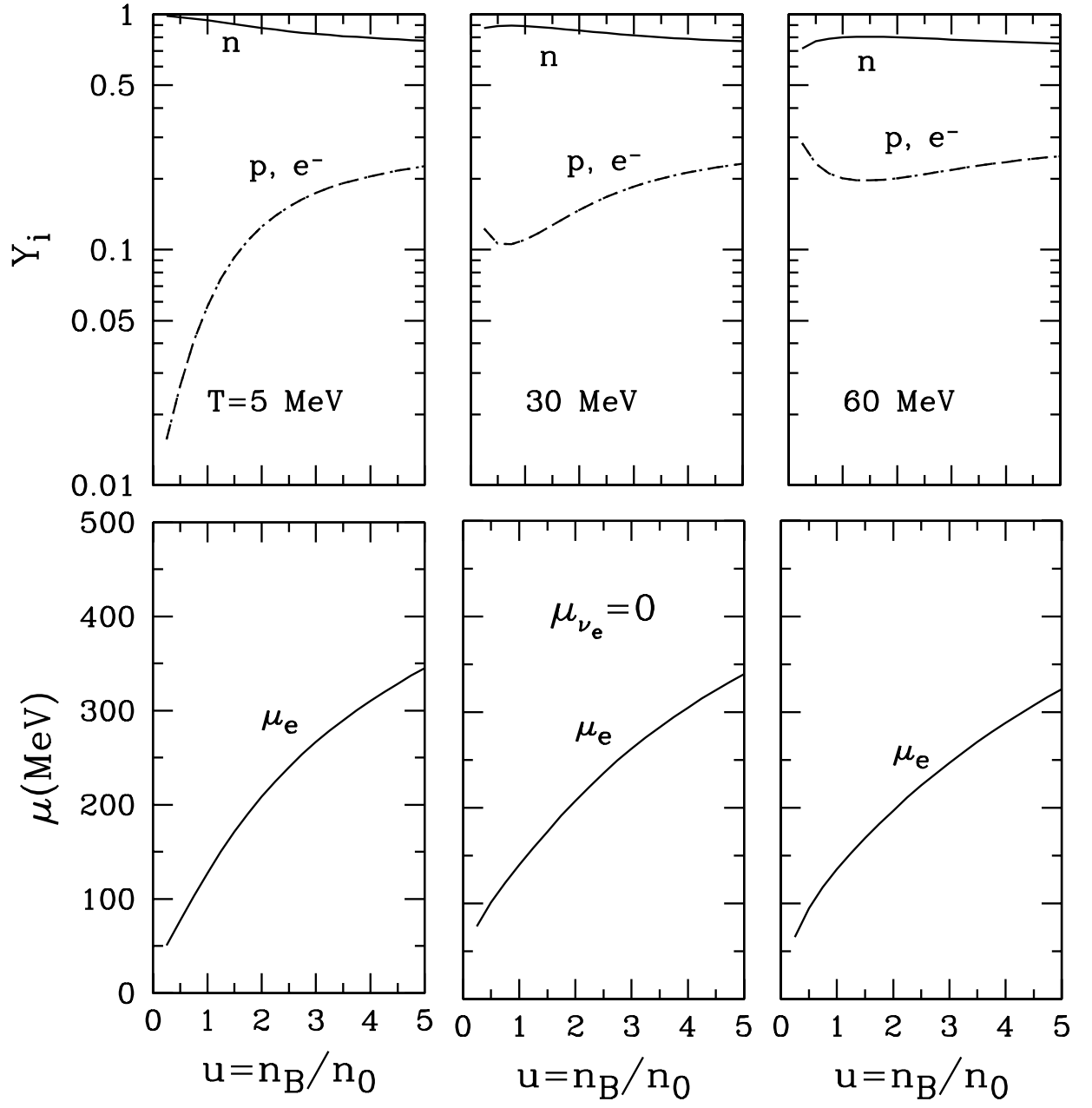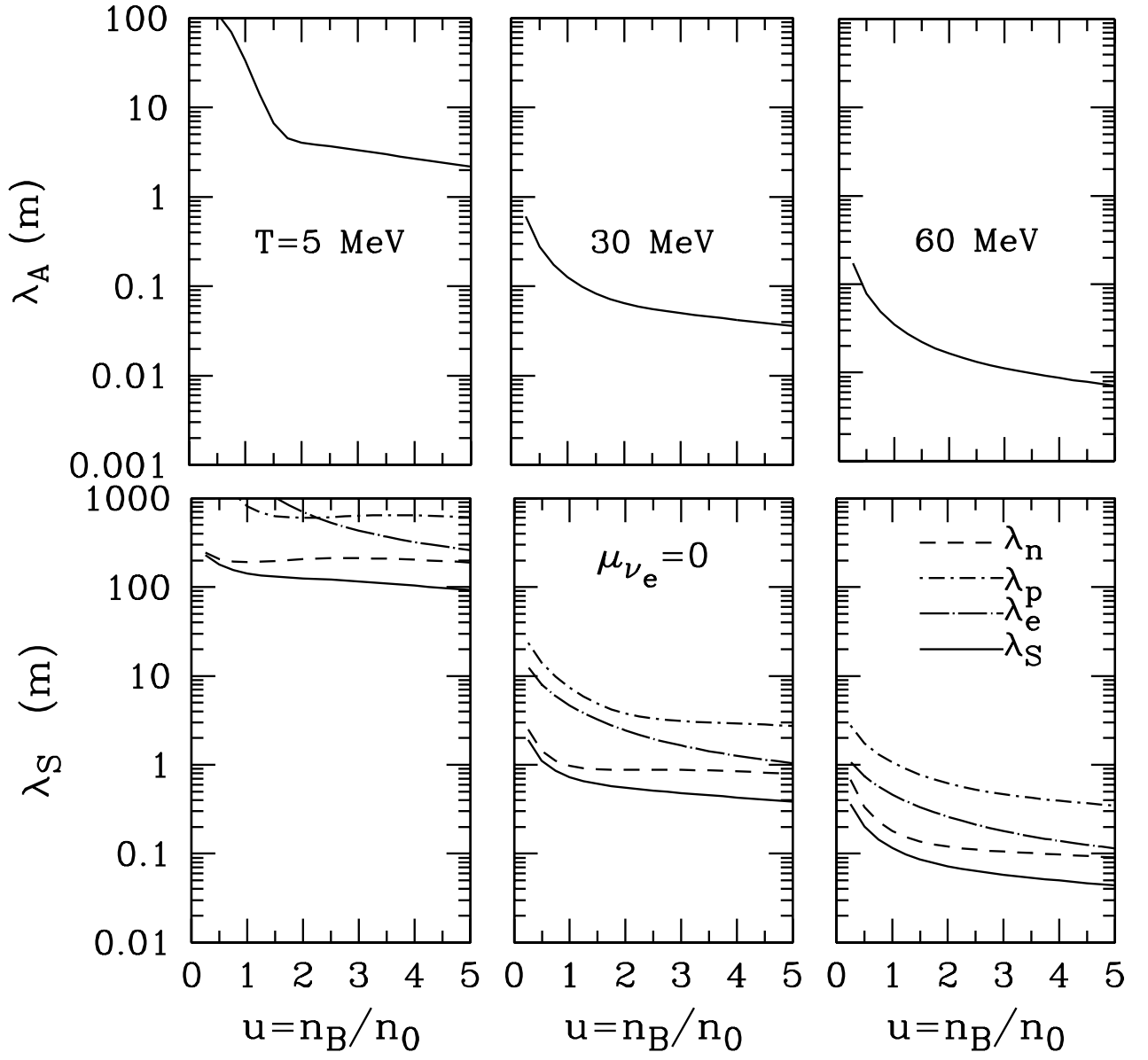
n

p

$u = n_B/n_0$

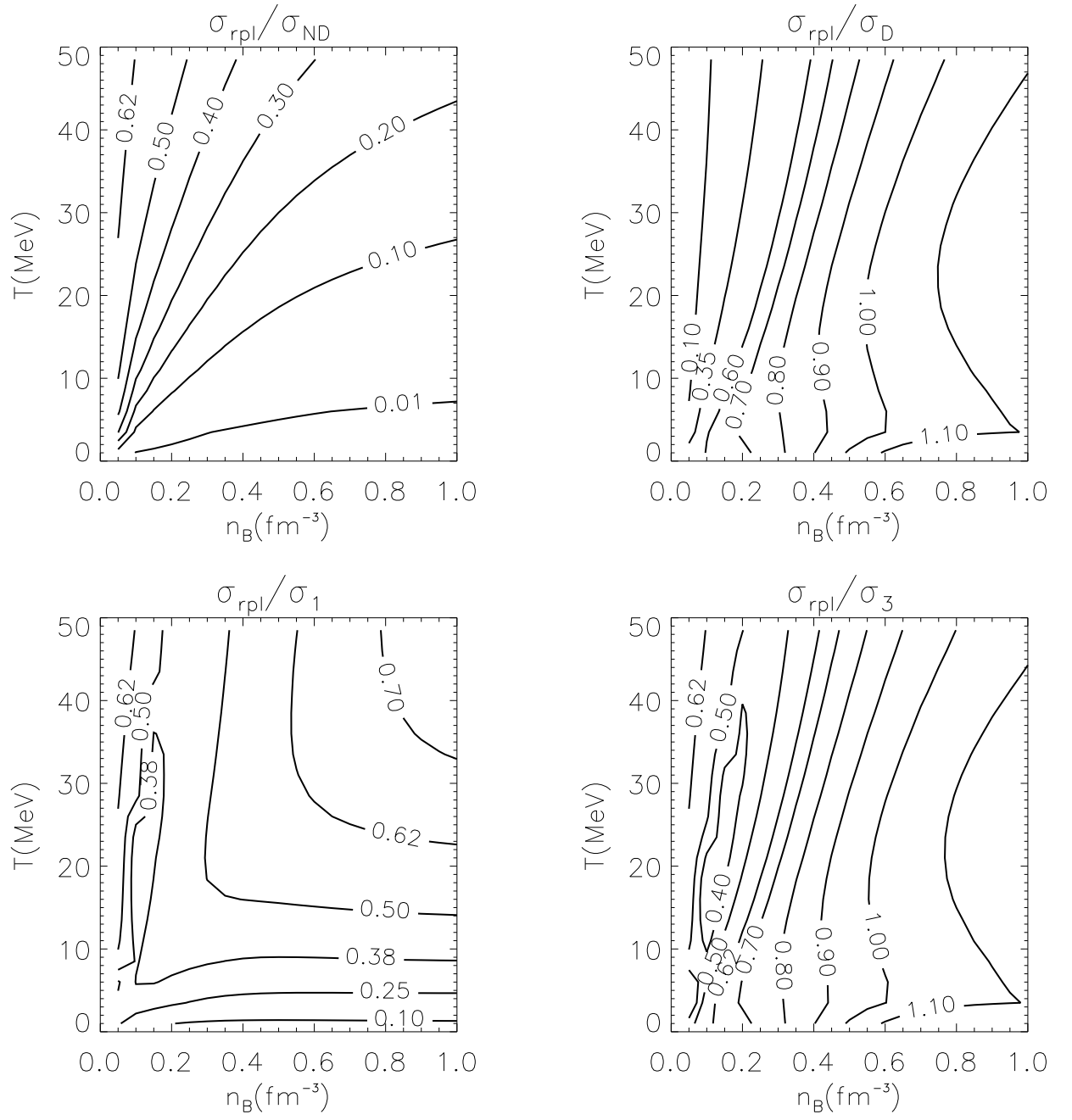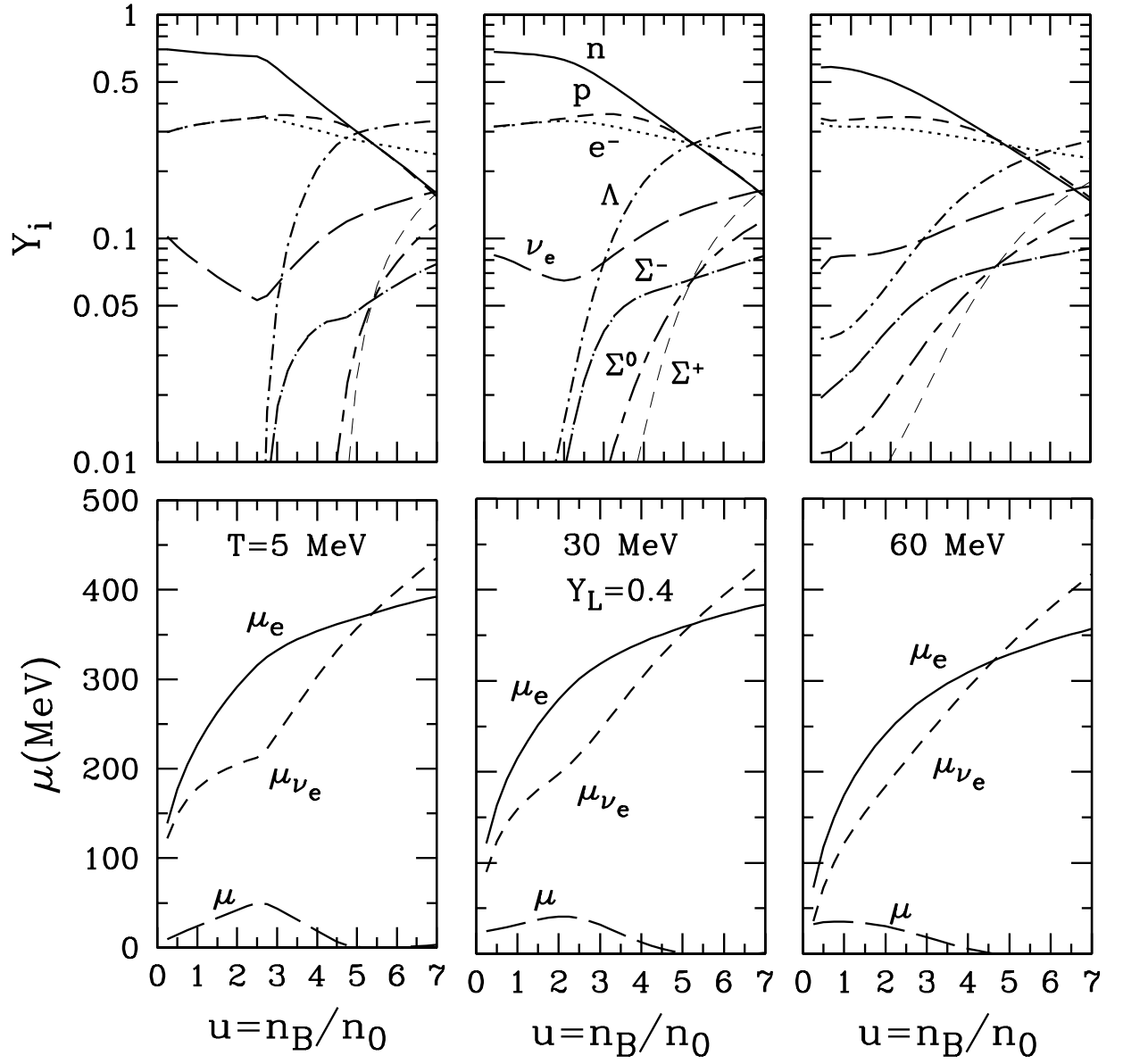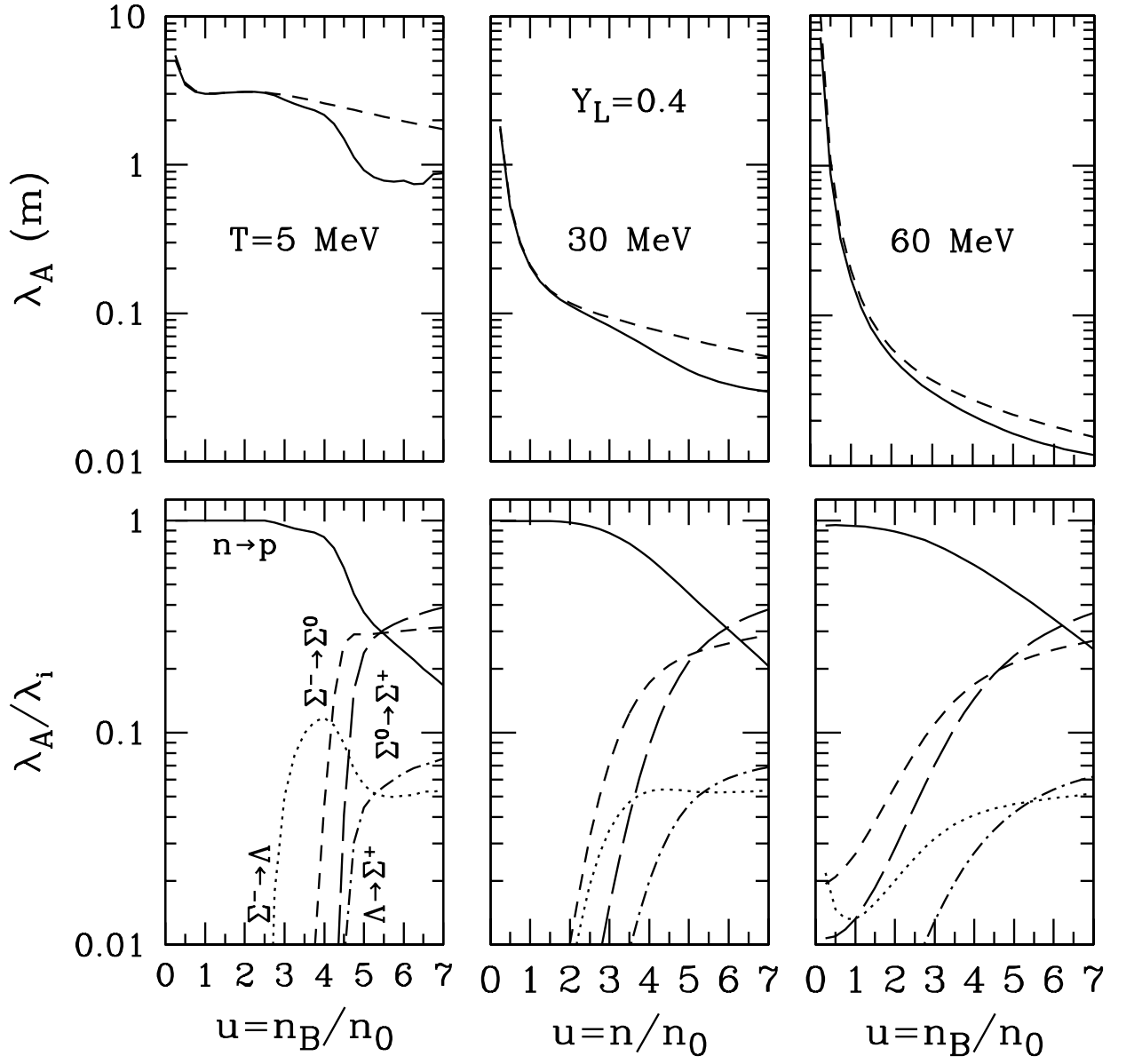FIG. 10.

51
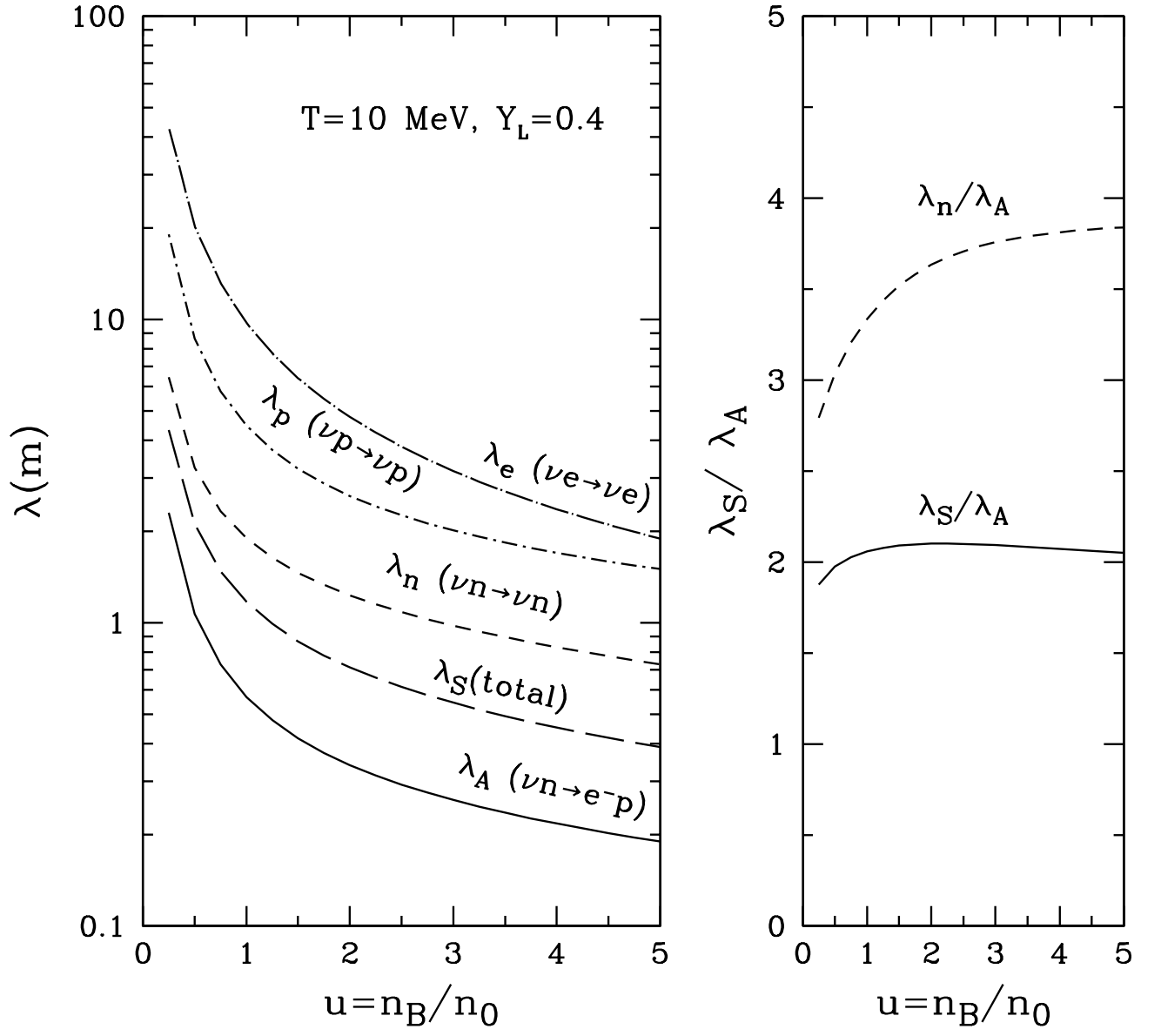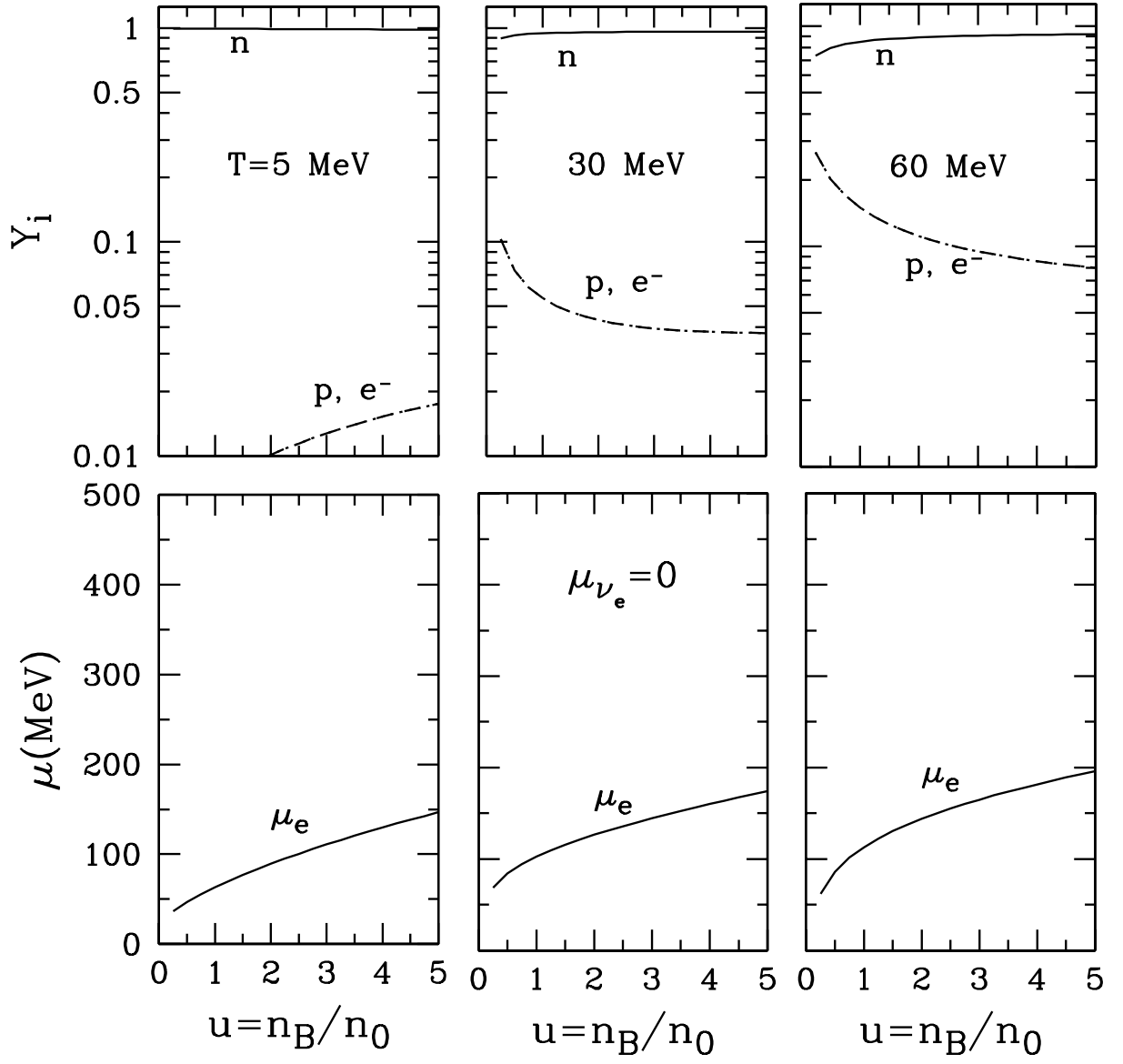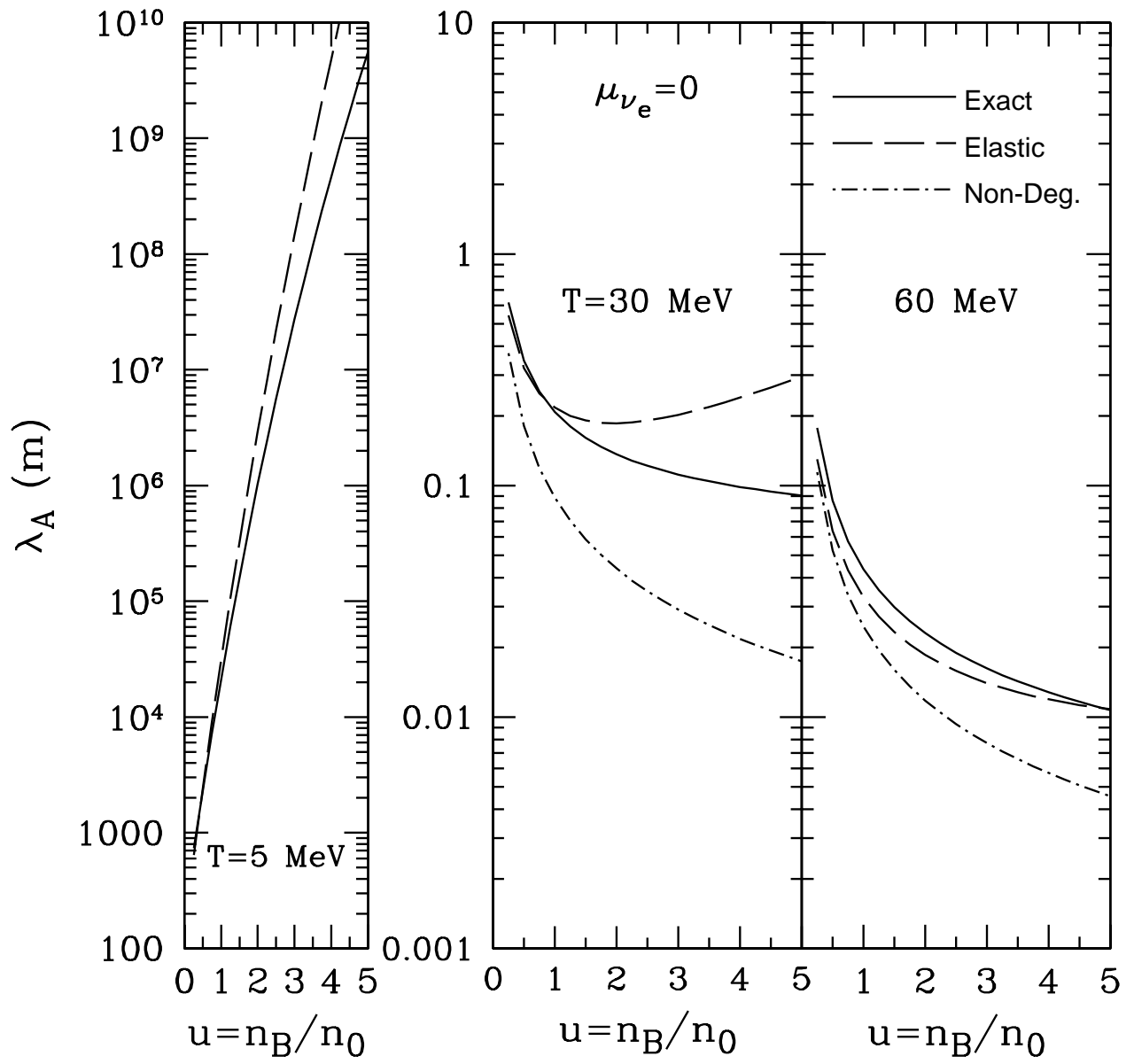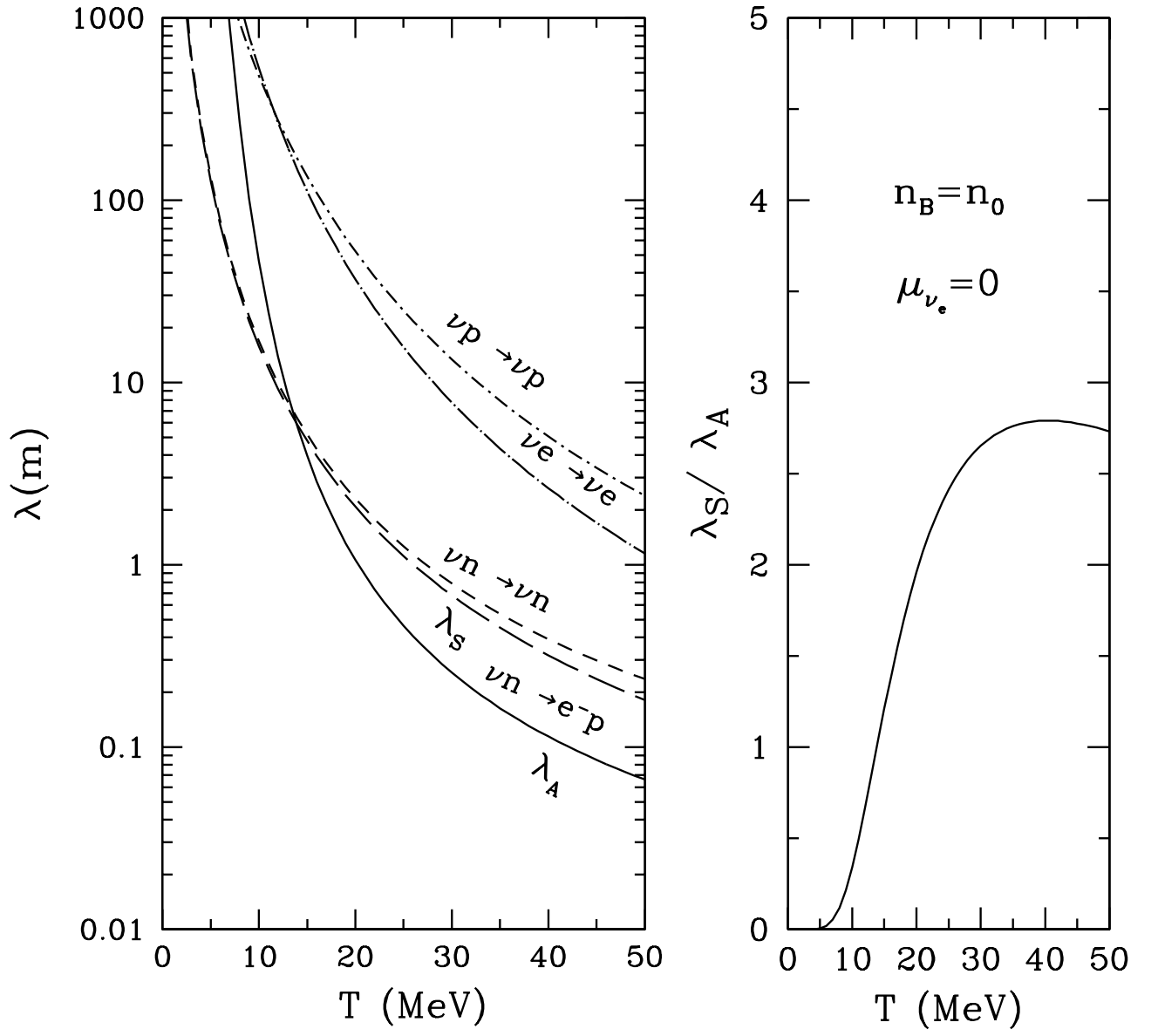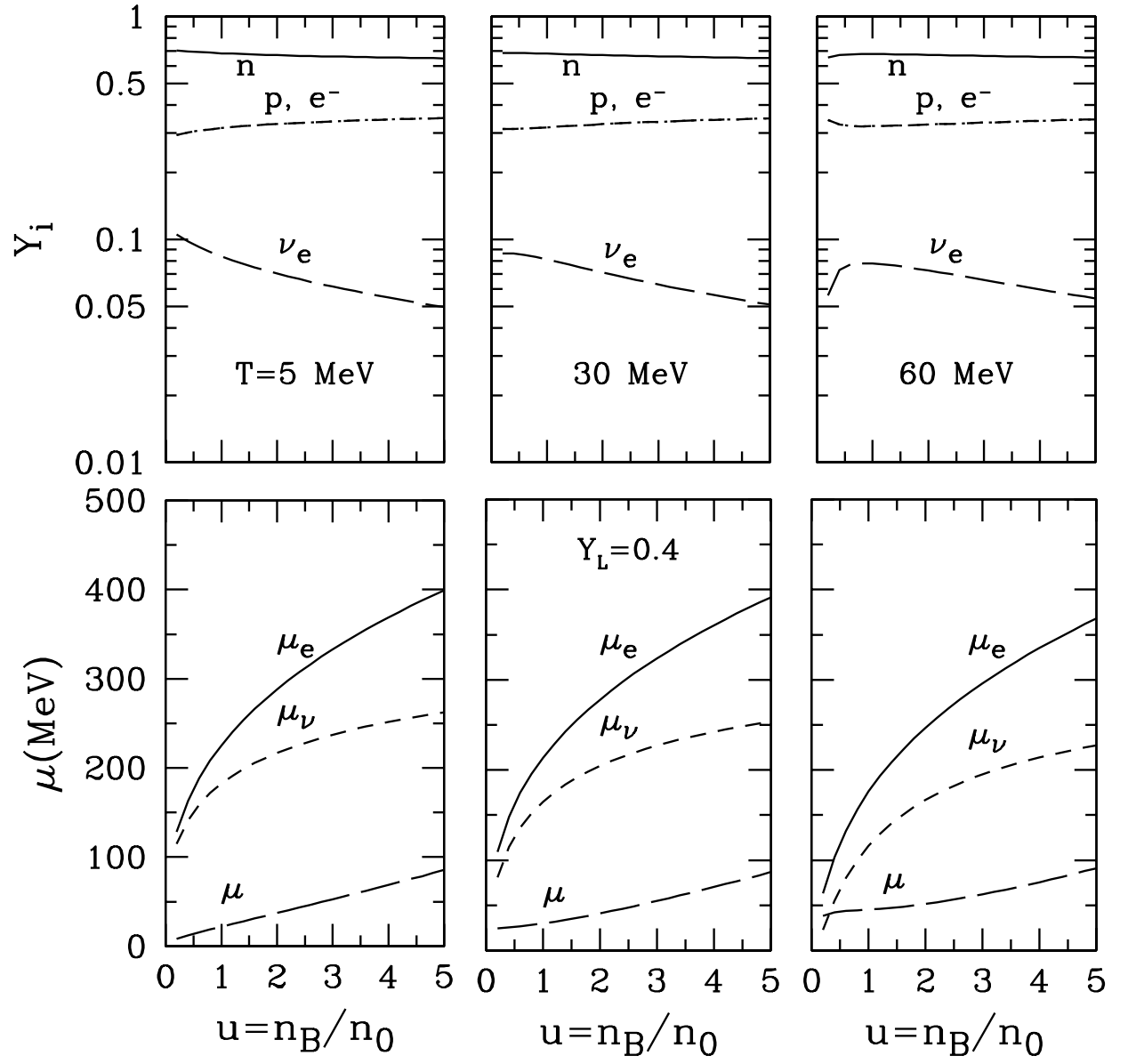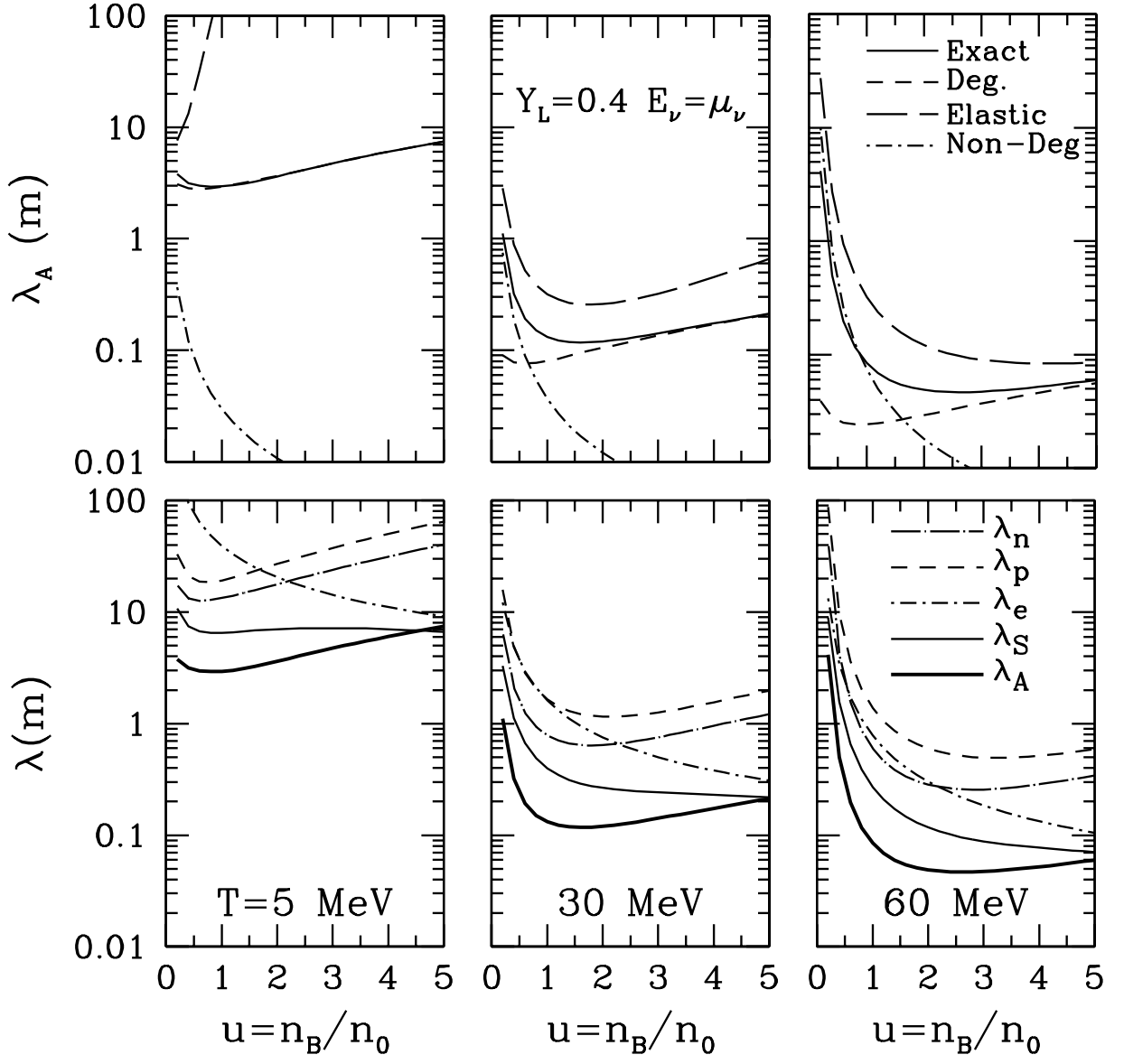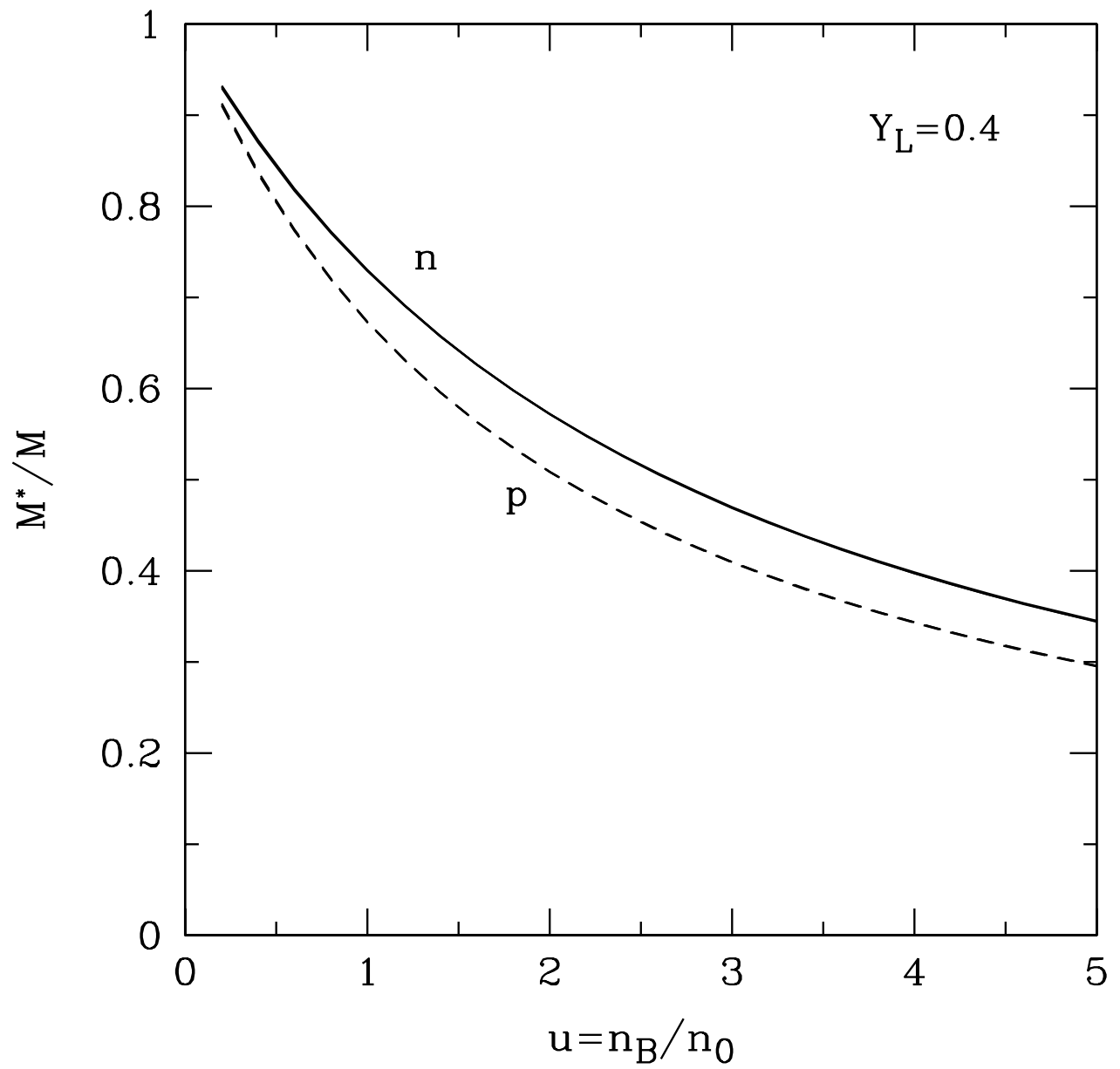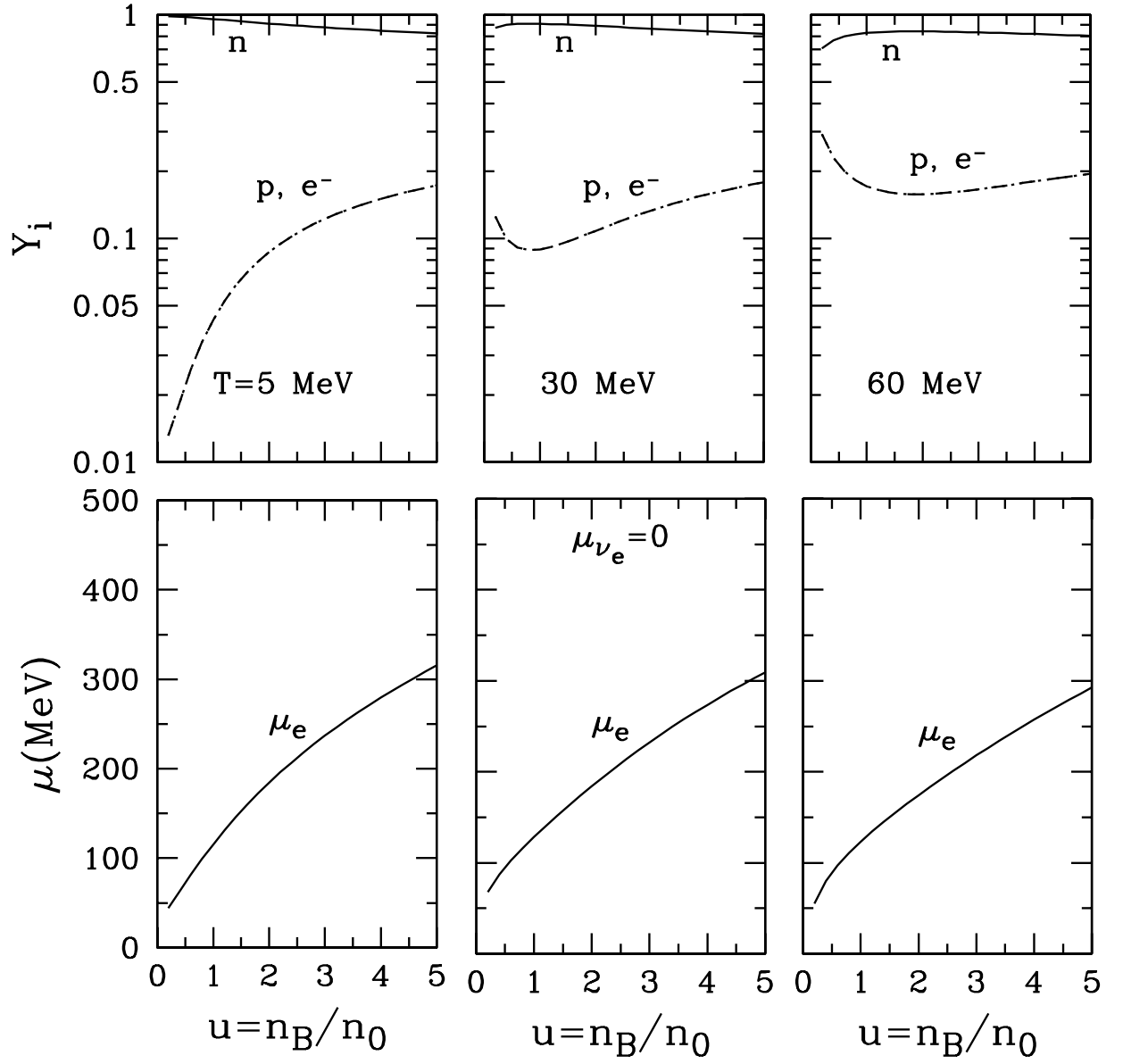
FIG. 11.
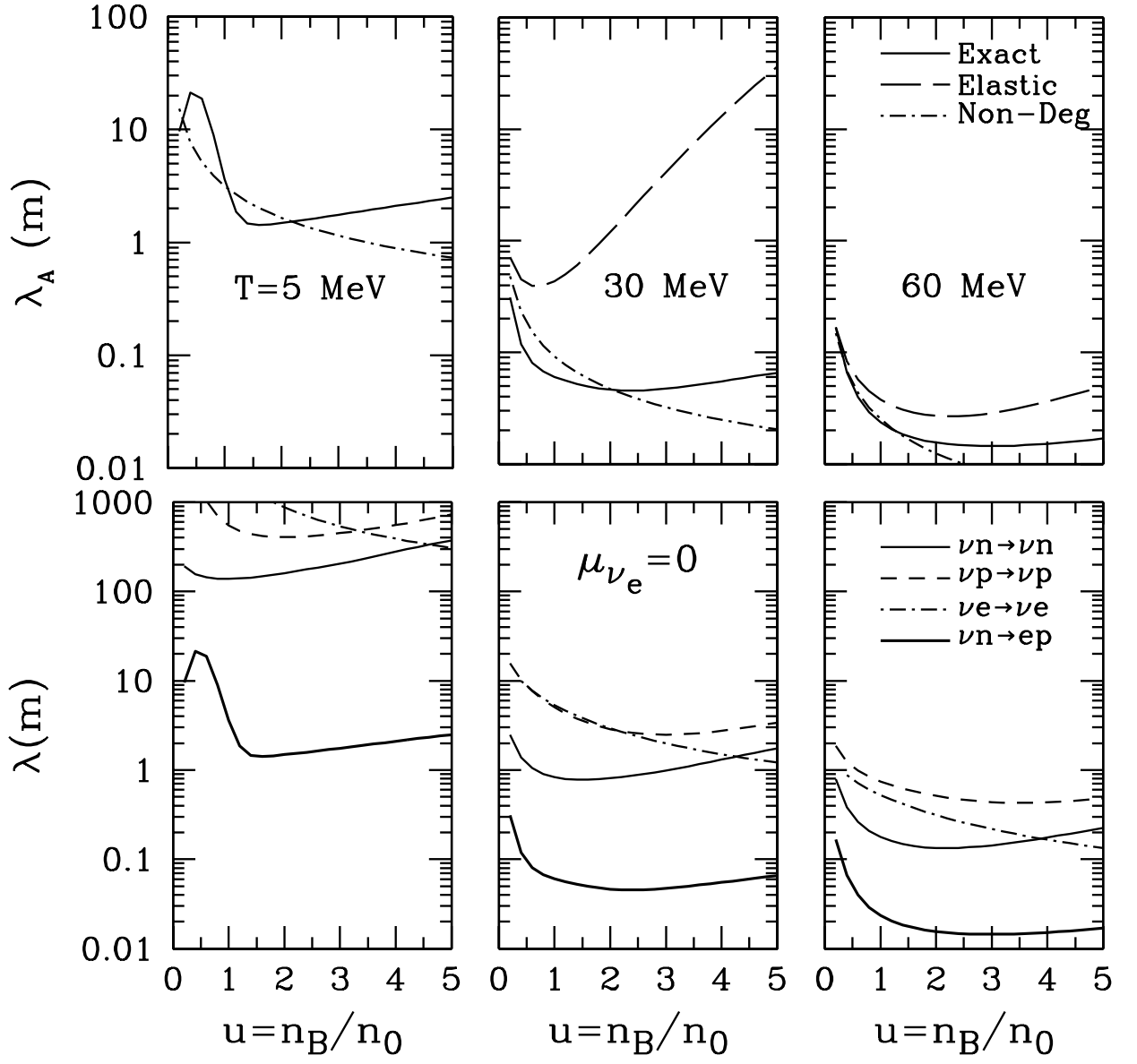
FIG. 12.
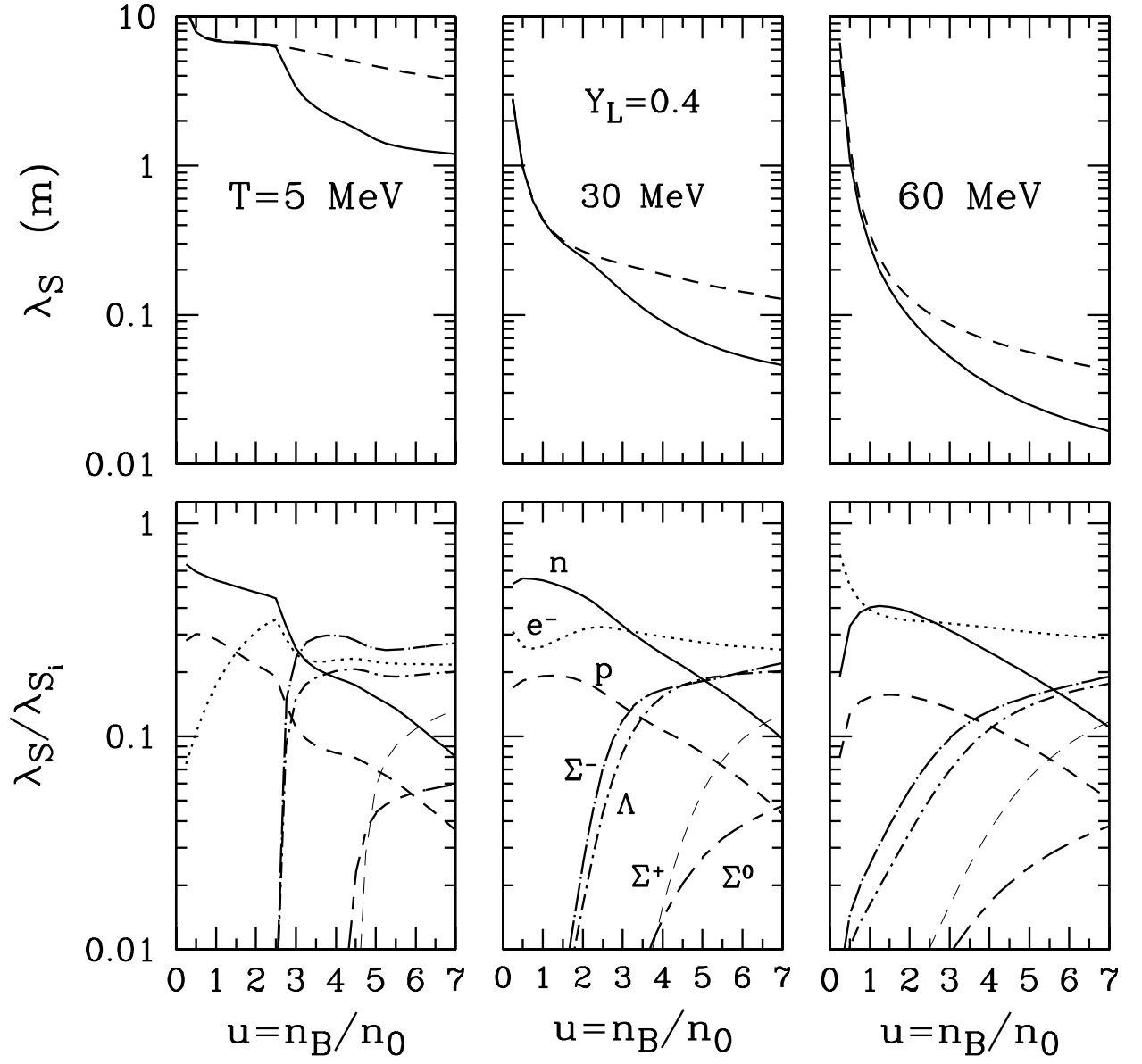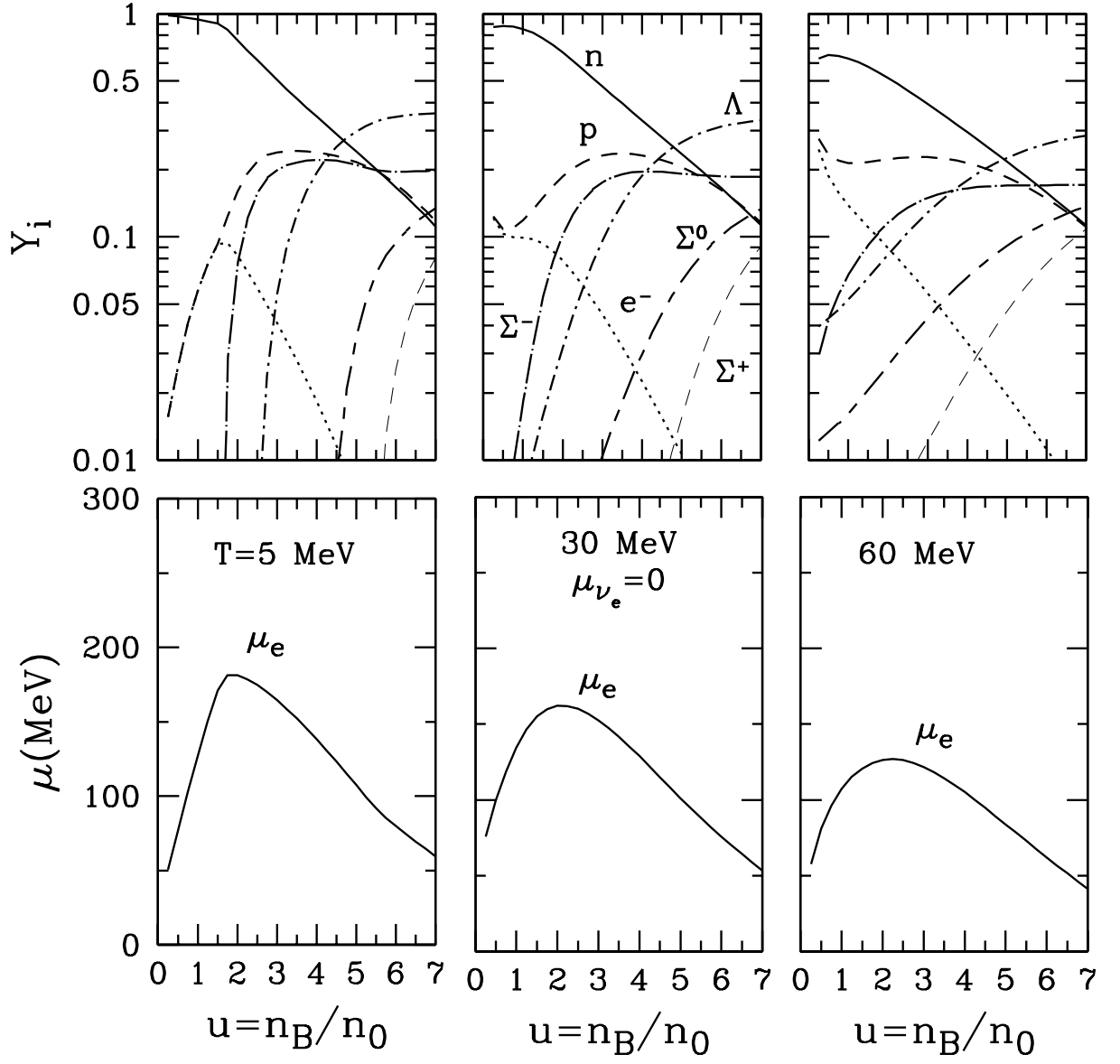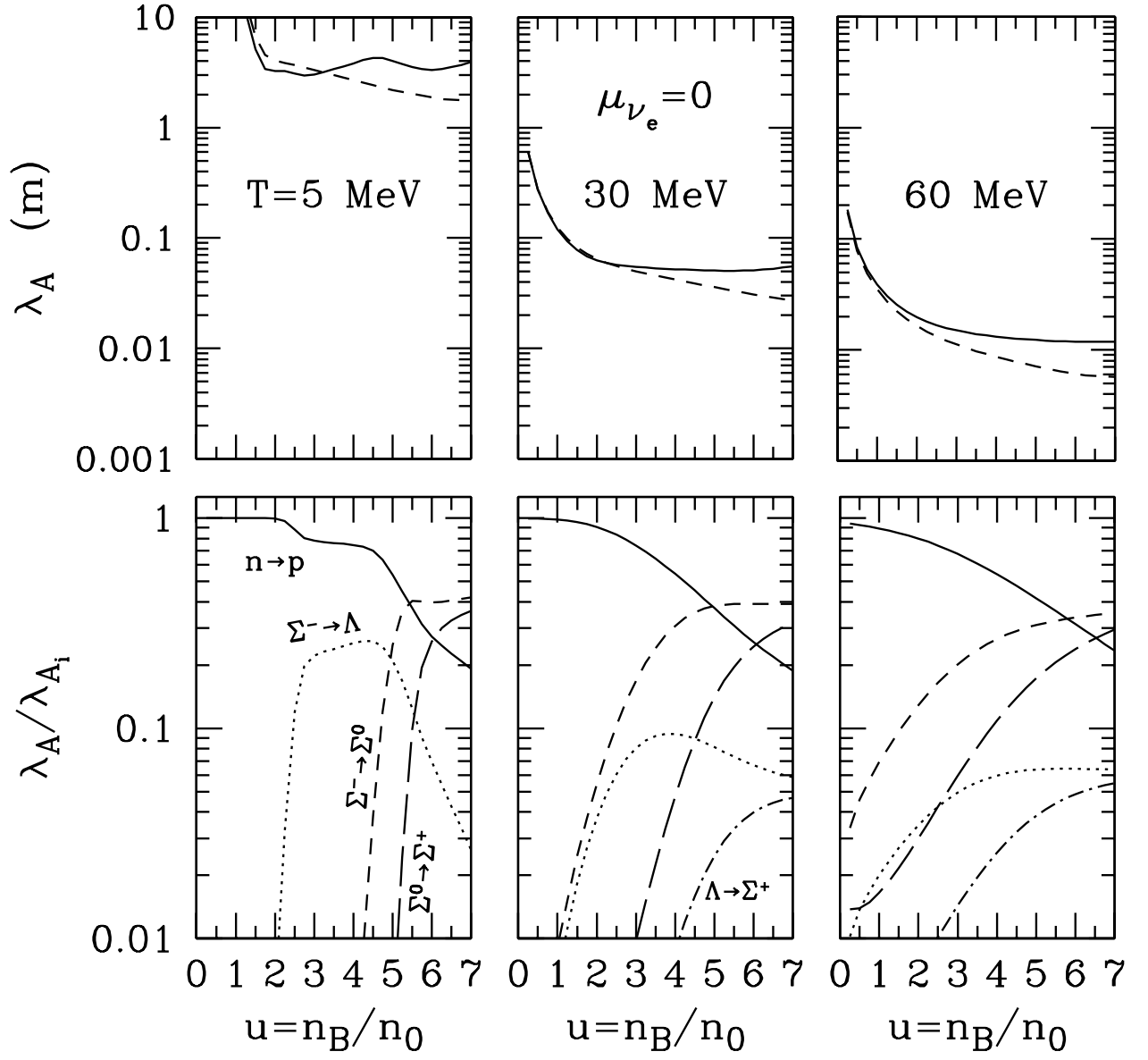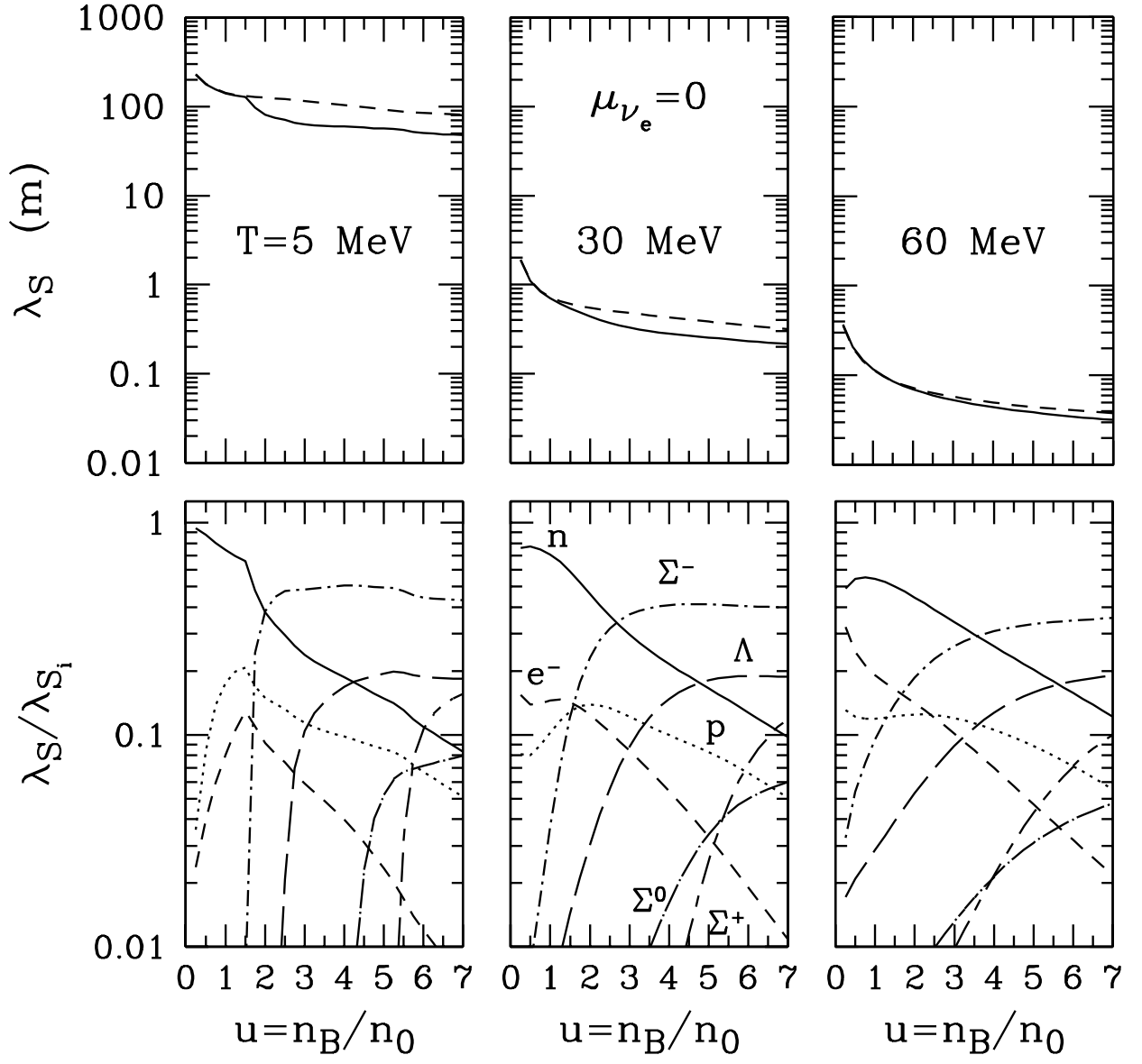
FIG. 13.

FIG. 14.

FIG. 15.

FIG. 16.

FIG. 17.

FIG. 18.

FIG. 19.

FIG. 20.

FIG. 21.

FIG. 22.

FIG. 23.

FIG. 24.

FIG. 25.